Corrosion Under Insulation In-Situ Testing in Marine Environment

By

©Alan Hillier

A Thesis submitted to the

School of Graduate Studies

In partial fulfilment of the requirements for the degree of

Doctor of Philosophy

Faculty of Engineering and Applied Science

Memorial University of Newfoundland and Labrador

May 2023

St. John's

Newfoundland and Labrador, Canada

ABSTRACT

Oil and gas pipelines in marine or coastal environments experience significant corrosion when moisture and chloride penetrate surface protections. There is lack of in-situ work studying corrosion under insulation (CUI) and corrosion under coating, especially in marine atmosphere. As well, monitoring and inspection of assets under corrosion attack is a concern, as it can spread insidiously in out of sight areas. Real time monitoring of pipelines and other assets is best to get information quickly, especially in difficult to reach areas. Electrochemical potential noise (EPN) is one proposed method to investigate CUI using simple equipment and should be further investigated in determining quantitative corrosion results.

This thesis investigates corrosion and pitting from pipelines which were coated, uncoated, insulated, and not, in a marine harsh environment field experiment. The surface morphology, and mechanisms of corrosion were also studied. Thirty-six A333 low temperature carbon steel pipelines were placed at Argentia, NL, Canada, an extremely corrosive environment (C5) near shoreline. High humidity, winds, and sea-spray are present throughout most of the year. Corrosion rate was assessed using mass loss and optical inspections were used for pit depth. X-ray diffraction and scanning electron microscope were used to determine corrosion products and surface morphology. Corrosion near the ends of the pipe were most severe, perhaps due to crevice corrosion, and ingress of moisture and chloride. Insulated uncoated pipes showed deepest pits, therefore when pipes are insulated, anti-corrosion protective coating should be applied. Corrosion and pitting rates were lowest in insulated and coated pipes.

Real time monitoring using EPN was explored, varying electrode size, temperature, and electrolytes. EPN was recorded using Keithly digital multimeter controlled by LabVIEW software. Potential was investigated using time and frequency domain methods to determine its usefulness

in monitoring corrosion. In this research the best way to relate potential to mass loss and corrosion type occurred using time-frequency domain power spectral density from raw potential noise generated from electrodes.

This in-situ testing enhanced the understanding of corrosion mechanisms and pitting in the environment. Important coating and insulation time to failure was recorded, which provides insights for oil and gas operations regarding inspection, maintenance, and design life. EPN tests proved a simple method and equipment can be used for in-situ corrosion detection, which can help ensure safety and asset integrity.

ACKNOWLEGEMENTS

First, I thank God for protecting, guiding, and providing me with the strength to complete this thesis.

First, I would like to express my gratitude to my supervisors Dr. Faisal Khan, Dr. Susan Caines, and the late Dr. John Shirokoff. I pray you always have blessings and happiness. They accepted me to perform and complete this research while providing mentorship, friendship, and valuable advice while contributing to my research and development. We shared many personal discussions and meals together, and for that I am very grateful. Specifically, to Dr. Khan living in your house was a hallmark of the happier times in St. John's, and I appreciate those memories. To Dr. Michael Hinchey, my progress has a come a long way since my first Fluids course with you, thank you for reviewing my thesis.

To my wonderful parents, Wade and Linda, who raised me with an excellent upbringing, provided love and anything I wanted, there are no words to express the level of gratitude and love I have for you. I appreciate you always encouraging me to work hard and finish this undertaking.

To my sisters' Caroline, Elizabeth, and Katherine, the fun times, and memories we have had together through the years will never be forgotten, and we will have many more.

To my beautiful wife Sarah, and my sweet children Maria, Malik, and Serene, your patience, help, and bliss you have provided me in every way, has been vital. You have brought much joy and happiness despite difficulties in recent years.

TABLE OF CONTENTS

LIST OF TABLES

LIST OF FIGURES

INDEX OF TERMS

ASM American Society for Metals

ASTM American Society for Testing and Materials

CR Corrosion Rate

CUI Corrosion Under Insulation

DMM Digital multi-meter

DNV Det Norske Veritas

ECN Electrochemical Current Noise

EN Electrochemical noise

EPN Electrochemical Potential Noise

FFS Fitness-for-service

LTCS Low temperature carbon steel

PF Probability of failure

RBI Risk-based Assessment

RE Reference Electrode

WE Working Electrode

RP Recommended practice

SCC Stress corrosion cracking

LTCS Low Temperature Carbon Steel

CHAPTER 1 - Introduction

1.1 Overview

Petroleum reserves continue to be pursued further offshore and in extreme environments as global demand requires. In many locations around the world insulation is used on pipelines to regulate product temperature and protect personnel (Eltai et al., 2019). Corrosion under insulation (CUI) is a major problem in petroleum and other industries (Javaherdashti, 2014; Winnik, 2016), occurring when moisture (rain, steam, sea spray, condensation, or other electrolytes) reaches metal surfaces under insulation and corrosion begins. Currently a high percentage of pipeline repairs occur externally due to CUI (Eltai et al., 2019), despite that corrosion and life information due to CUI are rarely found in literature. Corrosion also progresses under coating on pipe surfaces, and this is seldom discussed and should be further researched.

Steel is the most used metal for structures and in oil and gas pipe systems due to its low cost and good mechanical properties. Atmospheric corrosion of steel has been studied extensively with many books on the subject ("Atmospheric Corrosion" 2016; Evans, 1960; Graedel and McGill, 2002; Rozenfeld, 1972) and models exist (Melchers, 2012a, 2012b, "Molecular Modeling of Corrosion Processes," 2015) for bare metal corrosion in marine atmosphere. Until recently however, researchers paid little attention to corrosion action from marine chlorides, despite knowing that salt spray increases corrosion severely compared to non-marine atmospheres (Alcántara et al., 2017).

There are few resources to accurately determine lifespan of insulated or coated assets due to high variability in corrosion rate, insulation, coating, and weather information. Also, data is scarce on failure rates of insulation and coating. Though reliability and structural models exist using

probability distributions, accurate pitting and corrosion rate are required (Bhandari et al., 2015) to estimate life and evaluate risk. This information must come from physical processes recorded from a field experiment ("Heidary, R. et al" 2018) and this is a focus of this research.

Corrosion studies are done is to assess environment corrosion on metals, this information can be used to ensure design life. Most studies on marine atmosphere corrosion near ocean occur with flat metal coupons (or wire) mounted on racks and angled 30-45 degrees, while facing seashore (Alcántara et al., 2017; Fuente et al., 2011). Some standards that describe atmospheric corrosion testing are ASTM-G50 and ISO 8565 ("ASTM-G50" 2020; "ISO 8565," 2011). After samples are left for some time then they are removed, weighed, and corrosion rate by mass loss and other details are expressed. This information is used by engineers to ensure design life on different assets and create or test corrosion models. One issue with classical standards is they provide little guidance for field experiments on coating or insulation ("ASTM-G189"). A review completed by (Caines et al., 2015) provided a good overview of the needs and requirements to properly conduct a full-scale CUI experiment in-situ.

Corrosivity is variable to location, as hot dry weather would not produce the same corrosion as hot humid weather. Categories C1-C5 (CX, offshore corrosion, was added in 2018) are used to describe environments in ISO 12944-9. The scale describes C1 as a low corrosion environment and C5/CX as highly/extremely corrosive. As such, different environments require different protection from the elements.

Marine atmosphere is described with high salinity due to marine aerosol comprised of fine particles which are suspended. From the sea, wind and waves action bring different products into the air, where they may be liquid or solid, composed of brine, sea-salt, and/or other particles which affect corrosion severely (Li and Hihara, 2014). Newfoundland is rarely studied with corrosion tests

despite being a harsh marine environment according to Revie and presents an opportunity for research.

There is consensus that for steel in marine atmosphere, lepidocrocite is the early formed primary product, followed in time by geothite, akageneite, magnetite and others. Rust type and morphologies are observed by XRD, SEM and other methods and vary for different environments and surface protections. Though early and late state oxide and hydroxide formations are known for steel in marine atmosphere, the answer to what forms under insulation or coating is not and was not found in open literature. Thus, it should be investigated as almost all assets placed in such environments are coated and/or insulated (Alcántara et al., 2017).

It should be noted that morphologies of synthetic iron oxides and those formed by laboratory testing may be different than those formed in naturally in marine atmosphere (Waseda et al., 2006), as such, field tests are important research. As well, in environments of high corrosive activity (C4, C5) sheltered exposure of metals has shown that corrosion is increased (Morcillo et al., 2013), it is then valuable to investigate the effect of insulation and coating in this regard.

Other than corrosion rates and morphology, risk engineers also require up-to-date information on assets, including pipelines. Sometimes it is physically difficult to inspect due to inaccessible locations, intrusive insulation removal, or simply lacking information in standards to estimate failures. Currently technologies exist to help detect corrosion without removing insulation, like x-ray analysis, but it can be difficult to apply over areas (joints/flanges), and instruments are only used at intervals, it cannot monitor continuously. Therefore, new methods should be investigated. Traditional instruments used in electrochemical noise (EN) experiments are accurate in finding type and rate of corrosion but are difficult for field applications. Dr. Caines and her team developed a method to detect corrosion under insulation (Caines et al., 2017) using bulk materials, a digital

multimeter (DMM), and recording software. Early results related corrosion rate with potential linearly, but much more research is needed to understand its use with different electrolytes, electrode sizes, and other parameters, to understand if this method can properly quantify/qualify corrosion.

Therefore, this research investigates corrosion and CUI in Newfoundland, a marine harsh environment and investigates real time monitoring using potential noise.

1.2 Objectives

Corrosion processes are complex and have been investigated in numerous environments. However, applying coating or insulation to metal can change corrosion processes and chemical reactions. Corrosion information is necessary to ensure accurate design life of structures and pipelines. This study attempts to answer the following questions with a full-scale pipeline experiment that includes coated, uncoated, and insulated A333 steel pipes.

1. What are the details of pitting and corrosion which occur on coated and insulated pipelines in a marine harsh environment?
2. What are the surface features and corrosion products on coated and insulated pipelines which are present in marine harsh environment?
3. Can EN be used to monitor corrosion type or rate?

Therefore, this research focuses on detailed experimental analysis of corrosion, morphology, and mechanisms in a C5 class marine environment while describing the observed CUI, corrosion under coating, general corrosion, and pitting. Also, monitoring of corrosion using EN is investigated.

The general framework of this research includes setting up specific pipelines in the C5 environment based on design of experiments and then performing specific standards at intervals

discussed in Chapter 3, like, weighting and recording information. Also, XRD and SEM are used to describe the surface morphology in Chapter 4. This research may present results to create/influence corrosion models or information for risk and safety engineers.

1.3 Scope and Limitations

This thesis focuses on steel pipelines in a marine harsh environment and real time monitoring techniques, which can help engineers understand corrosion, and overall risks present for assets in similar environments. Standards may have high conservative or liberal estimates for C5 environment, as such, this study will add to relevant contributions in those areas. The objectives in the previous section guide the scope of this work. CUI is still not well understood, and assets placed in harsh marine environments face uncertainty and challenges. This work focuses on a C5 class site near high water mark in area that was allowed by the University and the Provincial Government and may not be applicable to other C5 sites. Though insulation and coating were used following standards, it may not meet the same as built for industry applications. Finding pitting and corrosion rates close to seashore possibly simulating offshore conditions may not have relevance for more dry environments, or environments far from sea.

For the second part of this research, real time monitoring using EPN was investigated, and sampling rate is important to show different information. The sampling frequency ~1hz is high enough to find corrosion details. Higher rates are better; however, the investigation was for as-simple-as-possible while being able to later work in field and store a smaller amount of data. The system measures at 3points+/sec while at 1hz per electrode.

1.4 Contribution and Novelty

CUI is still a significant issue and there is little information on insulation and coating failures for field tests in literature, especially in a C5 class environment. Therefore, different surface features are investigated throughout this novel experiment which generated corrosion, pitting and morphology data for different pipeline conditions for more than two years. This work provided added information from experimental insights with field data in harsh marine environment which was not available before.

S-EPN method developed by Dr. Susan Caines and her team was new method capable of finding corrosion information but, has only been investigated by the author. It was further investigated while expanding experiment parameters with longer testing times and different conditions to determine its applicability for monitoring corrosion.

1.5 Organization of Thesis

The thesis is written in manuscript format and includes 3 individual papers. Figure 1.1 presents a diagram to show the thesis organization.

Chapter 1 introduces the topics in the thesis and an overview. While there is extensive knowledge of bare metal atmospheric corrosion, corrosion near the sea has not had as much focus until recently, and CUI is still a critical issue causing failures. Also, real time monitoring of assets is best and EN applications should be investigated to detect corrosion.

Chapter 2 presents a literature review of the current knowledge of field tests and knowledge of CUI, coating, and monitoring techniques for corrosion. It was found that corrosion rates are highly variable, and that limited information is available (especially in marine environment) to detail CUI,

corrosion under coating, and design life. Currently, there is no reliable, simple method to monitor corrosion under insulation. This chapter provides the motivation for the research conducted.

Chapter 3 provides new data on corrosion, CUI, and corrosion under coating for pipelines over more than two years of exposure in a C5 marine environment. A version of this chapter was published as a peer-reviewed conference paper in ASME Offshore Mechanics and Arctic Engineering in 2021.

Chapter 4 focused on surface morphology and oxides on corroded pipelines from the in-situ experiment in Chapter 3. One interesting observance was magnetite forming a distance away from the substrate and accelerating corrosion with ferrihydrite in a sea water environment. A version of this chapter was published as a peer-reviewed conference paper in ASME Offshore Mechanics and Arctic Engineering in 2021.

Chapter 5 tested a simplified EN technique using three identical electrodes for corrosion observation. The method required further analysis using frequency (PSD) and/or time-frequency (wavelets) analysis to describe corrosion mechanisms. This paper will be submitted for publication after feedback is received.

Chapter 6 summarizes the findings of the thesis, presents a conclusion, and future work recommendations are provided.

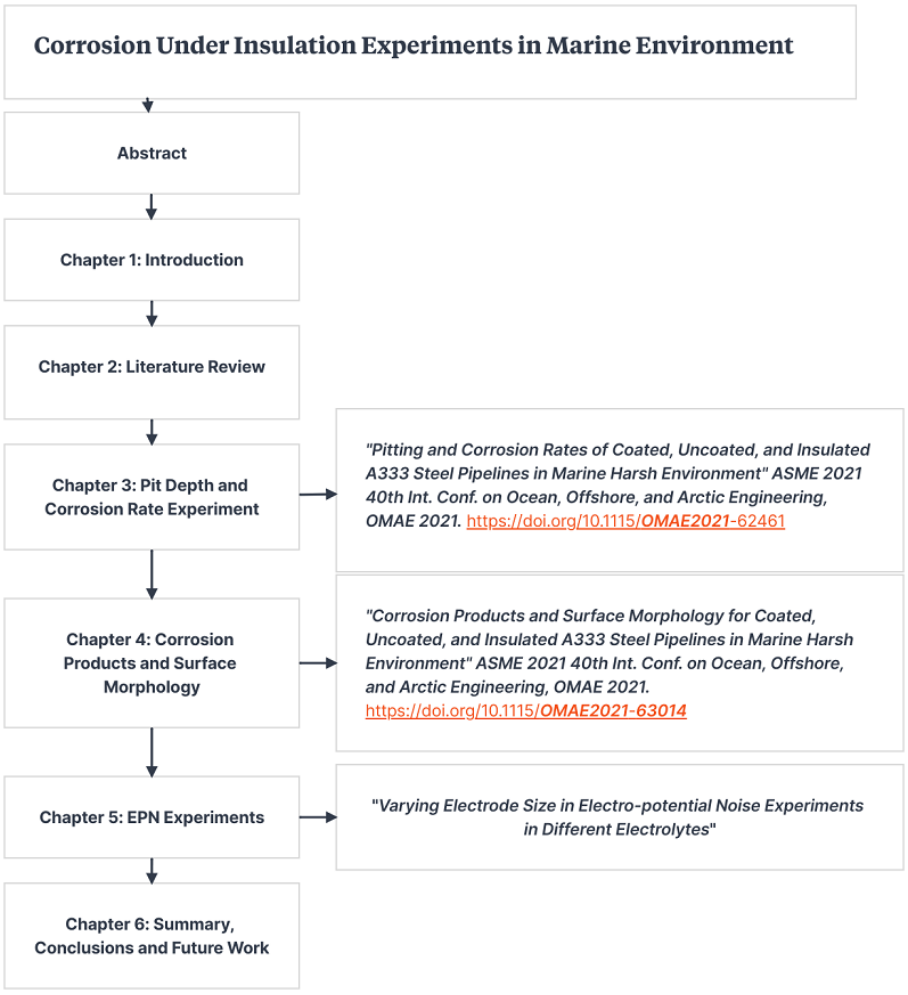

Figure 1.1: Thesis Layout

1.6 Co-authorship Statement

The PhD Candidate, Alan Hillier is the first author of the publication and created all drafts and is the main contributor to this work. Dr. Faisal Khan conceptualized the study, helped analyze the data and gave feedback to revise the manuscript. Dr. Susian Caines conceptualized the study and helped design experiments and setup equipment and provided feedback on the manuscripts.

1.7 References

A Review of Data-Driven Oil and Gas Pipeline Pitting Corrosion Growth Models Applicable for Prognostic and Health Management, 2018. . International journal of prognostics and health management 9.

Alcántara, J., Fuente, D. de la, Chico, B., Simancas, J., Díaz, I., Morcillo, M., 2017. Marine Atmospheric Corrosion of Carbon Steel: A Review. Materials (Basel) 10. https://doi.org/10.3390/ma10040406

ASTM-G50 | Standard Practice for Conducting Atmospheric Corrosion Tests on Metals [WWW Document], 2020. URL https://www.document-center.com/standards/show/ASTM-G50 (accessed 1.1.23).

Atmospheric Corrosion, 2nd Edition | Wiley [WWW Document], 2016. . Wiley.com. URL https://www.wiley.com/en-us/Atmospheric+Corrosion%2C+2nd+Edition-p-9781118762271 (accessed 1.1.23).

Bhandari, J., Khan, F., Abbassi, R., Garaniya, V., Ojeda, R., 2015. Modelling of pitting corrosion in marine and offshore steel structures – A technical review. Journal of loss prevention in the process industries 37, 39–62. https://doi.org/10.1016/j.jlp.2015.06.008

Caines, S., Khan, F., Shirokoff, J., Qiu, W., 2015. Experimental design to study corrosion under insulation in harsh marine environments. Journal of Loss Prevention in the Process Industries 33, 39–51. https://doi.org/10.1016/j.jlp.2014.10.014

Caines, S., Khan, F., Zhang, Y., Shirokoff, J., 2017. Simplified electrochemical potential noise method to predict corrosion and corrosion rate. Journal of Loss Prevention in the Process Industries 47, 72–84. https://doi.org/10.1016/j.jlp.2017.02.023

Corrosion Under Insulation Guidelines - 3rd Edition, 2020.

Eltai, E.O., Musharavati, F., Mahdi, E., 2019. Severity of corrosion under insulation (CUI) to structures and strategies to detect it. Corrosion Reviews 37, 553–564. https://doi.org/10.1515/corrrev-2018-0102

Evans, U.R., 1960. The Corrosion and Oxidation of Metals: Scientific Principles and Practical Applications. Edward Arnold, London.

Graedel, T.E., McGill, R., 2002. Degradation of materials in the atmosphere [WWW Document]. ACS Publications. https://doi.org/10.1021/es00153a003

ISO 8565: 2011, 2011.

Javaherdashti, R., 2014. Corrosion under insulation (CUI): A review of essential knowledge and practice. Journal of Materials Science and Surface Engineering.

Li, S., Hihara, L.H., 2014. Aerosol Salt Particle Deposition on Metals Exposed to Marine Environments: A Study Related to Marine Atmospheric Corrosion. J. Electrochem. Soc. 161, C268. https://doi.org/10.1149/2.071405jes

Melchers, R.E., 2012a. Modeling And Prediction of Long-Term Corrosion of Steel In Marine Environments. International Journal of Offshore and Polar Engineering 22.

Melchers, R.E., 2012b. Long-term corrosion of cast irons and steel in marine and atmospheric environments. Centre for Infrastructure Performance and Reliability, The University of Newcastle, NSW 2308, Australia, Corrosion Science Elsevier.

Molecular Modeling of Corrosion Processes: Scientific Development and Engineering Applications | Wiley [WWW Document], 2015. . Wiley.com. URL https://www.wiley.com/en-

gb/Molecular+Modeling+of+Corrosion+Processes%3A+Scientific+Development+and+Engineering+Applications-p-9781119057642 (accessed 1.1.23).

Morcillo, M., Chico, B., Díaz, I., Cano, H., de la Fuente, D., 2013. Atmospheric corrosion data of weathering steels. A review. Corrosion Science 77, 6–24. https://doi.org/10.1016/j.corsci.2013.08.021

Rozenfeld, I.L., 1972. Atmospheric corrosion of metals. National Association of Corrosion Engineers, Houston, TX.

Waseda, Y., Suzuki, S., Saito, M., 2006. Structural Characterization for a Complex System by Obtaining Middle-Range Ordering, in: Waseda, Y., Suzuki, S. (Eds.), Characterization of Corrosion Products on Steel Surfaces. Springer, Berlin, Heidelberg, pp. 77–104. https://doi.org/10.1007/978-3-540-35178-8_5

Winnik, S. (Ed.), 2016. 4 - The risk-based inspection methodology for CUI, in: Corrosion-Under-Insulation (CUI) Guidelines (Second Edition), European Federation of Corrosion (EFC) Series. Woodhead Publishing, pp. 17–42. https://doi.org/10.1016/B978-0-08-100714-3.00004-4

CHAPTER 2 – Background and Current Knowledge of Field Tests, Standards, and EPN

2.1 Introduction

In this chapter, literature was surveyed to determine current knowledge on CUI and field tests. An overview of CUI and coating standards are discussed. An overview of EN and applications regarding corrosion monitoring are presented. Other detailed historical field tests are presented in Chapter 3, while some historical applications of EN are detailed in Chapter 4.

2.1.1 CUI and Field Tests Overview

Corrosion mechanisms for steels in atmosphere are well documented (Melchers, 2005) but the effects and corrosion rates under insulation and coatings are not. Melchers mentioned many focused-on laboratory experiments and that there was a lack of field experiments. Also, others mentioned that some results of corrosion experiments differ from field exposed (Alcántara et al., 2017). It is very challenging to accurately simulate environmental corrosion due to the need to replicate much of natural environments (Wu et al., 2019). Therefore, an in-situ test can capture the most realistic corrosion information.

Some recent field test include an 8 year test (Lins et al., 2018) performed an 8 year field test in marine atmosphere using high resistant steels (also called weathering steels containing Ni, Cu, Si, Cr, etc.) near Rio de Janeiro State (classified as C4) and a 2-year nickel-steel test in Maldives (Jia et al., 2020). Both used coupons on racks. No recent CUI testing in field was found in literature.

(Khan et al., 2015) criticized API 581 as lacking quality to determine design life of assets under insulation. In reviewing CUI data available, (Caines et al., 2015) noted no data existed outside of laboratory accelerated testing. There is also a lack of consensus on localized corrosion models

(Caines et al., 2013) let alone CUI models. Even in (ASM International, 2015), few corrosion rates are presented even though breaks in coating, and mitigation strategies are often mentioned and discussed. Accurate corrosion and pitting rates are necessary for design life and models. Therefore, because information about CUI rates, insulation, and coating is rare, an experiment to investigate should be performed. Some other specific details of past field and accelerated experiments are presented in Chapter 3.

2.1.2 Standards of Pipeline Insulation and Coating:

Standards present guidance to estimate corrosion rates under insulation and include information on how to prevent and combat corrosion after initial attack. Also discussed are examples of what type of coating are required in different environments, and issues related to insulation. As mentioned previously limited CUI data is available, and most is limited to standards below:

- API RP 581 (2008), Risk-based inspection technology.
- API 583 (2014), Corrosion under insulation and fireproofing
- ASTM Standard G189, A. (2007), Laboratory Simulation of Corrosion Under Insulation
- Armacell CUI Technical paper 2019
- CINI Manual, 2018
- NACE SP0198 (2016), Control of Corrosion Under Thermal Insulation and Fireproofing Materials
- ASM Handbook 5b, Organic Coatings
- CUI Guidelines: Technical Guide for Managing CUI (2020)

To mitigate CUI, strategies must be developed that involve corrosion control, inspection, non-destructive evaluations, maintenance, and other means which control risk. These are a part of a broader risk-based inspection program detailed in API 581, CINI Manual 2018, and others. NACE

SP0198 describes methods for non-destructive planning and maintenance to prevent and treat CUI. Regarding coating and insulation recommendations for specific environments (and the break in protection which can occur), details are provided in ASM Handbook 5b, and Armacell CUI Technical Paper 2019.

One issue present is that corrosion rates presented in literature often have large variations for similar conditions. For example, in ASTM G189 and NACE SP0198 severe field CUI data is ~1mm/yr while ("API RP 581," 2008) gives corrosion for severe environments at 0.254mm/yr and (*Metals Handbook,* 1987) provides marine atmosphere rates 0.025 to 0.79mm/yr. Corrosion rates for marine environments are highly variable and rare, and as such may be unique to each geographical location and weather condition. Models require the input of corrosion data, and it is scarce and in cases of CUI based on accelerated testing, thus a field experiment is the appropriate way forward.

Protections like insulation and coating are required to ensure design life, but little information is available on how often they fail. Instead, most published literature is about post failure analysis and an estimate of what had occurred years prior (Geary, 2013; Geary and Parrott, 2016; Yang et al., 2017). Where failures did not take place, very little, or no information is presented. Pipeline coating is a crucial last line of defense, and little is discussed about investigations conducted where total failure did not occur. Failure analysis in these reports is not concerned where the pipe did not fail, even though it would greatly aid engineers in design life and other risk areas. Similarly, coating breaks down with age and weather conditions ("Armacell USA," 2018), but information is highly varied about its initial protective life (5-13 years). For these reasons, insulation and coating should be investigated in a field experiment presenting details on failures of surface protections.

2.1.3 Experiments involving CUI Literature Review outcome:

The review of CUI found that there is no consensus to assess CUI rates or corrosion under coating. Limited field tests data and industry failure data exist to currently provide this information. Guidance provided is usually based on laboratory accelerated experiments and may not be applicable to field. The high variability in the available corrosion, pitting, and CUI rates in literature may also be due to different short term laboratory tests.

While some guidance on CUI and coating in standards exist, the most practical way forward is a full-scale field test. A thorough review of current unknown information about field tests is found detailed Chapter 3.

2.1.4 Electrochemical Noise Literature Overview

Electrochemical noise (EN) describes fluctuations in potential and current on metal surfaces which occur in the presence of electrolyte. Instruments record passively, without the application of current or potential. It doesn't disturb the surface processes or influence corrosion. In 1968 when Iverson (Iverson, 1968) showed unique potential fluctuations occur on corroding surfaces. Later others (Hladky and Dawson, 1981) found that crevice and pitting corrosion produced "noise signatures" which could be detected. As time progressed standard methodologies like ASTM G199 ("Guide for Electrochemical Noise Measurement"), patents involving specific ranges of readings (*Patent*, 1992), and experiments involving time (Loto, 2018; Shahidi et al., 2012) and frequency (Acosta et al., 2014; Yi et al., 2018) domain and have shown it as a powerful technique to investigate corrosion. Recent reviews on EN applications and procedures were done by Obot (Obot et al., 2019) and Xia (Xia et al., 2020). The only way currently to confirm CUI is to remove the insulation and physically inspect the pipe, and because risk-based asset integrity surveys require current knowledge about assets, using real time monitoring process like EN may be ideal.

For most EN procedures, potential or current is recorded from working and a reference electrode (or two electrodes of the same material) and afterwards other analysis performed to learn what events may be occurring (Mahjani et al., 2014). Time domain statistical analysis (skew, kurtosis, and others), frequency domain (power spectra density (PSD) plots from Fourier transforms), and wavelets analysis (time-frequency analysis) are useful to interpret raw information from a recorded time series. Dr. Susan Caines (Caines et al., 2017) developed a simplified method to measure potential area in a time series and then related it to corrosion rate using simple equipment, it was called Simplified-EPN (S-EPN). This was not found in literature and so this method should be further investigated with longer testing and different parameters.

Researchers have recommended varying electrode area (Pistorius, 1997) while recording EN. Electrode area has an inverse effect on potential readings with larger electrodes generating smaller potential (Cottis, 2001). In one case researchers varied electrode area and found more details when compared to symmetrical electrodes (Shahidi et al., 2012). Larger areas may reduce standard deviation due to increase in capacitance and area for the cathodic reaction (Ma et al., 2017). It is rare in literature and should be further investigated. Therefore, new experiments modifying electrode size using simplified EPN methodology may present new information not found in literature. More specific experimental details and analysis are found in Chapter 5.

2.1.5 Electrochemical Noise Literature Review Outcome

S-EPN was found to be a new technique for monitoring CUI with standard materials and equipment. This research attempts to answer the if simplified EPN can provide information on corrosion rate, and any differences with varied electrode area.

2.2 Motivation

The motivation of this research comes from knowledge gaps found in the literature review:

1. Field tests are rare in marine environment.
2. Knowledge of CUI and corrosion under coating is limited.
3. Life of insulation and coating is rarely discussed.
4. Corrosion rates present in literature for similar environments are highly varied.
5. Extreme marine environment (C5) in Newfoundland may have different corrosion mechanisms and rates that have not been discussed elsewhere.
6. Currently no system exists that is simple, direct, and reliable to monitor corrosion for assets under insulation.

Because of the knowledge gaps present, a full-scale field test is required to be placed in a marine environment and will provide information on CUI and corrosion under coating. Life of the insulation and coating will be studied and compared to current literature. Surface morphology and products from environment will be completed and compared to other C5 sites. Also, real time monitoring will be investigated using EPN. In Figure 2.1 a general overview of the work to be completed from the Motivation.

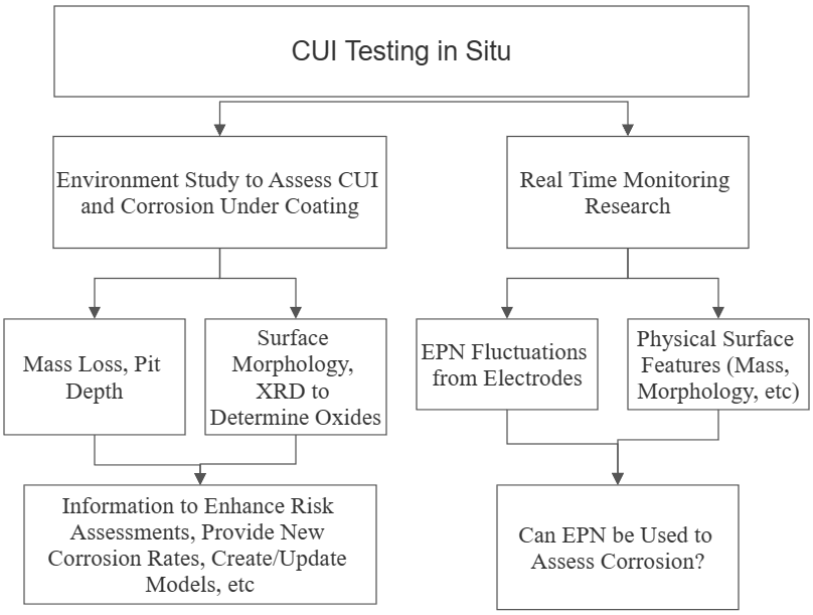

Figure 2.1: Work to be completed from the Motivation.

2.3 References

Acosta, G., Veleva, L., López, J., 2014. Power Spectral Density Analysis of the Corrosion Potential Fluctuation of Stainless Steel 316L in Early Stages of Exposure to Caribbean Sea Water. International journal of electrochemical science 9, 6464–6474.

Alcántara, J., Fuente, D. de la, Chico, B., Simancas, J., Díaz, I., Morcillo, M., 2017. Marine Atmospheric Corrosion of Carbon Steel: A Review. Materials (Basel) 10. https://doi.org/10.3390/ma10040406

Armacell USA [WWW Document], 2018. URL http://www.armacell.us/home/

ASM International, 2015. Corrosion in the Petrochemical Industry, Second Edition. A S M International, Materials Park, UNITED STATES.

Caines, S., Khan, F., Shirokoff, J., 2013. Analysis of pitting corrosion on steel under insulation in marine environments. Journal of Loss Prevention in the Process Industries 26, 1466–1483. https://doi.org/10.1016/j.jlp.2013.09.010

Caines, S., Khan, F., Shirokoff, J., Qiu, W., 2015. Experimental design to study corrosion under insulation in harsh marine environments. Journal of Loss Prevention in the Process Industries 33, 39–51. https://doi.org/10.1016/j.jlp.2014.10.014

Caines, S., Khan, F., Zhang, Y., Shirokoff, J., 2017. Simplified electrochemical potential noise method to predict corrosion and corrosion rate. Journal of Loss Prevention in the Process Industries 47, 72–84. https://doi.org/10.1016/j.jlp.2017.02.023

Cottis, R.A., 2001. Interpretation of Electrochemical Noise Data. CORROSION 57, 265–285. https://doi.org/10.5006/1.3290350

Geary, W., 2013. Analysis of a corrosion under insulation failure in a carbon steel refinery hydrocarbon line. Case Studies in Engineering Failure Analysis 1, 249–256. https://doi.org/10.1016/j.csefa.2013.09.001

Geary, W., Parrott, R., 2016. Two corrosion under insulation failure case studies. Loss Prevention Bulletin 2–6.

Hladky, K., Dawson, J.L., 1981. The measurement of localized corrosion using electrochemical noise. Corrosion Science 21, 317–322. https://doi.org/10.1016/0010-938X(81)90006-8

Iverson, W.P., 1968. Transient Voltage Changes Produced in Corroding Metals and Alloys. J. Electrochem. Soc. 115, 617. https://doi.org/10.1149/1.2411362

Khan, M., Mokhtar, A., Hussin, H., 2015. A Neural Based Fuzzy Logic Model to Determine Corrosion Rate for Carbon Steel Subject to Corrosion under Insulation. Applied Mechanics and Materials 789–790, 526–530. https://doi.org/10.4028/www.scientific.net/AMM.789-790.526

Loto, C.A., 2018. Electrochemical noise evaluation and data statistical analysis of stressed aluminium alloy in NaCl solution. Alexandria Engineering Journal 57, 1313–1321. https://doi.org/10.1016/j.aej.2017.05.009

Ma, C., Song, S., Gao, Z., Wang, J., Hu, W., Behnamian, Y., Xia, D.-H., 2017. Electrochemical noise monitoring of the atmospheric corrosion of steels: identifying corrosion form using wavelet analysis. Corrosion Engineering, Science and Technology 52, 432–440. https://doi.org/10.1080/1478422X.2017.1320117

Mahjani, M.G., Moshrefi, R., Jafarian, M., Neshati, J., 2014. Detecting pitting corrosion and its severity using wavelet entropy in electrochemical noise measurement. Physical Chemistry Research 2, 116–122. https://doi.org/10.22036/pcr.2014.4561

Melchers, R.E., 2005. The effect of corrosion on the structural reliability of steel offshore structures. Corrosion Science, International Symposium on Corrosion and Protection of Marine Structures—in memory of the late Professor Toshihei Misawa 47, 2391–2410. https://doi.org/10.1016/j.corsci.2005.04.004

Metals Handbook, Ninth Edition: Volume 13 - Corrosion, 1987. . ASM International Handbook Commitee, Metals Park, Oh.

Obot, I.B., Onyeachu, I.B., Zeino, A., Umoren, S.A., 2019. Electrochemical noise (EN) technique: review of recent practical applications to corrosion electrochemistry research. Journal of Adhesion Science and Technology 33, 1453–1496. https://doi.org/10.1080/01694243.2019.1587224

Official Gazette of the United States Patent and Trademark Office: Patents, 1992. . U.S. Department of Commerce, Patent and Trademark Office.

Pistorius, P.C., 1997. Design Aspects of Electrochemical Noise Measurements for Uncoated Metals: Electrode Size and Sampling Rate. CORROSION 53, 273–283. https://doi.org/10.5006/1.3280468

Risk-Based Inspection Technology, 2008.

Shahidi, M., Jafari, A.H., Hosseini, S., 2012. Comparison of Symmetrical and Asymmetrical Cells by Statistical and Wavelet Analysis of Electrochemical Noise Data. Corrosion -Houston Tx- 68. https://doi.org/10.5006/0626

Standard Guide for Electrochemical Noise Measurement [WWW Document], n.d. URL https://www.astm.org/g0199-09r20e01.html (accessed 10.17.22).

Wu, H., Lei, H., Chen, Y.F., Qiao, J., 2019. Comparison on corrosion behaviour and mechanical properties of structural steel exposed between urban industrial atmosphere and laboratory

simulated environment. Construction and Building Materials 211, 228–243. https://doi.org/10.1016/j.conbuildmat.2019.03.207

Xia, D.-H., Song, S., Behnamian, Y., Hu, W., Cheng, Y.F., Luo, J.-L., Huet, F., 2020. Review—Electrochemical Noise Applied in Corrosion Science: Theoretical and Mathematical Models towards Quantitative Analysis. Journal of The Electrochemical Society 167, 081507. https://doi.org/10.1149/1945-7111/ab8de3

Yang, Y., Khan, F., Thodi, P., Abbassi, R., 2017. Corrosion induced failure analysis of subsea pipelines. Reliability Engineering & System Safety 159, 214–222. https://doi.org/10.1016/j.ress.2016.11.014

Yi, C., Du, X., Yang, Y., Zhu, B., Zhang, Z., 2018. Correlation between the corrosion rate and electrochemical noise energy of copper in chloride electrolyte. RSC Adv. 8, 19208–19212. https://doi.org/10.1039/C8RA01203B

CHAPTER 3 – Coated, Uncoated, and Insulated Pipelines, A Field Test in Argentia, NL, Canada

3.1 Preface

A version of this paper was published in ASME 2021 40th International Conference on Ocean, Offshore and Arctic Engineering. Edits for clarity and updated references were added compared to previously published. The primary author is Alan Hillier and the co-authors for this manuscript include Dr. Faisal Khan and Dr. Susan Caines. The primary author completed literature review, setup experiment and performed test, lab analysis, and prepared the draft manuscript. Dr. Faisal Khan helped in developing concept, testing protocol, and provided feedback. Dr. Susan Caines developed the concept of experiment, provided feedback, and helped in tests and collecting data. Link: https://doi.org/10.1115/OMAE2021-62461

3.2 Abstract

Pipelines are a safe means of transporting useful materials, and their design life depends on protection mechanisms. Marine environments increase corrosion rate due to moisture, and elements like chloride which increase localized pitting. Thirty-six A333 low temperature carbon steel pipelines were placed at Argentia, NL, a C5 class environment. The experiment consisted of coated, uncoated, and insulated pipes that were exposed for more than two years. Corrosion rate, optical inspections, and pit depth were recorded at intervals. The highest average pit and maximum pit depth occurred in uncoated insulated pipes and coated uninsulated pipes. The highest average mass loss occurred in uncoated (insulated and uninsulated) pipes. The least mass loss and pit depths generally occurred in coated pipes (both insulated and uninsulated). Corrosion near the ends of the

pipes were more significant than other locations. Final averaged corrosion rates for insulated coated and uncoated pipes, were 0.017 and 0.021mm/yr respectively. Corrosion rates for uninsulated coated and uncoated pipes, were 0.014mm/yr and 0.023mm/yr respectively. Maximum and mean pit depths for insulated coated and uncoated pipes were, 180/156 and 271/207 microns, respectively, while for uninsulated coated and uncoated were 210/177 and 199/156 microns, respectively. Some coated and uncoated insulated pipes had negligible pitting and corrosion. Results provide an increased understanding of corrosion under insulation and under coating, and pitting data for pipelines in service in marine harsh environments.

3.3 Introduction

Pipelines are one of the most economical and safe means of transporting products in the petroleum industries, and their design life depends on protection mechanisms for the pipeline (Guo et al., 2014). External protections like insulation and coatings can fail. Though insulation can protect products within a pipeline from temperature fluctuations and outside environments, water ingress can cause catastrophic localized corrosion of carbon steel (Geary, 2013). Corrosion under insulation (CUI) is one of the costliest problems facing the oil and gas industry (Wilds, 2017). It was said 36% of pipelines failed due to external corrosion damage (Yang et al., 2017) and external corrosion is a primary factor in failure (Palmer and King, 2004).

The use of coatings on pipelines under insulation limit CUI, however quantitative values were not given (Geary and Parrott, 2016) and despite some case studies on pipeline failure due to external corrosion (Geary, 2013; Geary and Parrott, 2016; van Oostendorp et al., 2007) information is scarce and varied.

As CUI is difficult to detect (Caines et al., 2015) it is advantageous to pursue experimental research to improve our understanding of CUI and corrosion under coating is still limited compared to other areas of corrosion knowledge (like uncoated steels in atmospheric tests (Melchers, 2005)) (Caines et al., 2013). This is especially true in harsh marine environments. Asset management requires strict design of strength and integrity. Therefore, having information about how coated and insulated pipelines react in marine environments is advantageous.

(ASM International, 2015) contained only one example of corrosion rate for a coupon exposed to vapor, despite numerous discussions of coating, insulation, and inspection standards. CUI is mentioned several times yet no rates or how to estimate corrosion with coatings are presented. In ("API RP 581," 2008) severe environment CR are presented as 0.254mm/yr with guidance for CUI estimation. Therefore, information about coated and insulated metals is lacking.

(*Metals Handbook,* 1987) provides estimate for marine atmosphere from 0.025 to 0.79mm/yr. While other marine atmosphere include 0 to 0.3mm/yr and 0.1mm/yr near coaster zones in Japan (Zen, 2005). (Wall and Wadso, 2013) mentioned US Army Corps estimated marine corrosion rates from 0.05 to 0.25 mm/y but said the data was outdated. (Chico et al., 2017) used three international databases from global corrosion programs where marine sites had a range of 0.08 to 0.4mm/yr. (Lins et al., 2018) performed an 8 year field test in marine atmosphere using high resistant steels (also called weathering steels containing Ni, Cu, Si, Cr, etc.) near Rio de Janeiro State (classified as C4) and CRs were from 0.04 to 0.0125mm/year and generally decreased each year. Low carbon steel was also recorded, and its corrosion rate increased with time.

Marine atmosphere CRs are highly varied and different for each region. There is little mention of CRs in standards for coated/insulated pipes in marine environments, therefore, a physical experiment should be performed.

3.3.1 Review of Field Tests and Case Studies

In 1985 ASTM published Corrosion of Metals Under Thermal Insulation, a large volume of papers concerning CUI. (Ashbaugh and Laundrie, 1985) did an experiment near a cooling tower of a chemical plant to evaluate different CUI setups on pipes. It was mentioned that virtually no quantitative data existed about CUI. Long carbon steel pipes were placed on an atmospheric corrosion rack and sections of pipe had different insulation types. After 3 months some insulation was removed, and no corrosion was found. Afterwards testers injected water twice per week when it did not rain, accelerating the test. The water injection sites had nearly the same corrosion as the bare exposed steel. On pipes where ¼ of the surface was painted longitudinally using epoxy-phenolite, corrosion was nil. For insulated samples, the most severe location for corrosion was on the edge of the pipe. It was hypothesized that it had access to both water and oxygen easily. In conclusion: time of wetness, type of insulation and coating (epoxy-phonolite paint) had the most effect on CUI. Corrosion rates after the one-year exposure to test conditions were 0.23 to 1.57 mm/y.

(Geary and Parrott, 2016) discussed two failures from industry for CUI, one an offshore platform pipeline, and another a chlorine gas pipeline. Corrosion rates of CUI were mentioned as between 0.2 and 0.9mm/year. In both accidents it was noted that the pipes were coated but lost the protection and insulation. It was assumed that they offered protection to some extent, but it was not known how much and even the best coating will not prevent CUI (Geary, 2013). It was unknown how much the coating or insulation ironically contributed to the high corrosion rate.

A review by (Caines et al., 2013) found there were no long-term marine environment CUI tests outside of laboratory and that there was no model available specifically for marine environment CUI.

3.3.2 Coating Protection and CUI

When insulation or coating fail, how does this effect long term failure? In one recent explosion from a refinery pipeline, corrosion rates (CRs) between 0.5 and 0.9 mm/y (Geary, 2013) were estimated. The coating/epoxy/paint was assumed to have lasted for 5 years after insulation break, while this may, or not be the case, little evidence was found in literature about the effects of corrosion involving paint/epoxy protection and accepted life of coating is between 5-13 years (Fitzgerald and Winnik, 2005). (Long and Crawley, 1985) reported pitting for CUI in a ten-year-old chemical plant operating near the Gulf Coast that was then between 0.5 and 2mm. It occurred where aluminum jacketed insulation was visibly corroded, and water ingress was the likely. While it is known that external protections like insulation and coating are required to ensure design life little information is available. While ASTM G189 and NACE SP0198 worst-case field reported CUI data is ~1mm/yr though few other details are available.

In an accelerated test for CUI and coating, (Haraldsen, 2010) used pipelines with multiple flanges along the line with high temperature steam inside and flowing seawater outside. Pipelines had some corrosion before testing and were cleaned, and then coated, and different insulation applied. After only two months accelerated testing was stopped and most flanges were in near failed condition. Lab-accelerated testing was so harsh that the results for coatings and insulation were hard to interpret but, phenolic Norsok Type 7 ("NORSOK M501 ed. 6," 2013) was excellent even with different insulation types. (Abavarathna et al., 2015) used an ASTM G189-07 setup for three days to test corrosion coatings, then extrapolated corrosion rates per year with polarization resistance data. (Bai et al., 2017) also used the same standard for a corrosion cell to test aluminum coatings on steel pipe under insulation. (Caines et al., 2017) again used a similar setup with a new electrochemical potential noise method to prove that corrosion increases under insulation with

water ingress. (Melchers, 2005) mentions that remaining life is influenced by the loss of thickness via pitting corrosion, and so it is critical to find areas where protection (like coating) is no longer effective.

Thankfully, process safety incidents have been decreasing for the last several years, partly because of auditing programs focused on asset integrity and especially CUI inspection and repair (Morey, 2018). However, due to limited data on pipelines in harsh marine environments, coating protection, and pitting rates, further field tests are necessary. Despite CUI being a relatively basic problem (water/electrolyte under insulation on a steel pipe) very few studies are published with field data since 1985 and CRs and pit depths mentioned are very scarce.

This research is presented as an early effort to help understand and quantify uncertainties involved in CUI in harsh marine environment.

3.3.3 Materials and Methods

In this section the materials and methods for the experiment are described. First the location, then the pipeline materials chosen, then inspection schedule, and then the insulation and coating type are described. The equation for calculation of CR is also presented in this section. This section provides the start of the experiment and the time frame.

Argentia, NL is a small commercial seaport on the southwest coast of the Avalon Peninsula of Newfoundland and Labrador, Canada. Exposed to high winds and precipitation throughout the year (135 rainy days, in top six rainiest towns in Canada), the site was approximately 30m from high tide mark to witness the effects of simulated topside marine conditions, and often experiences high humidity, having similar conditions of being offshore, and being further away from the sea would reduce the ocean spray exposure. It is known that salt/chloride in marine atmosphere have direct relation to corrosion rate (*Metals Handbook,* 1987) and time of wetness plays an important

role where electrochemical processes take place (Shifler, 2005). The site is classified as extremely severe corrosion (C5) based on (Revie, 2002).

ASTM A333 low temperature carbon steel is used for transporting high pressure liquids, gasses, and fluids from refineries, and oil and gas sites where toughness is needed at very low temperatures (Brady et al., 2002). It has a high strength to weight ratio, good corrosion resistance, and ductile. Detailed product analysis from manufacturer shown in Table 3.2.

After finding the location and the material for the experiment then the surface protections were applied to the pipes before being placed in environment. The experiment consisted of four different types of surface protections for the pipelines as shown in Figure 3.2 showing bare metal (insulated and not) and coated (insulated and not). Of these four types of protections, two different lengths of pipelines were used. 24 pipes were constructed of three sections of 6in length pipe (with a dielectric plastic divider between), and 12 pipes were constructed with 18in long single pipe, some examples are shown in Figure 3.2 following general design of experiment parameters in (Caines et al., 2015). In total 36 model pipelines were fabricated and followed an inspection schedule first observed at 1 year, and after every 6 months as in Table 3.1. During inspections pipes were dismantled weighted and photographed, and then moved back to field after reassembly. Destructive sampling was taken from randomly selected pipes of each type from second field inspection (at 1.5 years and 2 years) and continued to end of experiment to find corrosion rate and pit depth (ASTM G46, G1, and NACE RP0775). The overview of the data recording procedure is described in Figure 3.1 and is related to Figure 2.1. Corrosion rates were calculated using ASTM G1 2003 below. Originally the experiment was planned as 3 years but was cut short due to the provincial government closing the site.

Table 3.1: Inspection schedule, initial time was Sept 2015.

Inspection Schedule for Argentia, NL					
Removal	1	2	3	4	5
Time	+1 Year	+6 months	+6 months	+6 months	+6 months

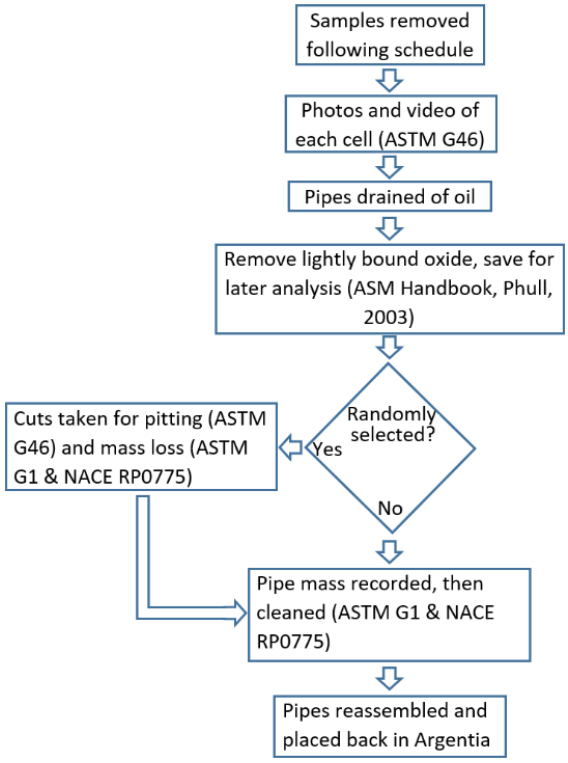

Figure 3.1: Procedure during pipe inspection and cleaning

Table 3.2: Pipeline chemical composition from manufacturer

Hot Rolled Steel Pipe Chemical Composition														
C	Si	Mn	P	S	Ni	Cr	Mo	Cu	Al	V	Nb	Ti	B	Ca
0.16	0.26	0.95	0.013	0.004	0.06	0.11	0.05	0.07	0.02	<0.01	0.01	<0.01	<0.0005	0.0021

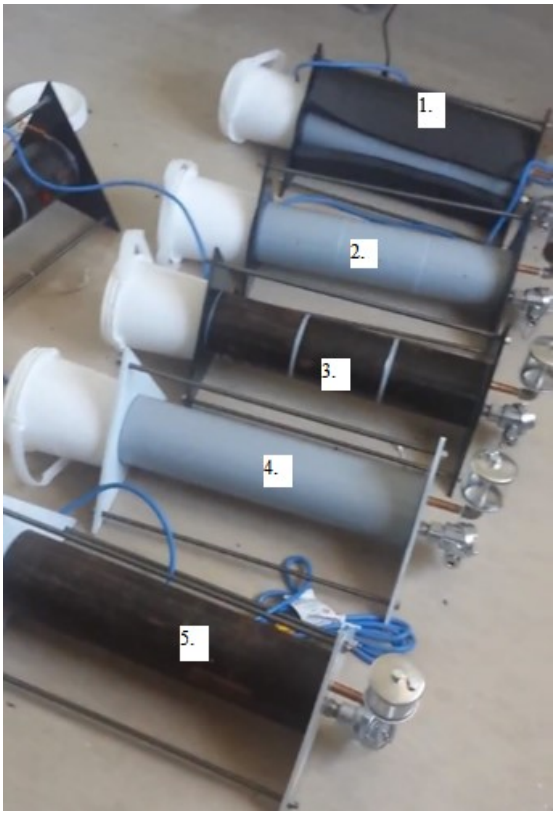

Figure 3.2**:** Four types of pipelines were placed, some pipes including those are shown from top to bottom as: 1. Insulated coated, 2. uninsulated coated, 3. uninsulated uncoated, 4. uninsulated coated, and 5. uninsulated uncoated. Not shown here is insulated uncoated.

Corrosion rate (ASTM G1 2003)

$$CR = \frac{(K \times W)}{(A \times T \times D)} \qquad (1)$$

Where K = constant $8.76 * 10^4$,

T = time of exposure in hours,

A = area of exposed corroding surface in cm^2

W = mass loss in grams

D = density in g/cm^3 (estimated at 7.85)

Armacell ("Armacell USA," 2018) rubber foam 1-inch thick 4.5" diameter was used over the pipes and secured with zip ties and silicone. Following guideline from SPO 198-2010, Norsok number

6C coating was used with one coat epoxy phenolic primer, and one topcoat (each 150µm). Pipes that were not coated were used as received with Rust-preventing Spraying Hard-film Agent (RSH-3A/Lucency with 50% acrylic, 10% phenolic, 20% hydrocarbon solvent, 10% suphonate, 10% miscellaneous) on the surface of pipes.

Figure 3.3: Argentia research site view from experimental setup towards (1) south-east and (2) south-west. Sea is 30m away.

Assembled pipelines were placed on racks approximately 1.5m high, 30m from high water mark, approximately 5-7m above sea level as shown in Figure 3.3. October 2015 pipelines were deployed and exposed to environment until first weighting November 2016.

3.4 Results

In the first scheduled mass recording, 12 samples were removed and studied. Nine six-inch pipes including six uncoated and uninsulated, two coated and insulated, and one coated uninsulated. From 18inch pipes, two uncoated and uninsulated, and one coated insulated were studied. Samples were weighted, and then corrosion products removed from specimens scrapping using nylon brush and ultrasonic cleaning and then reweighted. Visual and lab inspection showed little surface bound oxide and no corrosion on the coated and insulated samples. Negligible mass loss was recorded. Heated diammonium citrate cleaning method (*ASTM G01-03*, 2003) was used for uninsulated pipes 6" to remove corrosion products. Afterward insignificant changes occurred, as shown in Table 3.3. Heated citrate bath was not used further as it was not effective in removing surface corrosion bound products and issues involved with heated acidic baths and large diameter pipe samples. Figure 3.4 shows before and after cleaning.

Table 3.3: November 2016 mass recording. Pipes which were UI: Uninsulated I: Insulated UC: Uncoated C: Coated for first mass recording.

Condition	Number	Position	Fall 2015	Fall 2016	Change
UI UC	2	A	2.345	2.345	0
UI UC	2	B	2.355	2.36	0
UI UC	2	C	2.355	2.36	0
UI UC	4	A	2.34	2.345	0.005
UI UC	4	B	2.355	2.36	0.005
UI UC	4	C	2.35	2.355	-0.005
UI UC	6	A	2.33	2.335	0.005
UI UC	6	B	2.35	2.35	0
UI UC	6	C	2.345	2.345	0
UI UC	8	A	2.335	2.335	-0.005
UI UC	8	B	2.35	2.35	0
UI UC	8	C	2.355	2.35	-0.005
UI UC	10	A	2.33	2.33	0
UI UC	10	B	2.35	2.355	0.005
UI UC	10	C	2.36	2.365	-0.005
UI UC	12	A	2.35	2.355	0.005
UI UC	12	B	2.335	2.33	-0.005
UI UC	12	C	2.35	2.36	0.01
I C	20	A	2.37	2.37	0
I C	20	B	2.38	2.38	0
I C	20	C	2.385	2.39	0.005
I C	22	A	2.38	2.38	0
I C	22	B	2.39	2.39	0
I C	22	C	2.38	2.38	0
UI UC	23	A	2.39	2.39	0
UI UC	23	B	2.37	2.37	0
UI UC	23	C	2.385	2.385	0
UI UC	25	N/A	7.56	7.57	0.01
UI UC	27	N/A	7.475	7.485	0.01
I UC	28	N/A	7.58	7.595	0.015

Figure 3.4: 1.) Pipeline 2, in top left initial condition Fall 2015, 2.) to the immediate right top and 3.) to the second right top Pipe 2 during Fall 2016, 4.) bottom center and 5.) bottom right after cleaning Fall 2016.

The second sampling occurred six months later, one and a half years from first exposure, all samples were inspected, photographed, and weighted. Eight randomly selected pipelines (four from both 18" and 6") had slices removed for analysis of mass loss and pit depth (Figure 1). Cut samples were cleaned in HCL+DBT for mass loss and checked for pits, and then measured using guidelines from (*ASTM G 46*, 1994) with calibrated microscope. Pit measurement was taken across surfaces and the five deepest pits were averaged.

Most pits found were circular and oval shape. Figure 3.9, Figure 3.10, and Figure 3.11 show examples of pits, coating cracks, and corrosion under coating. In Figure 3.11 the reason for the highest pit depths may be due to the lack of accessible oxygen under the coating. Figure 3.5 shows

corrosion under insulation of an uncoated pipe. Mass updates are available in Table 3.4 and pitting and corrosion rates for random samples in Table 3.9 and Table 3.10.

Table 3.4: June 2017 mass data. Pipes not listed (13-24) were same as initial mass. Spring 2017 cut pipes for destructive testing bolded, change in mass was before destructive testing. Mass presented is in kilograms. Scale resolution is 0.005 kg.

Condition	Number	Position	Fall 2015	Spring 2017	Change
UI UC	1	A	2.355	**2.07**	0
UI UC	1	B	2.34	**2.07**	0
UI UC	1	C	2.34	**2.07**	0
UI UC	2	A	2.345	2.34	-0.005
UI UC	2	B	2.355	2.355	0
UI UC	2	C	2.355	2.35	-0.005
UI UC	3	A	2.335	2.335	0
UI UC	3	B	2.335	2.335	0
UI UC	3	C	2.345	2.345	0
UI UC	4	A	2.34	**2.01**	-0.005
UI UC	4	B	2.355	**2.075**	0
UI UC	4	C	2.35	**2.05**	-0.005
UI UC	5	A	2.355	2.355	0
UI UC	5	B	2.35	2.35	0
UI UC	5	C	2.355	2.355	0
UI UC	6	A	2.33	2.33	0
UI UC	6	B	2.35	2.35	0
UI UC	6	C	2.345	2.345	0
UI UC	7	A	2.345	2.35	0.005
UI UC	7	B	2.345	2.35	0.005
UI UC	7	C	2.355	2.355	0
UI UC	8	A	2.335	2.33	-0.005
UI UC	8	B	2.35	2.35	0
UI UC	8	C	2.355	2.35	-0.005

Condition	Number	Position	Fall 2015	Spring 2017	Change
UI UC	9	A	2.34	2.34	0
UI UC	9	B	2.335	2.33	-0.005
UI UC	9	C	2.355	2.36	0.005
UI UC	10	A	2.33	2.33	0
UI UC	10	B	2.35	2.35	0
UI UC	10	C	2.36	2.36	0
UI UC	11	A	2.345	2.345	0
UI UC	11	B	2.345	2.335	-0.01
UI UC	11	C	2.34	2.34	0
UI UC	12	A	2.35	2.345	-0.005
UI UC	12	B	2.335	2.33	-0.005
UI UC	12	C	2.35	2.35	0
UI UC	25	N/A	7.56	7.565	0.005
I UC	26	N/A	7.495	7.495	0
UI UC	27	N/A	7.48	7.48	0
UI UC	28	N/A	7.58	**7.115**	-0.01
I UC	29	N/A	7.545	**6.985**	0
I UC	30	N/A	7.535	7.535	0
I C	31	N/A	7.615	7.61	-0.005
UI C	32	N/A	7.595	7.595	0
I C	33	N/A	7.625	7.625	0
UI C	34	N/A	7.575	**7.21**	0
UI C	35	N/A	7.635	**7.155**	0
I C	36	N/A	7.625	7.625	0

Figure 3.5: I UP pipe 26 June 2017, underwent significant CUI compared to others when inspected. Lightly bound oxide and exfoliation was over the entire surface.

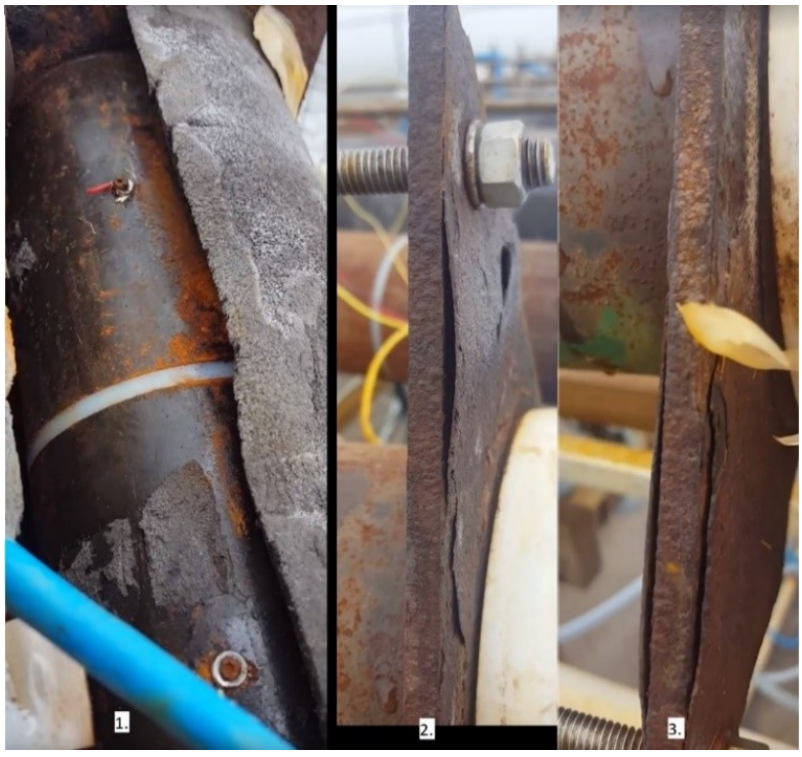

Figure 3.6: 1. One sample opened showing slight corrosion under insulation. 2. & 3. Low carbon steel triangles used for holding pipes together often flaked in large sections as exfoliation.

At the third scheduled removal for pipe inspection the environment research center in Argentia, NL was abruptly closed by government and so it is the last data point available. Final mass recordings, pit information and corrosion rate date are available in the following tables.

Table 3.5: Final weighing of pipelines 1-16 December 2017. Weights in kg, scale resolution 0.005 kg.

Condition	Number	Position	Fall 2015	Dec-17	Change	Condition	Number	Position	Fall 2015	Dec-17	Change
UI UC	1	A	2.355	2.07	0	UI UC	9	A	2.34	2.34	0
UI UC	1	B	2.34	2.07	0	UI UC	9	B	2.335	2.335	0
UI UC	1	C	2.34	2.07	0	UI UC	9	C	2.355	2.36	0.005
UI UC	2	A	2.345	2.345	0	UI UC	10	A	2.33	2.33	0
UI UC	2	B	2.355	2.355	0	UI UC	10	B	2.35	2.35	0
UI UC	2	C	2.355	2.355	0	UI UC	10	C	2.36	2.36	0
UI UC	3	A	2.335	2.34	0.005	UI UC	11	A	2.345	2.345	0
UI UC	3	B	2.335	2.34	0.005	UI UC	11	B	2.345	2.345	0
UI UC	3	C	2.345	2.35	0.005	UI UC	11	C	2.34	2.34	0
UI UC	4	A	2.34	2.015	-0.005	UI UC	12	A	2.35	2.35	0
UI UC	4	B	2.355	2.075	0	UI UC	12	B	2.335	2.33	-0.005
UI UC	4	C	2.35	2.055	-0.005	UI UC	12	C	2.35	2.35	0
UI UC	5	A	2.355	2.355	0	UI UC	13	A	2.375	2.37	-0.005
UI UC	5	B	2.35	2.35	0	I UC	13	B	2.385	2.385	0
UI UC	5	C	2.355	2.355	0	I UC	13	C	2.395	2.395	0
UI UC	6	A	2.33	2.335	0.005	I UC	14	A	2.385	2.385	0
UI UC	6	B	2.35	2.35	0	I UC	14	B	2.37	2.37	0
UI UC	6	C	2.345	2.345	0	I UC	14	C	2.38	2.38	0
UI UC	7	A	2.345	2.35	0.005	I UC	15	A	2.395	2.395	0
UI UC	7	B	2.345	2.35	0.005	I UC	15	B	2.385	2.385	0
UI UC	7	C	2.355	2.36	0.005	I UC	15	C	2.385	2.385	0
UI UC	8	A	2.335	2.33	-0.005	I UC	16	A	2.375	2.375	0
UI UC	8	B	2.35	2.35	0	I UC	16	B	2.39	2.385	-0.005
UI UC	8	C	2.355	2.35	-0.005	I UC	16	C	2.38	2.38	0

Table 3.6: Final weighing of pipelines 17-36 December 2017. Weights in kg, scale resolution 0.005 kg.

Condition	Number	Position	Fall 2015	Dec-17	Change	Condition	Number	Position	Fall 2015	Dec-17	Change
I UC	17	A	2.355	2.07	0	I UC	23	A	2.34	2.34	0
I UC	17	B	2.34	2.07	0	I UC	23	B	2.335	2.33	-0.005
I UC	17	C	2.34	2.07	0	I UC	23	C	2.355	2.36	0.005
I UC	18	A	2.345	2.34	-0.005	I UC	24	A	2.33	2.33	0
I UC	18	B	2.355	2.355	0	I UC	24	B	2.35	2.35	0
I UC	18	C	2.355	2.35	-0.005	I UC	24	C	2.36	2.36	0
I UC	19	A	2.335	2.335	0	UI UC	25	N/A	7.56	7.565	0.005
I UC	19	B	2.335	2.335	0	UI UC	26	N/A	7.495	7.505	0.01
I UC	19	C	2.345	2.345	0	UI UC	27	N/A	7.475	7.48	0.005
I UC	20	A	2.34	2.01	-0.005	UI UC	28	N/A	7.58	7.12	-0.05
I UC	20	B	2.355	2.075	0	UI UC	29	N/A	7.545	6.985	-0.05
I UC	20	C	2.35	2.05	-0.005	UI UC	30	N/A	7.535	7.535	0
I UC	21	A	2.355	2.355	0	UI C	31	N/A	7.615	7.61	-0.005
I UC	21	B	2.35	2.35	0	I C	32	N/A	7.595	7.6	0.005
I UC	21	C	2.355	2.355	0	UI C	33	N/A	7.625	7.625	0
I UC	22	A	2.33	2.33	0	UI C	34	N/A	7.575	7.21	-0.01
I UC	22	B	2.35	2.35	0	I C	35	N/A	7.635	7.635	0
I UC	22	C	2.345	2.345	0	I C	36	N/A	7.625	7.625	0

Table 3.7: Averaged mass loss, pit depth, max pit depth, and CRs for different surfaces of pipes. CR in mm/yr. Pit depth +/- 3% error. CR +/- 0.6% error.

Pipe - 2017 June	Average % Mass Loss	Average Pit Depth (microns)	Max Pit Depth (microns)	CR
Ins. Uncoated	0.47	203	240	0.019
Ins. Coated	0.00	0	0	n/a
Unins. Coated	0.00	0	0	n/a
Unins. Uncoated	0.70	139	165	0.028

Pipe - 2017 Dec	Average % Mass Loss	Average Pit Depth (microns)	Max Pit Depth (microns)	CR
Ins. Uncoated	0.84	207	271	0.023
Ins. Coated	0.62	156	180	0.017
Unins. Coated	0.49	177	210	0.014
Unins. Uncoated	0.72	156	199	0.019

Table 3.8: June and December averaged data, CR in mm/yr. Pit depth +/- 3% error. CR +/- 0.6% error.

June+December	Average % Mass Loss	Average Pit Depth (microns)	Max Pit Depth (microns)	CR
Ins. Uncoated	0.65	205	256	0.021
Ins. Coated	0.62	156	180	0.17
Unins. Coated	0.49	177	210	0.14
Unins. Uncoated	0.71	148	182	0.023

3.5 Discussion

The highest average mass loss and corrosion rates occurred in uninsulated uncoated, and then insulated uncoated pipes as shown in Table 3.7 and Table 3.8. Another representation of these tables is Figure 3.7 and Figure 3.8 The highest average and maximum pit depth were in insulated uncoated pipes. In June 2017 all randomly selected insulated coated and uninsulated coated samples had no corrosion, similar was observed at the 1-year mark of the experiment where some coated and insulated pipes were dissembled. Figure 3.9 and Figure 3.11 show examples of cracks in coating and localized corrosion.

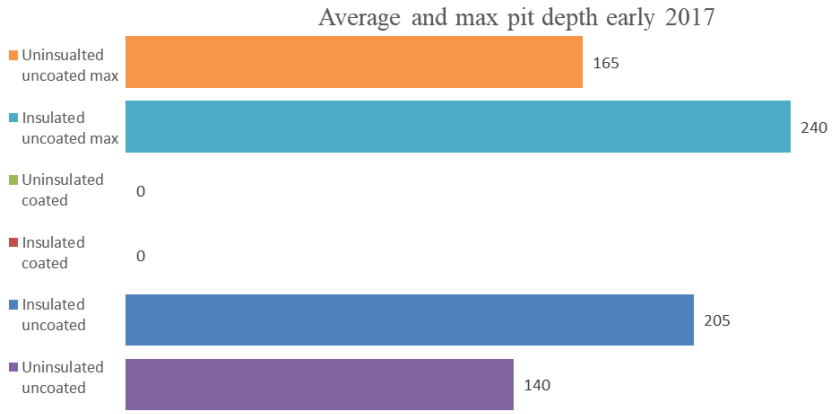

Figure 3.7: Average and max pit depth early 2017. No pitting on insulated and uninsulated coated samples.

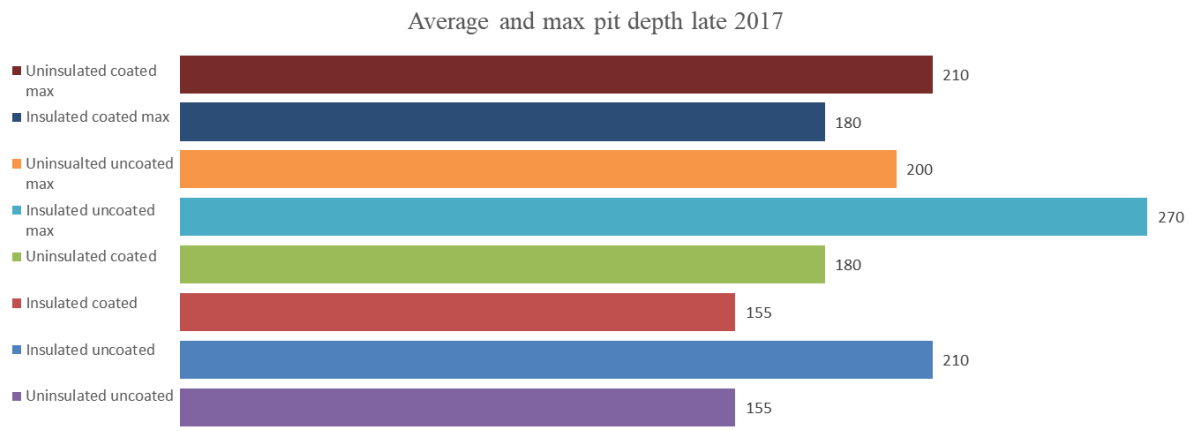

Figure 3.8: Average and max pit depth in late 2017.

Most insulated coated pipes selected during random destructive tests (Pipes 16, 34, 35 June 2017, and 31,32 in Dec 2017) had almost no measurable corrosion, and other insulated and uncoated pipes (Pipe 1 June 2017) had no measurable corrosion present (Table 3.9). When there is no break in coating or insulation protection, corrosion is reduced or is not measurable during this experiment time.

During general mass recordings using a calibrated scale, some pipes gained or lost 0.005kg during experiment, more loss was not observed for ~2.35kg pipes (1-24). The most mass loss from beginning to end of experiment was ~0.05kg (10x scale resolution) for a 7.5kg pipe from pipe 28 and 29 exposed for two years, with a computed corrosion rate of ~0.021mm/yr. Destructive tests also showed a similar CR in Table 3.9 and Table 3.10. It should be mentioned that many pipes did not change values from first placement, though some visual corrosion is present. Also, some pipes measurements were increased by 5 grams (which was the scale resolution) and this may be due to scale error or trapped moisture inside oxides. However, as many smaller destructive tests showed similar CR as calculated from larger pipe weighing, the error present is apparently low. A333 steel

is manufactured and used in corrosive cold environments and for many uncoated pipes the effective mass loss over the experiment was 0.

When coating or insulation fail pitting corrosion proceeds faster and deeper compared to uninsulated and uncoated steel in this experiment. In Figure 3.10 pipe 26 (insulated uncoated) randomly selected during December 2017, had water ingress through insulation with deepest pits measured at near ~0.5mm after two years of exposure to a C5 corrosion environment. In the case of Figure 3.11 pipe 20 (insulated coated) damaged coating had pits measured near ~0.2mm and were similar in size to uncoated uninsulated as shown in Figure 3.10 and Table 3.10.

Table 3.9: June 2017 pit and corrosion rate information. “I” is insulated, and “C” is coated. “X” signifies the surface protection. Pit depth +/- 3% error. CR +/- 0.6% error.

Pipe - June 2017	I	C	Max Pit Depth (microns)	Avg Pit Depth (microns)	Initial Mass (g)	Final Mass (g)	Loss (g)	% Loss	CR
1	x		n/a	n/a	n/a	n/a	n/a	n/a	n/a
3B	x		240	203	39.50	39.39	0.11	0.28	0.010
4A			120	90	26.95	26.79	0.16	0.60	0.023
4A			130	116	28.34	28.15	0.19	0.67	0.026
4B					25.94	25.76	0.18	0.68	0.025
4B			150	126	22.75	22.57	0.18	0.78	0.028
4B					21.04	20.86	0.18	0.86	0.031
8A			180	170	42.96	42.86	0.10	0.24	n/a
13C		x	200	152	34.55	34.43	0.12	0.35	0.015
16	x	x	n/a	n/a	n/a	n/a	n/a	n/a	n/a
23		x	200	190	46.40	46.32	0.08	0.17	n/a
28	x		260	196	20.32	20.21	0.11	0.56	0.013
28	x		220	211	90.28	89.76	0.52	0.57	0.034
29			210	184	45.02	44.55	0.46	1.03	0.050
29			200	150	54.26	53.87	0.38	0.71	0.014
34		x	n/a	n/a	n/a	n/a	n/a	n/a	n/a
35	x	x	n/a	n/a	n/a	n/a	n/a	n/a	n/a

Table 3.10: December 2017 pit and corrosion rate information. CR is mm/yr. “I” is insulated, and “C” is coated. “X” signifies the surface protection. Pit depth +/- 3% error. CR +/- 0.6% error.

Pipe - Dec 2017	I	C	Max Pit Depth (microns)	Avg Pit Depth (microns)	Initial Mass (g)	Final Mass (g)	Loss (g)	% Loss	CR
2A			180	144	16.92	16.81	0.11	0.64	0.018
2B			140	108	34.10	33.95	0.15	0.43	0.010
2B			n/a	n/a	10.35	10.25	0.10	0.96	n/a
4B			200	182	49.80	49.23	0.57	1.15	0.033
7A	x		230	174	39.88	39.61	0.27	0.67	0.019
7C	x		230	174	33.22	32.97	0.25	0.76	0.013
7C	x		180	144	16.92	16.81	0.11	0.64	n/a
12A			240	184	59.08	58.72	0.35	0.59	0.022
13C		x	200	160	31.45	31.26	0.18	0.58	0.017
17C		x	220	193	24.36	24.26	0.10	0.40	0.010
20B	x	x	170	146	60.60	60.44	0.17	0.27	0.010
20B	x	x	190	166	10.35	10.25	0.10	0.96	0.025
26	x		495	304	29.47	29.25	0.22	0.74	0.021
26	x		345	303	90.43	89.77	0.66	0.73	0.023
26	x		250	212	55.21	54.80	0.40	0.73	0.022
26	x		n/a	n/a	37.18	36.63	0.55	1.47	0.041
27			340	246	24.66	24.45	0.21	0.86	0.021
27			145	119	19.52	19.40	0.13	0.65	0.013
28	x		170	140	58.59	58.09	0.50	0.85	0.023
28	x				10.35	10.25	0.10	0.96	0.026
29			150	110	115.25	114.71	0.53	0.46	0.014
31		x	n/a	n/a	n/a	n/a	n/a	n/a	n/a
32	x	x	n/a	n/a	n/a	n/a	n/a	n/a	n/a

The largest pits and corrosion were near the ends of the pipe where crevice corrosion may occur due to low carbon steel holding the pipes together (though physically separated with a dielectric polymer material) as seen in Figure 3.2 and Figure 3.6. Moisture and corrosion accelerators such as chloride may enter near the ends of the pipe more readily near the insulation sealing and this was observed in the field as in Figure 3.10. Also, in Table 3.10, pipe 28 had deeper pits in the first cut than in the second, leading to the same conclusion, along with other authors (Long and Crawley, 1985).

In coated pipe 13 (Figure 3.9) a break in the coating was investigated in random destructive testing. In December 2017, the pits and CR were higher than 6 months previous, for coated pipes corrosion was not as dependent on being close to the ends of the pipes as seen previously in uncoated inspections. Pipe 13 had an area shown in the white circle (Figure 3.11) which was smaller than a dime. When the coating was removed during destructive testing, the corroded area was more than ~10x the exposed original visible area. The deepest pits were in the areas circled in red, away from the aerated surface/coating break. The bottoms of the pipes (4 to 6 on a 12-hour clock location) generally appeared more corroded than the top 10-2pm position and this was similarly noted by other researchers (Ashbaugh and Laundrie, 1985), likely due to lack of sunshine and water runoff plus longer drying time.

Insulated and coated samples' CR and mass loss were lowest. For a process like pitting, when surface protections are working, probability of corrosion is greatly reduced. This was also noted by Geary (2013) when examining failure and assuming from industry knowledge that coatings would have no corrosion for ~5 years. In current results, some coating, as well as insulation failed in less than two years. On average, the highest corrosion rates were observed in insulated uncoated, and then uninsulated uncoated, samples. Coated insulated pipes had protection to the pipeline and observed the lowest CR and pit depths.

Uncoated uninsulated pipes had lower mean and maximum pit depth compared to uncoated insulated and uninsulated coated. This shows A333 steel, with similar properties to weathering steel, endures the environment better when exposed bare to the environment compared to a single protection (i.e., when it has only coating or insulation, not both). When insulation or coating fails, pitting is accelerated. It should be noted that this experiment completed in a little over two years and different results may occur over longer time frames.

3.5.1 Statistical and Calculation Errors

When producing experimental results, a question arises on the reproducibility of results, and the amount of uncertainty in each variable. Percent uncertainties come from size measurement of coupons, field time (and immersion time for Chapter 4 experiments), and mass balance. Using the mean average value of each data set, and the uncertainty of each variable x 100% will provide a basic uncertainty estimate.

For the case of measurement errors in the research the following applies, from the mass scale with resolution 0.01g and a mean weight of coupon as 39.3g would give a 0.025% error. Average measurement error was 0.2mm each way with an average area of 0.00174m^2 would be an error of 0.002%. For the field experiment the time standard deviation was 5 days over the experiment 2.25 years, or 0.6%. Calculating sum of squared errors gives ~+/-0.6% error in the results for corrosion rates. About the pit depth measurements, the average pit depth was 175 microns, but the readings were only accurate to 5 micros from the device, which computes to ~+/- 3% error.

Interestingly, the data also shows that for the 24x3 pipeline sections (~2.5kg) in weighing, and 12 (7.5kg) longer pipes, the highest corrosion rates compare with the highest in the random selection, and similarly for low corrosion. Therefore, though small percent changes in measurement would change results, the similarity of large pipes to random selection (and for similar surface protections) shows that the results are accurate. In the case of the EPN experiments in chapter 4, a 15 min deviation over 12 hours would be 2% and using sum of individual squared errors gives +/- 2%.

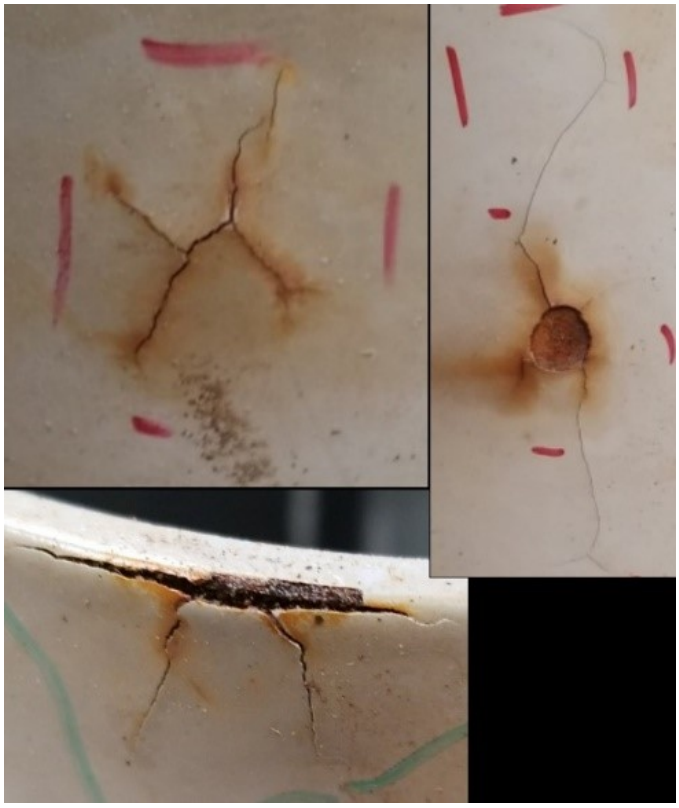

Figure 3.9: Pipe 13, Cracks in coating. Top right further examined in Figure 3.11.

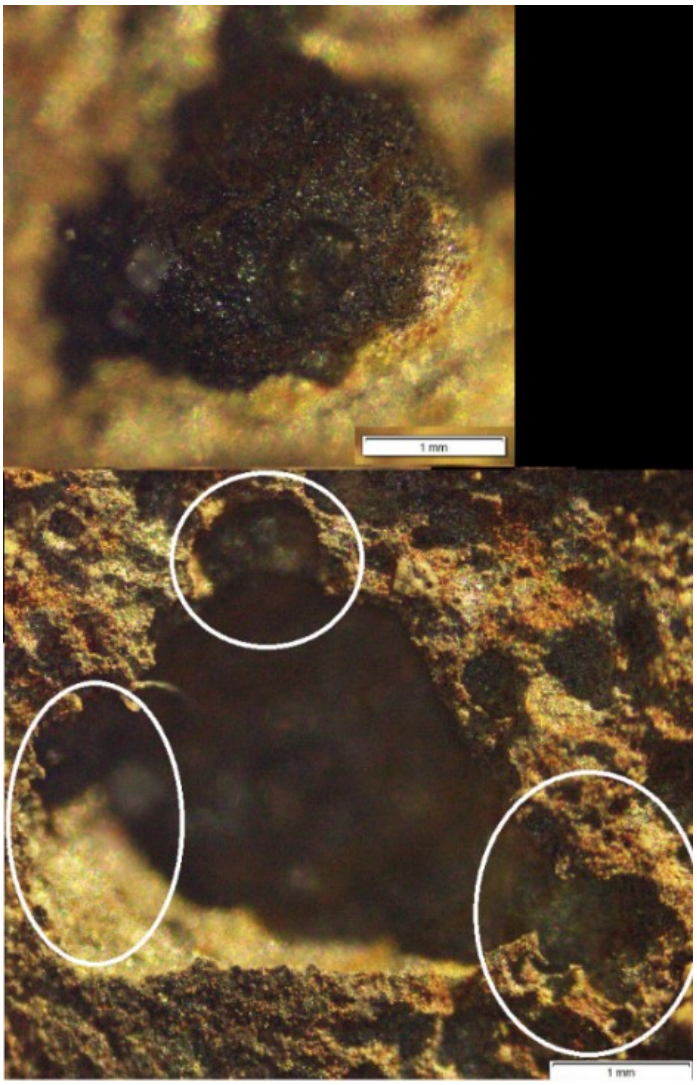

Figure 3.10: One of the largest pits measured from Pipe 26, insulated and uncoated. Scale bar is 1mm. The insulation, which should protect the pipeline became an insulated that did not allow O2 to enter and create protective surface oxides.

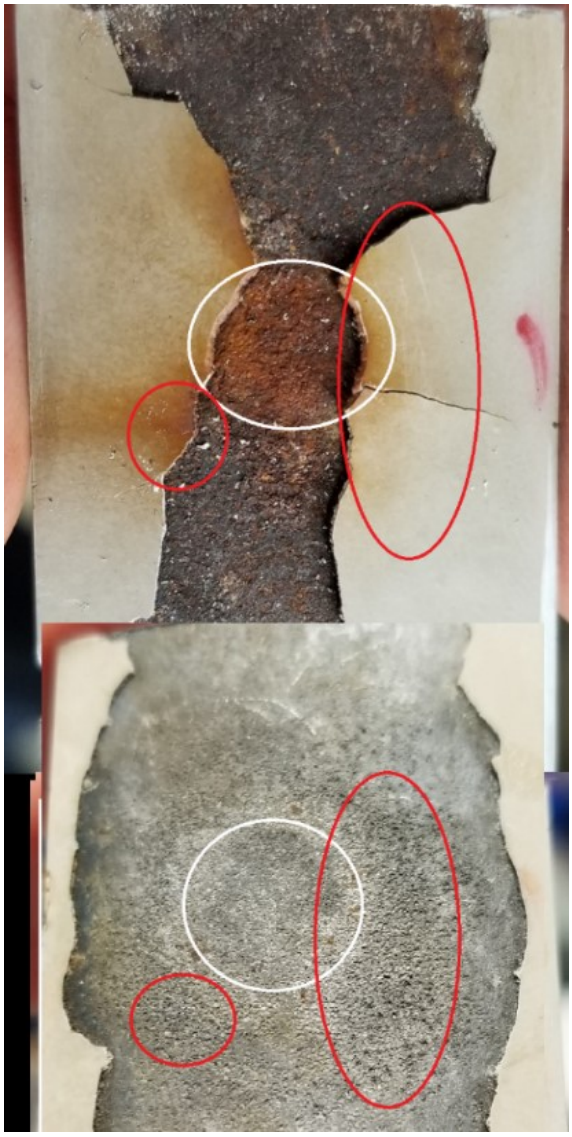

Figure 3.11: Pipe 20 which had one paint section damaged. Red circles were deepest pits. They occurred here perhaps due to the lack of free flow 02, while away from the open surface, and away from the area still protected by coating but no electrolyte ingress.

3.6 Conclusion

The results add new knowledge of CUI, corrosion under coating, and pitting rates not available before using A333 steel (LTCS) in harsh marine environment. This data may allow for new model development, standard updates, and quantification of risks where previously ranked scores were used for harsh environments where CUI could take place (Winnik, 2016).

Differences in mass loss, CR, and pitting were observed in pipelines as coated, insulated, and not, in a harsh marine environment. The corrosion near ends of pipe were most severe, likely due to crevice corrosion, and ingress of corrosion accelerating substances (moisture, chloride). Uninsulated uncoated pipes generally had the highest CRs with 18" and 6" pipe at 0.05mm/yr and 0.031mm/yr respectively as shown in Table 3.9 and Table 3.10, while insulated uncoated CRs were slightly less than uninsulated uncoated, however, insulated uncoated pipes had the deepest pits. Therefore, if pipelines are insulated and will be exposed to moisture an anti-corrosion protective coating should first be applied. Insulated and coated samples' corrosion and pitting rates were lowest of all. Probability of corrosion is very low when insulation and coating do not fail. Deepest pits found in uninsulated coated and insulated uncoated are perhaps due to lack of oxygen, and protection ironically becoming an area for trapped moisture and corrosion accelerated substances. Insulated uncoated has a much higher CR than uninsulated coated, despite both having 1 layer of protection against the outside environment. A large difference between them is that, when coating fails the surface area is small and the hole will be exposed to oxygen in and around the cracked area. The oxides expand, further exposing the metal surface to the air. However, in the case of water ingress under insulation, the water pools in the bottom, does not evaporate, and little new oxygen comes to the surface of metal under the insulation. This gives rise to much of the pipe being covered with electrolyte with reduced oxygen. Localized corrosion was worse on those pipes, and this is observed in Figure 3.8. Average corrosion rates (+/- 0.6%) from destructive tests are in Figure 3.12.

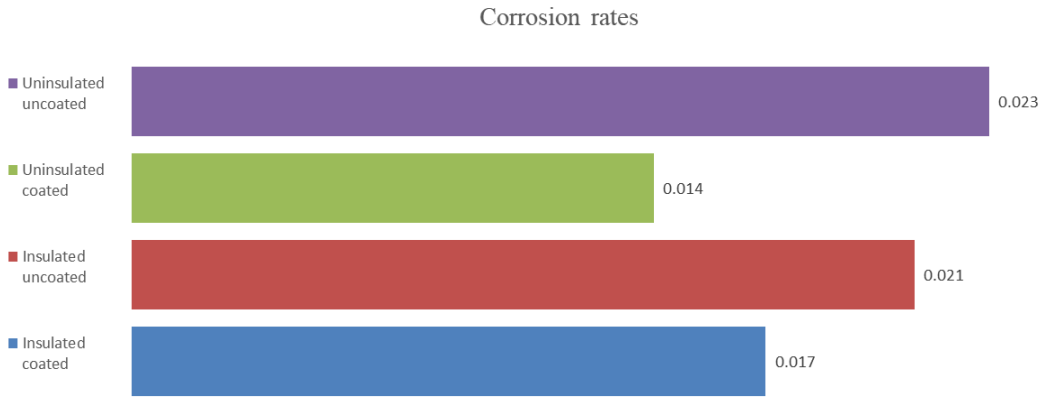

Figure 3.12: Average CRs from destructive tests.

These rates were comparable with other recent researchers (Lins et al., 2018) but were lower than many in Introduction section which may be due to A333 steel having high corrosion resistance properties compared to some steels in standards, overestimating corrosion rates due to extrapolation from lab accelerated results, or few industry failure cases published where CR is high.

3.7 Acknowledgments

The authors appreciate and thank the late Dr. John Shirokoff for his help, talks, measurement of sample sizes, and input throughout this research. Thanks to Dr. Wanda Alyward for her help and use of her lab facilities for XRD, EDS, and SEM imaging.

3.8 References

Abavarathna, D., Ashbaugh, W., Kanev, R., McGowan, N., Heimann, B., 2015. Measurement of corrosion under insulation and effectiveness of protective coatings.

Armacell USA, 2018. URL http://www.armacell.us/home/

Ashbaugh, W.G., Laundrie, Thomas.F., 1985. A Study of Corrosion of Steel Under a Variety of Thermal Insulation Materials. ASTM STP 880 W. I. Pollock and J. M Barnhart, Eds. ASTM, Philidelphia, 121–131.

ASM International, 2015. Corrosion in the Petrochemical Industry, Second Edition. A S M International, Materials Park, UNITED STATES.

Bai, X., Tang, J., Gong, J., Lü, X., 2017. Corrosion performance of Al–Al2O3 cold sprayed coatings on mild carbon steel pipe under thermal insulation. Chinese Journal of Chemical Engineering 25, 533–539. https://doi.org/10.1016/j.cjche.2016.10.004

Brady, G.S., Clauser, H.R., Vaccari, J.A., 2002. Materials Handbook: an Encyclopeida for Managers, Technical Professionals, Purchasing and Production Managers, TEchnicians, and Supervisors. McGraw-Hill Professional, New York.

Caines, S., Khan, F., Shirokoff, J., 2017. Demonstration of increased corrosion activity for insulated pipe systems using a simplified electrochemical potential noise method. Journal of Loss Prevention in the Process Industries 47, 189–202. https://doi.org/10.1016/j.jlp.2017.03.012

Caines, S., Khan, F., Shirokoff, J., 2013. Analysis of pitting corrosion on steel under insulation in marine environments. Journal of Loss Prevention in the Process Industries 26, 1466–1483. https://doi.org/10.1016/j.jlp.2013.09.010

Caines, S., Khan, F., Shirokoff, J., Qiu, W., 2015. Experimental design to study corrosion under insulation in harsh marine environments. Journal of Loss Prevention in the Process Industries 33, 39–51. https://doi.org/10.1016/j.jlp.2014.10.014

Chico, B., Fuente, D. de la, Diaz, I., Simancas, J., Morcillo, M., 2017. Annual Atmospheric Corrosion of Carbon Steel Worldwide. An Integration of ISOCORRAG, ICP/UNECE and MICAT Databases. Materials 10. https://doi.org/10.3390/ma10060601

Fitzgerald, B., Winnik, S., 2005. A Strategy for Preventing Corrosion Under Insulation on Pipeline in the Petrochemical Industry. Journal of Protective Coatings and Linings 52–57.

Geary, W., 2013. Analysis of a corrosion under insulation failure in a carbon steel refinery hydrocarbon line. Case Studies in Engineering Failure Analysis 1, 249–256. https://doi.org/10.1016/j.csefa.2013.09.001

Geary, W., Parrott, R., 2016. Two corrosion under insulation failure case studies. Loss Prevention Bulletin 2–6.

Guo, B., Song, S., Ghalambor, A., Lin, T.R., 2014. Chapter 8 - Pipeline External Corrosion Protection, in: Guo, B., Song, S., Ghalambor, A., Lin, T.R. (Eds.), Offshore Pipelines (Second Edition). Gulf Professional Publishing, Boston, pp. 103–112. https://doi.org/10.1016/B978-0-12-397949-0.00008-X

Haraldsen, K., 2010. Corrosion under insulation - testing of protective systems at high temperatures. NACE. https://doi.org/Paper No. 10022

Lins, V., Gomes, E.A., Costa, C.G., Castro, M. das M.R., Carneiro, R.A., 2018. Corrosion behavior of experimental nickel-bearing carbon steels evaluated using field and electrochemical tests. Metallurgy and materials 71(4), 613–620. https://doi.org/10.1590/0370-44672016710173

Long, V.C., Crawley, P.G., 1985. Recent Experiences with Corrosion Beneath Thermal Insulation in a Chemical Plant. ASTM STP 880 Corrosion of Metals Under Thermal Insulation, 86–94.

Melchers, R.E., 2005. The effect of corrosion on the structural reliability of steel offshore structures. Corrosion Science, International Symposium on Corrosion and Protection of Marine Structures—in memory of the late Professor Toshihei Misawa 47, 2391–2410. https://doi.org/10.1016/j.corsci.2005.04.004

Metals Handbook, Ninth Edition: Volume 13 - Corrosion, 1987. . ASM International Handbook Commitee, Metals Park, Oh.

Morey, A., 2018. Corrosion under insulation revisited: Aren't we about to finish that project? Process Safety Progress 37, 502–505. https://doi.org/10.1002/prs.12007

NORSOK M501 ed. 6, 2013.

Palmer, A.C., King, R.A., 2004. Subsea Pipeline Engineering. PennWell Books.

Practice for Preparing, Cleaning, and Evaluating Corrosion Test Specimens, 2003. . ASTM International. https://doi.org/10.1520/G0001-03R17E01

Revie, R.W., 2002. Chapter 18: Atmospheric Corrosion, in: Uhlig's Corrosion Handbook (2nd Edition). John Wiley & Sons.

Risk-Based Inspection Technology, 2008.

Shifler, D.A., 2005. Corrosion in Marine and Saltwater Environments II: Proceedings of the International Symposium. The Electrochemical Society.

Standard Guide for Examination and Evaluation of Pitting Corrosion, 1994. . ASTM International.

van Oostendorp, D.L., Earle, R.N., Forbes, R., 2007. Gas Distribution Transmission Pipelines External Corrosion Direct Assessment - A Case Study. Presented at the CORROSION 2007, NACE International.

Wall, H., Wadso, L., 2013. Corrosion rate measurements in steel sheet pile walls in a marine environment. Marine Structures 33, 21–32.

Wilds, N., 2017. 17 - Corrosion under insulation, in: El-Sherik, A.M. (Ed.), Trends in Oil and Gas Corrosion Research and Technologies, Woodhead Publishing Series in Energy. Woodhead Publishing, Boston, pp. 409–429. https://doi.org/10.1016/B978-0-08-101105-8.00017-6

Winnik, S. (Ed.), 2016. 4 - The risk-based inspection methodology for CUI, in: Corrosion-Under-Insulation (CUI) Guidelines (Second Edition), European Federation of Corrosion (EFC) Series. Woodhead Publishing, pp. 17–42. https://doi.org/10.1016/B978-0-08-100714-3.00004-4

Yang, Y., Khan, F., Thodi, P., Abbassi, R., 2017. Corrosion induced failure analysis of subsea pipelines. Reliability Engineering & System Safety 159, 214–222. https://doi.org/10.1016/j.ress.2016.11.014

Zen, K., 2005. Corrosion and life cycle management of port structures. Corrosion Science 47, 2353–2360. https://doi.org/10.1016/j.corsci.2005.04.003

CHAPTER 4 – Coated, Uncoated, and Insulated Pipelines, A Field Test Morphology Analysis

4.1 Preface

A version of this paper was published in ASME 2021 40th International Conference on Ocean, Offshore and Arctic Engineering. The primary author is Alan Hillier and the co-authors for this manuscript include Dr. Faisal Khan and Dr. Susan Caines. The primary author setup experiment and performed testing, lab analysis, completed literature review and prepared the draft of the manuscript. The co-author Faisal Khan helped in developing concept, analyzing data, drawing conclusion, and provided feedback on the draft manuscript. Dr. Susan Caines developed the concept of experiment, helped setup the research site and analysis of lab interpretation. Link: https://doi.org/10.1115/OMAE2021-63014

4.2 Abstract

In situ studies involving CUI and corrosion under coating are rare, especially in marine harsh environment. A333 low temperature carbon steel is selected for its versatile use in cold environments and corrosion resistance properties. It has not been studied widely in marine environment and so, this work reports corrosion type, products, morphology, and mechanism for thirty-six model pipelines (insulated, uninsulated, coated and uncoated) placed at Argentia, NL. Corrosion products were identified using x-ray diffraction (XRD). Detection and semi-quantification of elements was performed using energy disruptive spectroscopy (EDS) which was coupled to a scanning electron microscope (SEM). SEM images confirmed the formation of characteristic morphological structures such as sandy crystal (lepidocrocite γ-FeOOH), cotton ball

(goethite α-FeOOH), and small grain (akageneite β-FeOOH) structures. For insulated uncoated pipes, the main phases were goethite, akageneite, and hematite(α-Fe_20_3). For uncoated uninsulated pipes, akageneite, goethite, and hematite were main phases. For coated pipes, goethite was the main phase. When ferrihydrite was detected with akageneite, there was less lepidocrocite and goethite than when ferrihydrite was not present. Uncoated pipes had deepest pits and highest corrosion rates as previously reported in (Hillier et al., 2021) and magnetite (Fe_30_4) was present only in year two. It is a passive oxide formed on the iron surface but can be a product of microbial reduction of ferrihydrite in certain conditions. A proposed mechanism for the high corrosion rate and pits in uncoated pipes is due to the localized corrosion from excess chloride and moisture from seawater spray (exfoliation was observed) as well as stabilized ferrihydrite limiting goethite formation, thus reducing steel pipe surface passivity.

4.3 Introduction

This research is a continuation of the work by Hillier et al (Hillier et al., 2021) where insulated, uninsulated, coated, and uncoated pipes were exposed and studied in harsh weather marine environment ~30m from high tide near Argentia, Newfoundland and Labrador, Canada for more than 2 years based on experimental design in Caines et al (Caines et al., 2015).

Years of research have been completed to determine the performance of steels in industrial, rural, urban and marine atmospheres (Raman et al., 1986) (Morcillo et al., 2019) (Antunes et al., 2003) (Oh et al., 1998) (Alcántara et al., 2015) (Cano et al., 2014) (Antunes et al., 2014) (Fuente et al., 2011) (Melchers, 2012). Corrosion characteristics and oxide formations on metals help to create models giving engineers insight into structural life for different environments and circumstances.

Composition and formation of oxides depend on environment conditions and the consensus for weathering steels in marine environments (Alcántara et al., 2017) is that the primary corrosion product is lepidocrocite (γ-FeOOH). As time passes, it transforms into goethite (α-FeOOH) and later magnetite (Fe_3O_4). Akageneite (β-FeOOH) can form when there is high chloride concentration in aqueous solutions on steel. Most research conducted in atmospheric corrosion tests have used metal coupons on racks, and there are few cases of insulated or coated pipelines to determine corrosion products and surface morphology. Corrosion under insulation (CUI) and under coating is not widely studied and so there is a lack of knowledge in this area. It is important as coating and insulation are an initial protection preventing corrosion and when one or both fail, corrosion and eventual failure may occur (Javaherdashti, 2014).

CUI is difficult to detect, and our understanding is low compared to other areas of corrosion knowledge (Caines et al., 2013). Little knowledge on morphology and rust phases formed on steels in situ in marine atmosphere are available (Alcántara et al., 2016). Corrosion under coating, and CUI may have different mechanisms, products, and morphology which have not been reported in literature. This research advances knowledge with A333 low temperature carbon steel (with comparable properties to weathering steels) exposed to C5 class marine corrosion environment with insulated, uninsulated, coated, and uncoated pipelines using SEM, EDS, and XRD analysis.

4.3.1 Other Marine Environment Studies

Steel was placed for two years in a marine environment and characterized by optical microscope, SEM/EDS, XRD and mass loss by (Cano et al., 2014). The main species found were ferrihydrite, maghemite (γ-Fe2O3), and goethite in the inner corrosion layer, and lepidocrocite in the outer layer. They mentioned corrosion is often constituted by a wide variety of oxides such as goethite, lepidocrocite, feroxyhyte, magnetite and amorphous phases.

(Cook et al., 1999) exposed weathering and carbon steel to marine atmosphere and found oxides consisted of goethite, akageneite, lepidocrocite, magnetite, and amorphous matter. Cu, Cr, and Si were on the inner layer while P and Ni were distributed on the entire rust layer.

Authors in (Alcántara et al., 2016) used carbon steel exposed on open air racks in marine atmosphere. Typical atmospheric corrosion specimens found were lepidocrocite, goethite, akageneite, and magnetite. The work used SEM and Raman analysis for species, and SEM for rust characterization. It contains extensive references and definitions for the typical structures which occur on weathering steels based on the work of (Cornell and Schwertmann, 2006) and the many works of Raman.

Low carbon steel was exposed to marine sites for three years by (Surnam et al., 2016). Early during exposure lepidocrocite and akageneite were observed, however after 3 years of exposure magnetite was the most probable product, and this surface had a more compact rust layer.

(Jaen et al., 2012) found that lepidocrocite formed after 6 months atmospheric corrosion, and at 12 months, goethite formed on samples. Akageneite was prominent in high chloride environments.

For most researchers, lepidocrocite is reported as the earliest corrosion product and afterwards, goethite and then magnetite appear. These are known to passivate and protect the steel from further oxidation. Akageneite was reported in marine environments rich in moisture and chlorides, acting as an agent to increase localized corrosion such as pitting. Most references on ferrihydrite in iron in atmospheric corrosion come from long term corrosion studies (Bouchar et al., 2017, 2013). It forms reactive islands away from the iron surface, in contrast to magnetite, which forms on it and passivates it.

4.4 Experiment and Results

A JEOL JSM 7100F field emission SEM equipped with a Thermo EDS system was used to observe surface morphologies of the rust film and detect the elemental distribution. Power X-ray diffraction (XRD) was taken on a SmartLab analyzer at a range of 10-90 with a scanning rate of 20/min to characterize the crystalline phases of the corrosion products. The parameters of the generator were set as 40 kV and 44 mA.

Following guideline from SPO 198-2010, Norsok number 6C coating was used with one coat epoxy phenolic primer, and one topcoat (each 150μm). Pipes that were not coated were used as received with Rust-preventing Spraying Hard-film Agent (RSH-3A/Lucency with 50% acrylic, 10% phenolic, 20% hydrocarbon solvent, 10% suphonate, 10% miscellaneous) on the surface of pipes. Armacell ("Armacell USA," 2018) rubber foam 1-inch thick approximately 4.5-inch diameter was used over half of the pipes and secured with zip ties and silicone.

Samples of A333 low temperature carbon steel pipes (properties in Table 4.1 from manufacturer) were randomly selected for SEM, EDS, and XRD data for the four surface protections (Uncoated uninsulated, coated insulated, coated uninsulated, and uncoated insulated pipes). Samples were cut using a pipe cutter and band saw. Slices of pipe were observed under SEM for surface features, and EDS scans which are presented in some tables after the SEM images. The EDS scans present elemental mass percent and are different for different surface protections and may be investigated further. Surface rust was taken off by scraping or prying off from the surfaces of pipes, and then crushed for XRD analysis. Details for each type of pipe surface protection studied and experimental results are presented below.

Table 4.1: A333 steel properties.

Hot Rolled Steel Pipe Chemical Composition														
C	Si	Mn	P	S	Ni	Cr	Mo	Cu	Al	V	Nb	Ti	B	Ca
0.16	0.26	0.95	0.013	0.004	0.06	0.11	0.05	0.07	0.02	<0.01	0.01	<0.01	<0.0005	0.0021

4.4.1 Uncoated Uninsulated Pipes

Pipes in this section were used as received. Figure 4.1 is an uncoated uninsulated and corroded in Argentia, NL for two years. While received black and smooth, after corrosion it appears red and brown, with non-smooth surface. Some rust could be easily removed and flaked off by touching as in Figure 4.8, this was generally an outside layer, while the darker inner layer was more compact. In some cases, it was difficult to remove a tightly bound oxide on the surface without a sharp tool.

Figure 4.1: Pipe 27 showing compact light layer of surface oxide in patches. Left July, right December.

SEM image in Figure 4.2 shows a cracked and broken, uneven surface oxide on the left, while the right side is more compact, smooth. Such surfaces generally protect the steel from elements like chloride. Figure 4.3 shows a pit. EDS scans in Table 4.2 show typical marine atmosphere elements.

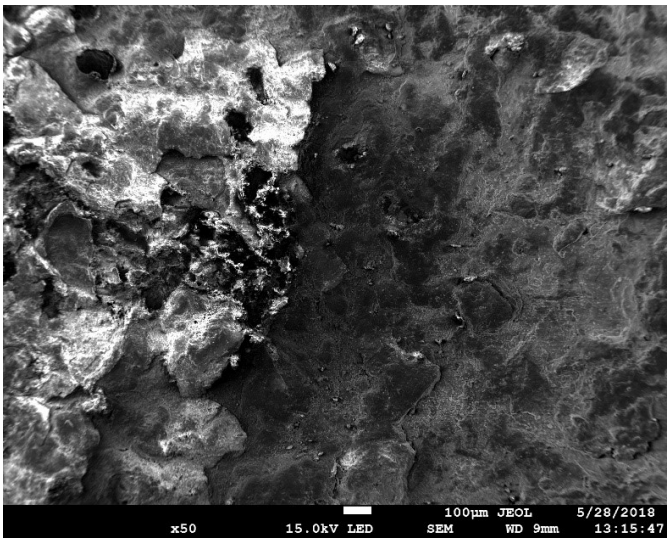

Figure 4.2: Pipe 27, Uncoated uninsulated, easily removed flaky oxide on the left side and the more compact darker underlayer on the right.

Table 4.2: EDS scan of points on Figure 4.2: Pipe 27

	C-K	O-K	Na-K	Mg-K	Al-K	Si-K	S-K	Cl-K	Ca-K	Ti-K	Mn-K	Fe-K	Br-L
27 pt1	24.39	13.27		0.24	0.51	1.28	0.57	0.15	0.89	0.28		58.42	
27 pt2	8.92	29.38	0.63			0.58	0.38				0.59	58.95	0.58
27 pt3	14.02	33.77	0.43	0.12	0.17	0.40	0.24	0.12				50.73	

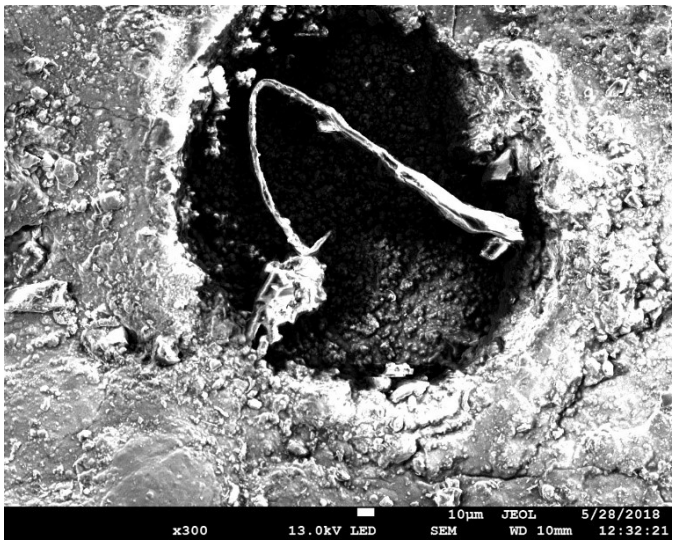

Figure 4.3: A pit on Pipe 27 with sandy grains, globules (spread over different areas of the surface).

Table 4.3: EDS 3 points across Figure 4.3, having chloride near the pit.

	C-K	O-K	Al-K	Si-K	P-K	S-K	Cl-K	Ca-K	Mn-K	Fe-K
27 pt1	42.07	5.15	0.73	1.08	0.60	0.93	2.04	10.36		37.03
27 pt2	12.99	3.10		0.19						83.72
27 pt3	34.43			0.35					0.69	64.54

Pipe 27 XRD oxides displayed (by mass percent largest to smallest) akageneite, lepidocrocite, hematite.

Figure 4.4: Pipe 2B in July showing thin compact oxide layer.

Figure 4.5, Figure 4.6, and Figure 4.7 have cracks and flattened area like valleys. Cracked and easily removed oxide surface may not protect the steel surface as well as a uniform oxide layer with a smooth surface. Typical marine elements were found on the surface listed in Table 4.4. Figure 4.8 shows typical exfoliation in marine environments where chloride oxides form higher volume below other Fe oxides, raising up layers of Fe which are easily removed.

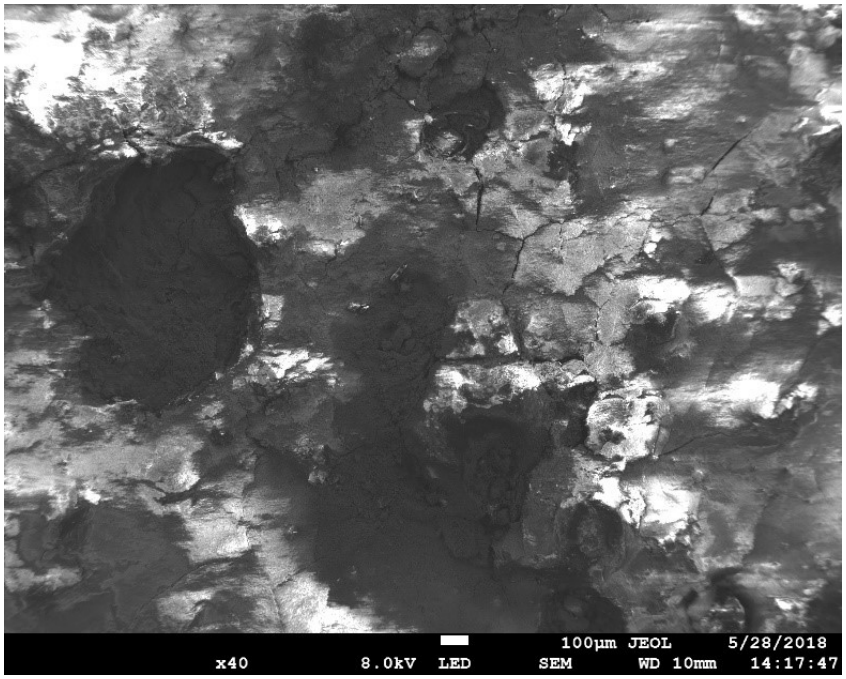

Figure 4.5: Pipe 2B showing non protective oxide, with cracks and non-smooth surface. In the darkened areas, sandy grains appear.

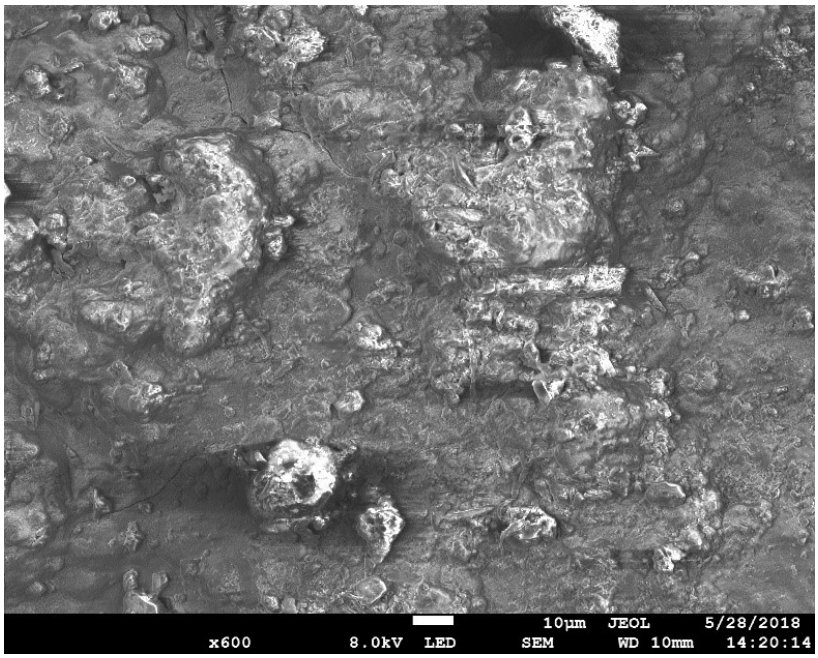

Figure 4.6: Pipe 2B zoomed in.

Table 4.4: Pipe 2B EDS scans across Figure 4.6.

	C-K	*O-K*	*Na-K*	*Mg-K*	*Al-K*	*Si-K*	*S-K*	*Cl-K*	*K-K*	*Ca-K*	*Fe-K*
2b pt1		2.95			0.22	0.52			0.35	1.13	94.83
2b pt2	16.68	43.56	1.52	0.58	1.27	2.84	0.37	0.28	0.22		32.67
2b pt3	8.66	35.88	1.55	0.16	0.14	0.23	0.16	0.36		0.27	52.59

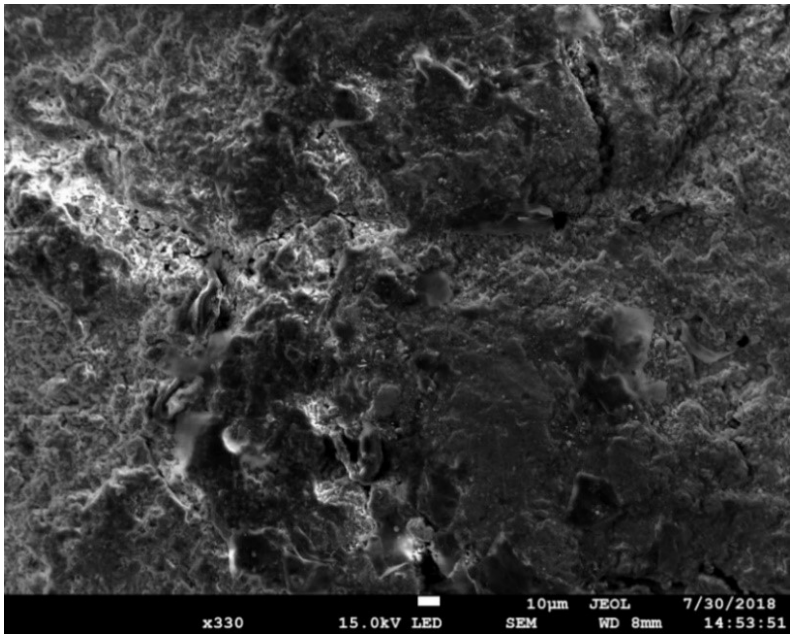

Figure 4.7: Pipe 2B showing what may be lepidocrocite and globular goethite in cracks, and globular goethite in areas of the surface. The oxide shown here is more compact than other images taken.

Figure 4.8: Early exfoliation, typical outer (lightly bound) and inner (strongly bound) oxides.

4.4.2 Coated Insulated Pipes

Only one random sampled pipe experienced broken coating with corrosion as seen in Figure 4.9, Figure 4.10, and Figure 4.11 showing different features and oxides. EDS scans are shown in Table 4.5. In this sample, marine moisture penetrated the insulation and attacked an area of broken coating. Corrosion then spread under the coating. This coating failed in under 2 years, while in industry coating is generally given life of 5-13years (Geary, 2013). However, 7/36 pipes which were coated and insulated did not suffer any coating breaks.

Figure 4.9: Pipe 20, July (left) vs December (right). Coating failure led to corrosion under coating which spread multiple times its initial size under the coating in 6 months.

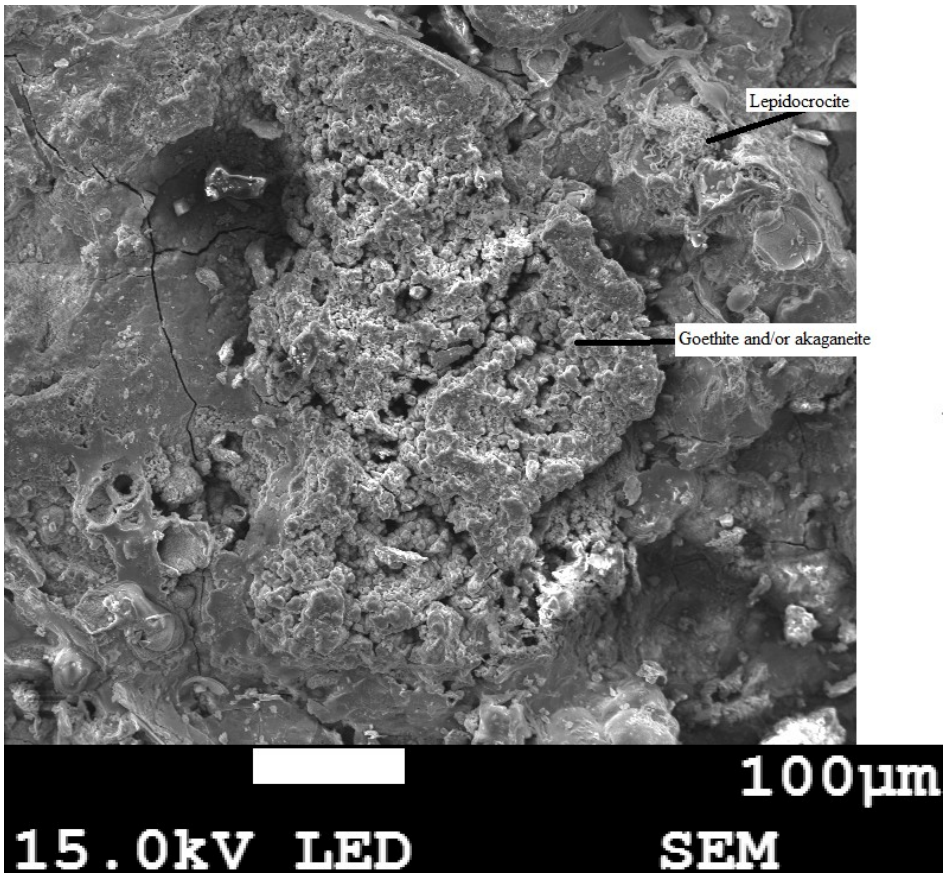

Figure 4.10: 20B showing lepidocrocite in worm nest pattern and globular goethite and/or akageneite in center.

Table 4.5: Atomic percent from EDS scan from surface of Figure 4.10. Typical seaside elements.

	C-K	O-K	Na-K	Mg-K	Al-K	Si-K	S-K	Cl-K	K-K	Ca-K	Mn-K	Fe-K	Ba-L
20B	9.39	31.98	0.67	0.81	0.11	0.33					0.77	55.94	
20B	6.81	21.90			0.18	0.76				0.20	1.04	69.10	
20B	6.19	3.70										90.11	
20B	20.80	32.21		0.34	0.17	0.40	1.33	0.22	0.60	0.28	0.70	38.56	4.39

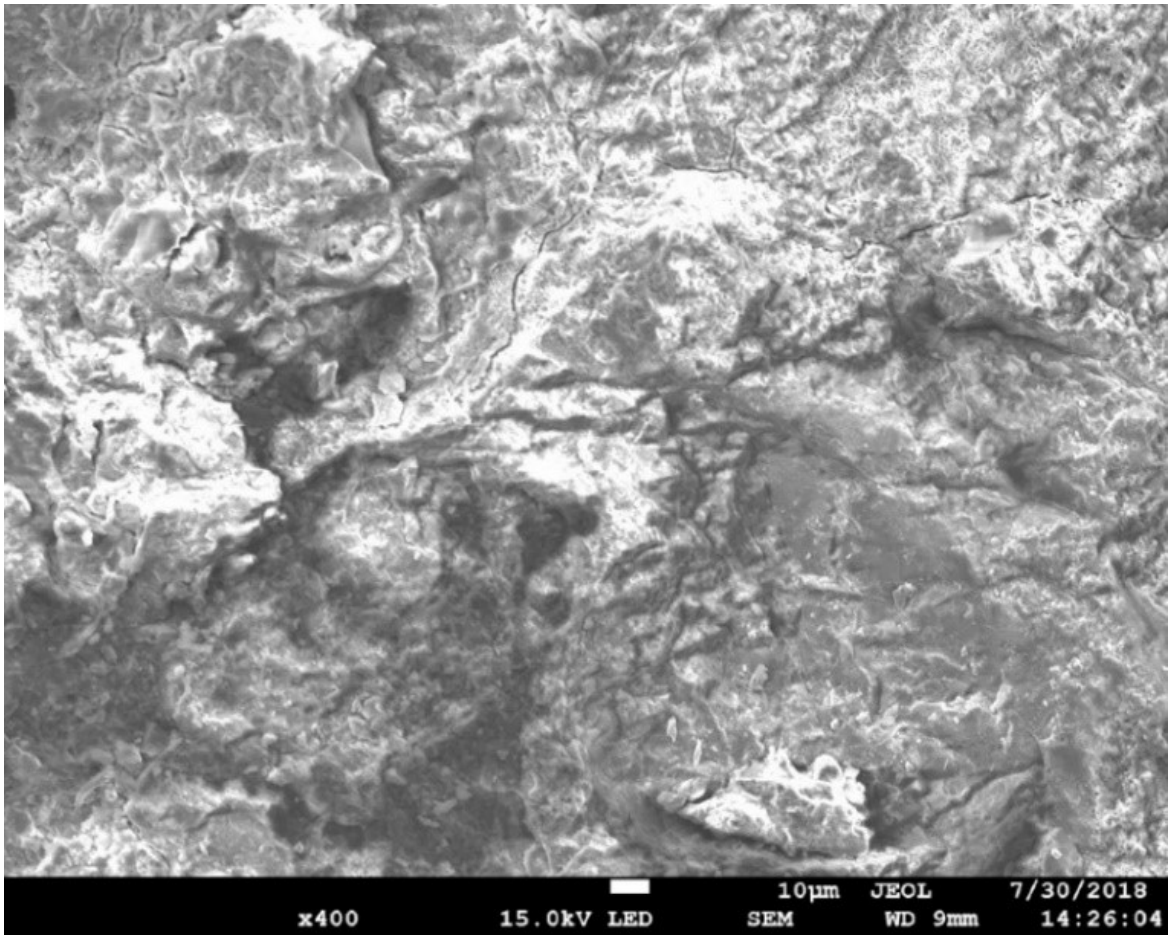

Figure 4.11: Pipe 20B (uninsulated and coated) showing lepidocrocite in and around cracks.

4.4.3 Coated Uninsulated Pipes

Pipes in this section experienced corrosion around instrumentation and other surface breaks in coating. When iron oxides form under the coating the rise in volume expands and cracks the coating (Figure 4.12), leaving more areas exposed to the environment, thus accelerating the corrosion of the steel. During the first year, no corrosion occurred on random sample pipes, and

so no mass loss or pit depth was recorded for the previous paper research (Hillier et al., 2021). Interestingly, many pipes in this section exhibit clear lepidocrocite formation, an early iron oxide.

Figure 4.12: Pipe 17 showing July (left) and December (right) surfaces near instrumentation.

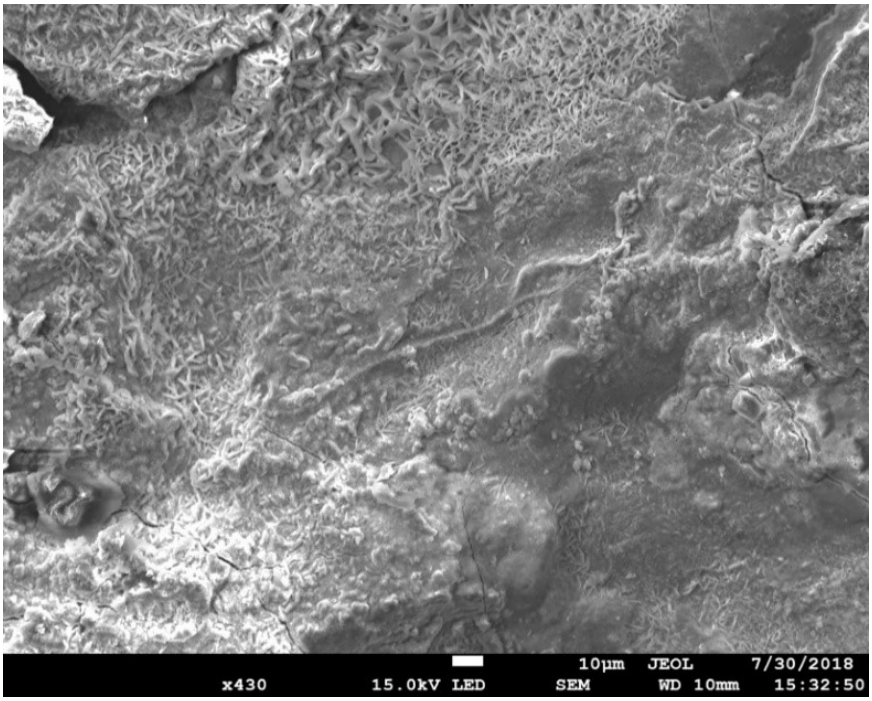

Figure 4.13: Laminar lepidocrocite over pipe 17.

Table 4.6: Pipe 17 atomic weight percent of 3 points on surface. Chloride percent mass is higher than other samples.

	C-K	O-K	Na-K	Mg-K	Al-K	Si-K	S-K	Cl-K	K-K	Fe-K	Ba-L
17		6.46	0.00					0.32		93.22	
17	31.85	13.06		0.19		0.58	2.99	1.37	1.22	39.39	9.35
17		44.02			0.08		0.50	1.16		54.25	

Figure 4.13 shows laminar lepidocrocite over the surface, with what appears to be some globular goethite starting to form in the center. The surface is not deeply cracked compared to uncoated pipe samples in previous section. Pipe 17 was from the first year, while pipe 13 was from the second.

Figure 4.14: Corrosion under coating of 13C. SEM preformed on epicenter of break until right edge of coating still attached. See Figure 4.15 to Figure 4.21.

In Figure 4.14 a break in coating around instrumentation lead to moisture inside. As the corrosion layer increased in size, expanding, it pushed the coating off the surface allowing corrosion on new areas of the pipe further from the initial break. As seen on coating chip, corrosion products near the initial break were redder in colour, while moving under the coating away from the break a darker color appears. In (Hillier et al., 2021) similar was investigated and the largest pits occurred between the epicenter and the edge of coating where no corrosion had taken place. XRD was

preformed on for pipe 13 but due to some issue, oxides were underneath the background curve, and only SEM and EDS results were available.

In Figure 4.15 to Figure 4.21 shows from the initial break, middle of the break to the outside coating edge, and near the coating edge are shown. In Figure 4.17 the stacks are sharp, deep, and were found in the mid region from epicenter to coating edge with little corrosion, previously this area was shown with deepest pits. In Figure 4.19 near to the epicenter the surface shows advanced corrosion with surface looking smoother, even though more globules are shown rather than individual larger stacks. Figure 4.21 near edge of coating shows debris and fiber/crystalline features, which may be the coating rather than an oxide formed. Figure 4.22 shows another random sample with more advanced corrosion, the surface appears smoother.

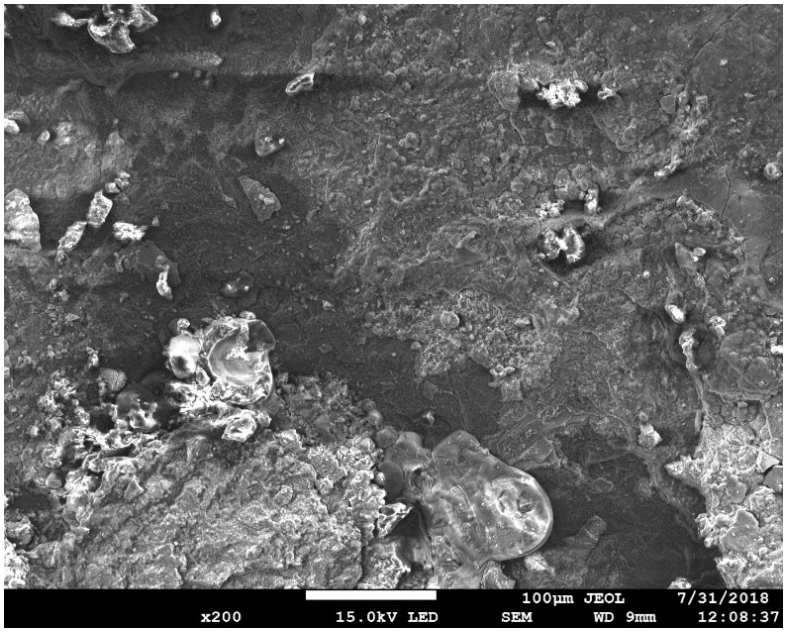

Figure 4.15: Pipe 13C showing cracks, uneven surface.

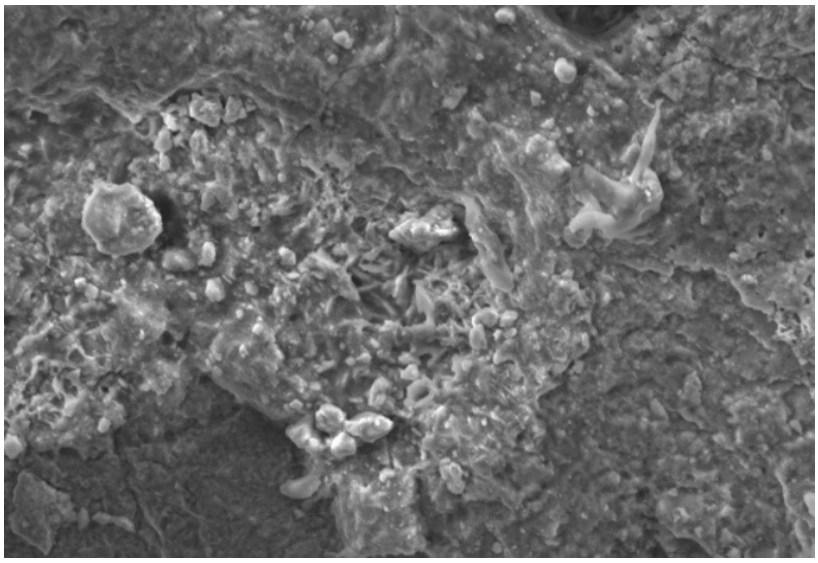

Figure 4.16: Enlarged center from Figure 4.16 showing lepidocrocite and goethite and small pits on layered sheets on bottom right side. XRD of similar pipe in Figure 4.30.

Table 4.7: 13C areas from Figure 15

	C-K	O-K	Mg-K	Al-K	Si-K	S-K	Cl-K	K-K	Ca-K	Ti-K	Cr-K	Fe-K	Ba-L
13C(2)_pt1	25.98	29.32	0.29		0.18	1.86	0.65		0.25			33.61	7.86
13C(2)_pt2	18.48	5.08					1.84			0.46		73.28	0.87
13C(2)_pt4	11.76	2.16			0.17	0.43	0.59					82.38	2.51
13C(2)_pt5	27.31	14.35	0.12	0.13	0.68	0.34	0.46	0.26	0.30	1.01		55.03	
13C(2)_pt6	25.46	39.31		0.12	0.42	0.25	2.70				0.22	31.52	

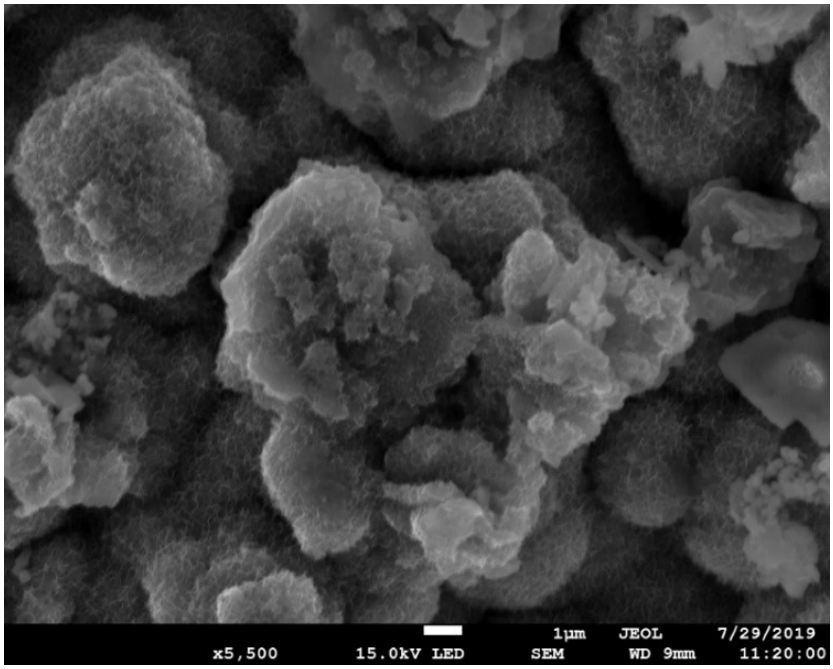

Figure 4.17: 13C mid region from coating edge to coating break location. Corrosion surface appears porous with small laminar slivers on stacks.

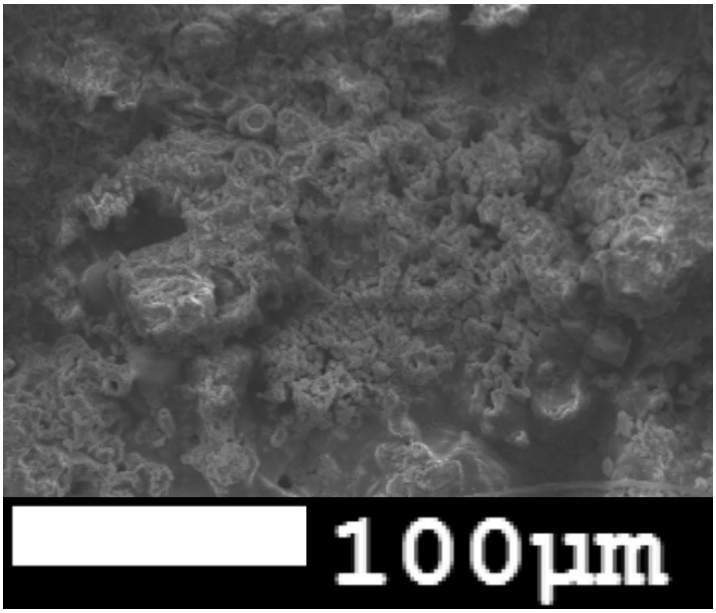

Figure 4.18: 13C near coating break showing a donut shapes, typically magnetite, in top center left.

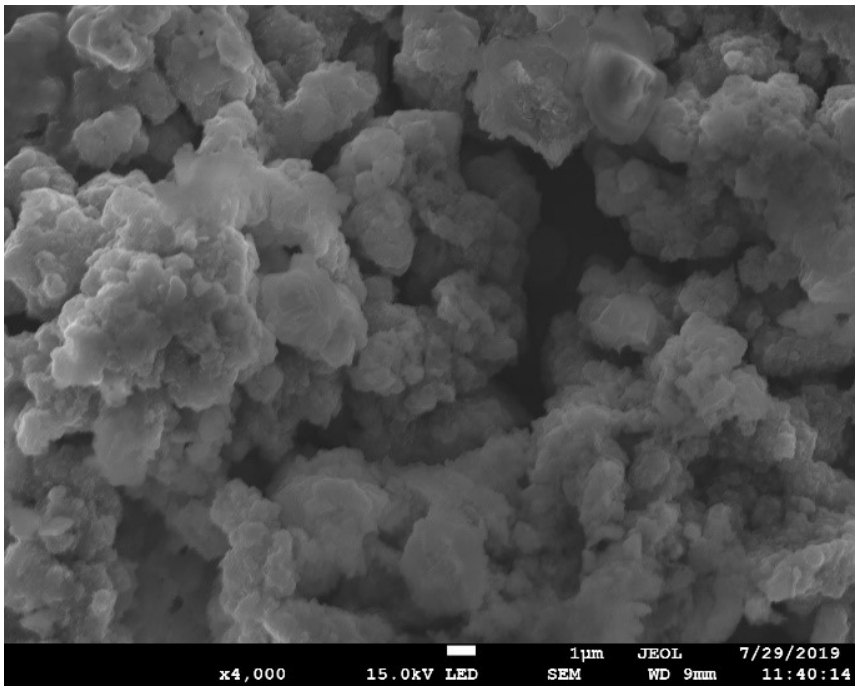

Figure 4.19: Pipe 13C near epicenter of coating break, the stacks appear with globules, smoother than in Figure 4.17.

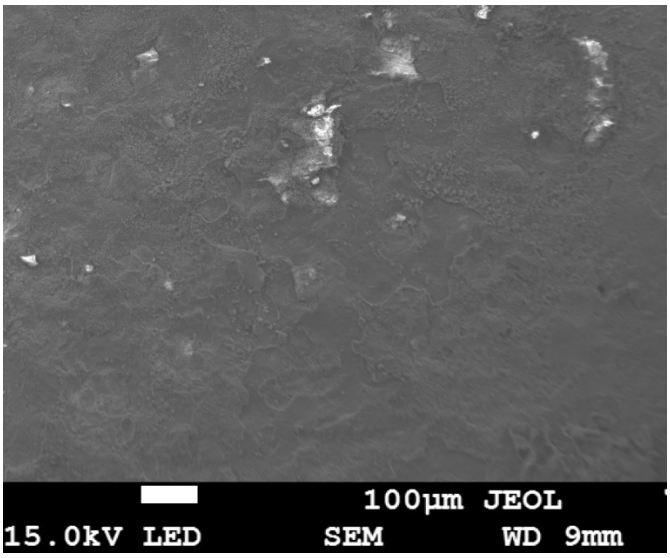

Figure 4.20: 13C further from the break only sandy grain lepidocrocite over a generally flat surface are seen.

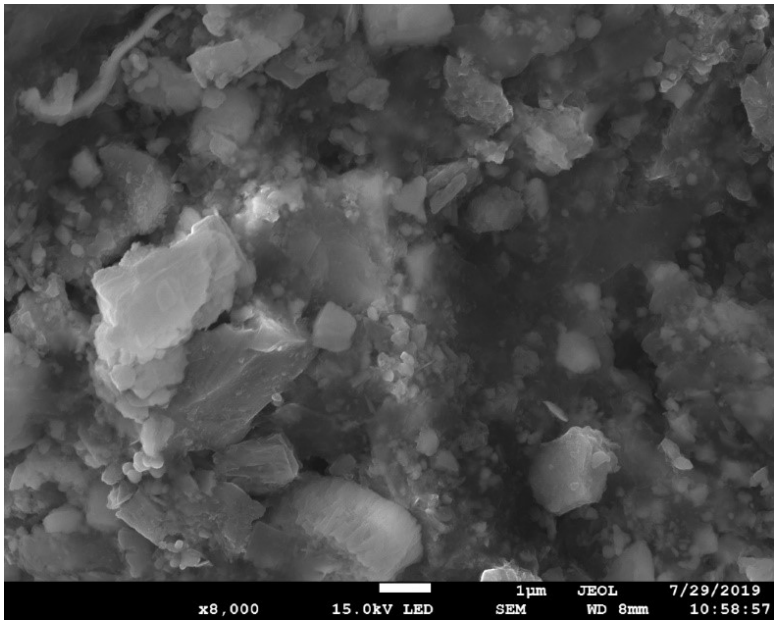

Figure 4.21: 13C Further from initial break shows crystalline species present. It may be organic matter or part of the coating still on the surface where corrosion did not yet progress.

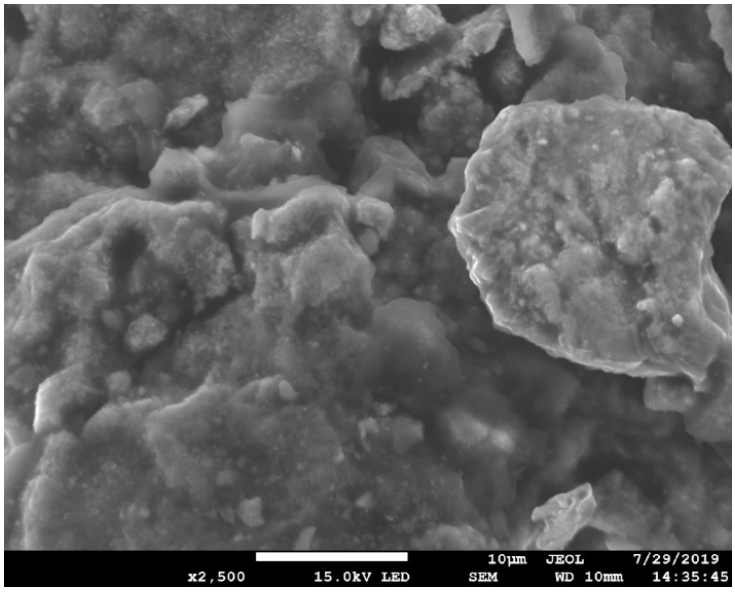

Figure 4.22: Pipe 23B showing relatively matured, smoothed surface compared to other pipes in this section. Mature products found in XRD in Figure 4.31 a similar coated uninsulated pipe.

4.4.4 Uncoated Insulated Pipes

Much of the surface of the uncoated samples under insulation remained as they were received, as shown in Figure 4.23, i.e., visible surface corrosion across the whole surface was less than uninsulated (i.e., Figure 4.4 and Figure 4.8). Most visible corrosion was near the bottom of the pipe, where the ingress of water would remain under insulation for some time. The figures in this section are from the bottom of insulated uncoated pipes. Figure 4.23 shows red oxide progression, Figure 4.24 possibly elongated akageneite which was also found on XRD tests, Figure 4.25 showing possible lepidocrocite to goethite formation, and Table 4.8 showing EDS scans.

Figure 4.23: Pipe 3B in July (left) and December (right)

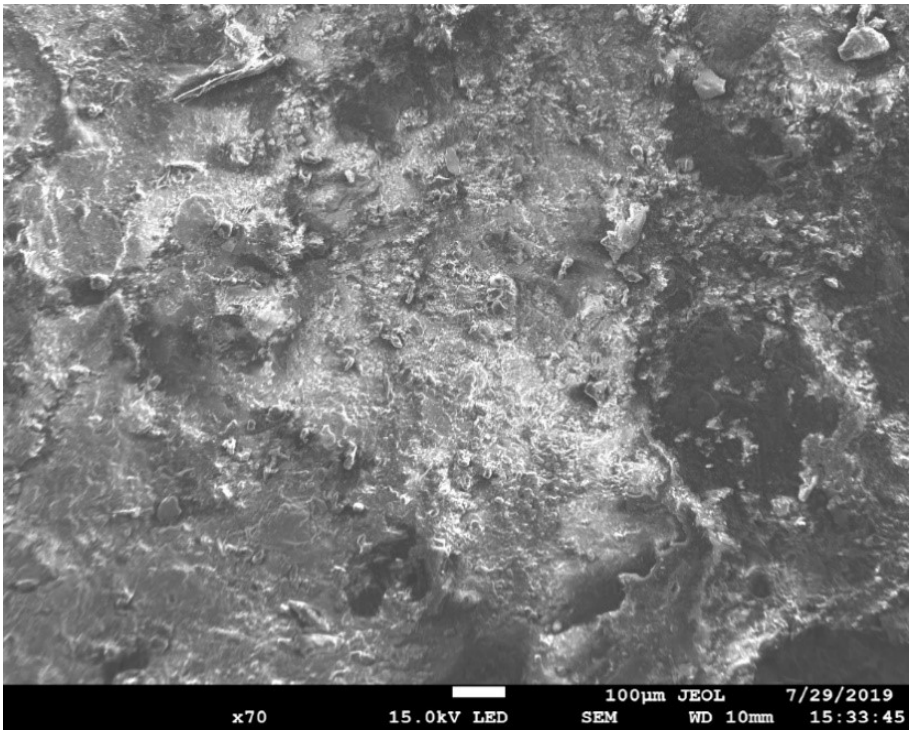

Figure 4.24: Pipe 3B showing globules and elongated cigar shapes, possibly akageneite, matching XRD in Figure 4.26: Pipe 3 XRD analysis.

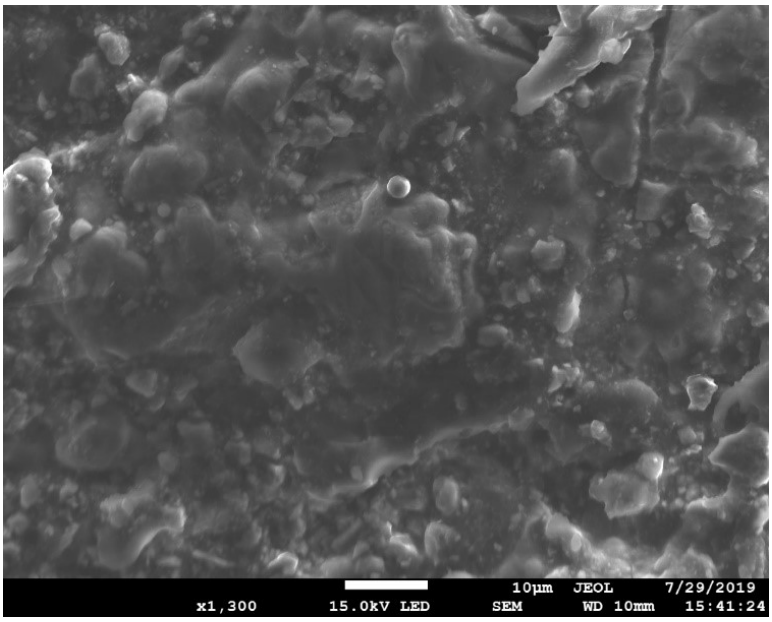

Figure 4.25: Pipe 3B globules. Compared to Figure 4.11 and Figure 4.13 the oxide is more compact and smoother showing lepidocrocite to goethite transformation and matches XRD found in Figure 4.26

Table 4.8: EDS scans for Pipe 3

	C-K	O-K	Na-K	Al-K	Si-K	S-K	Cl-K	K-K	Ca-K	Mn-K	Fe-K	Ba-L
3B pt1	76.82	15.43	1.40	0.26	0.17	0.66	0.80		0.71		3.74	
3B pt2	40.35										59.65	
3B pt3	61.25	14.68	0.47		0.33	0.33	0.60	0.18	0.99		21.15	
3B pt4	49.41	25.51	0.69	0.14	0.28	0.47					22.77	0.72
3B pt5	43.32	11.35		0.39	0.16	0.26				0.99	43.53	

4.4.5 XRD Analysis

Samples were taken from the oxides and underwent XRD, some of those sample figures are below. Pipe 3C (insulated uncoated), 8A (uninsulated uncoated) 27 (uninsulated uncoated), 28 (insulated uncoated), 12 (uninsulated coated) and 23 (insulated coated).

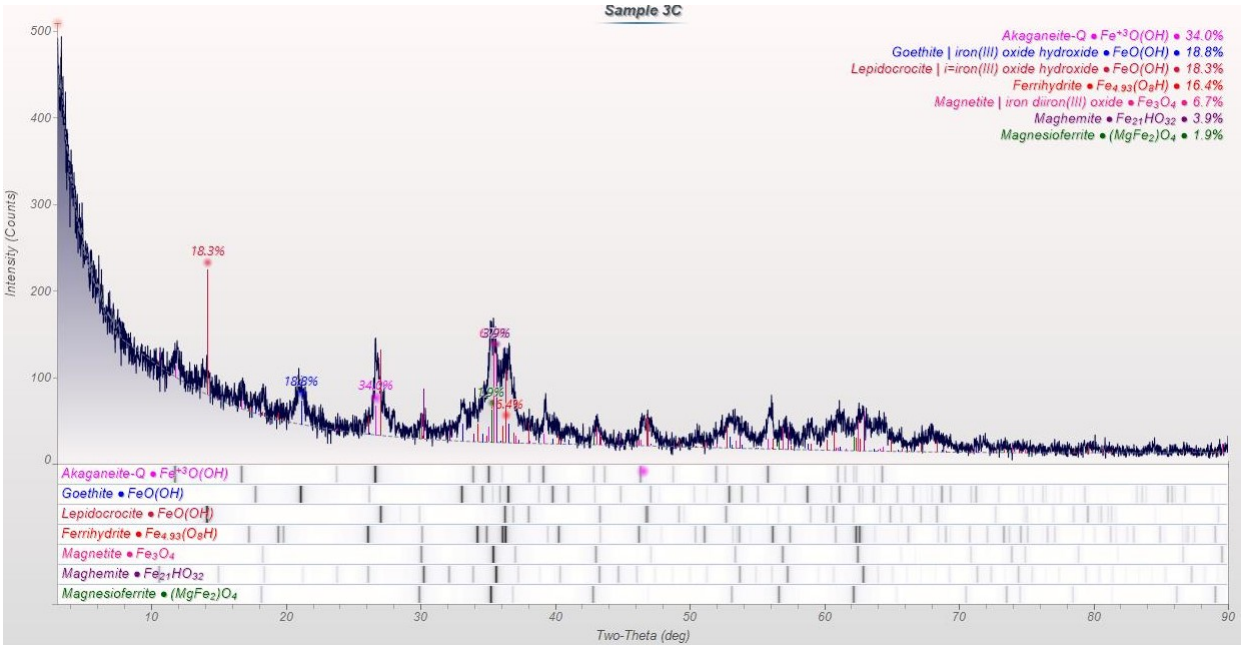

Figure 4.26: Pipe 3 XRD analysis

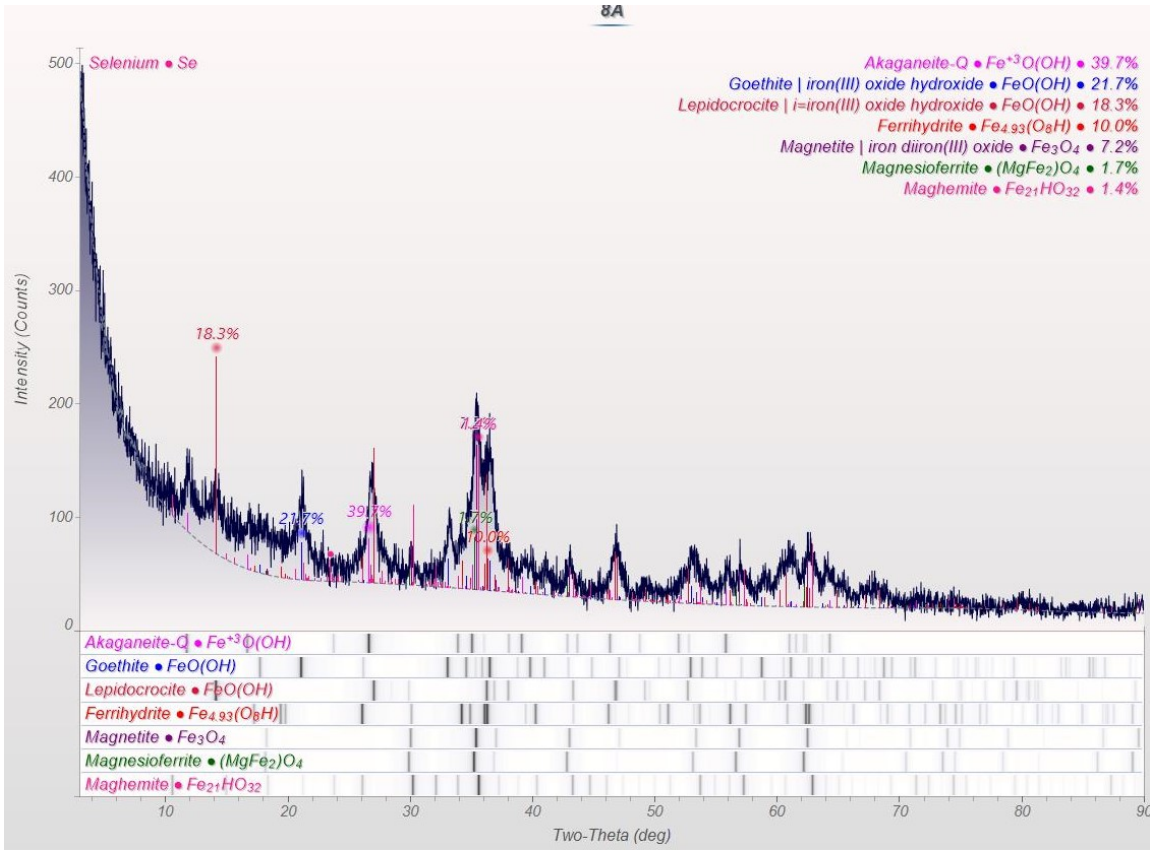

Figure 4.27: Pipe 8 XRD analysis

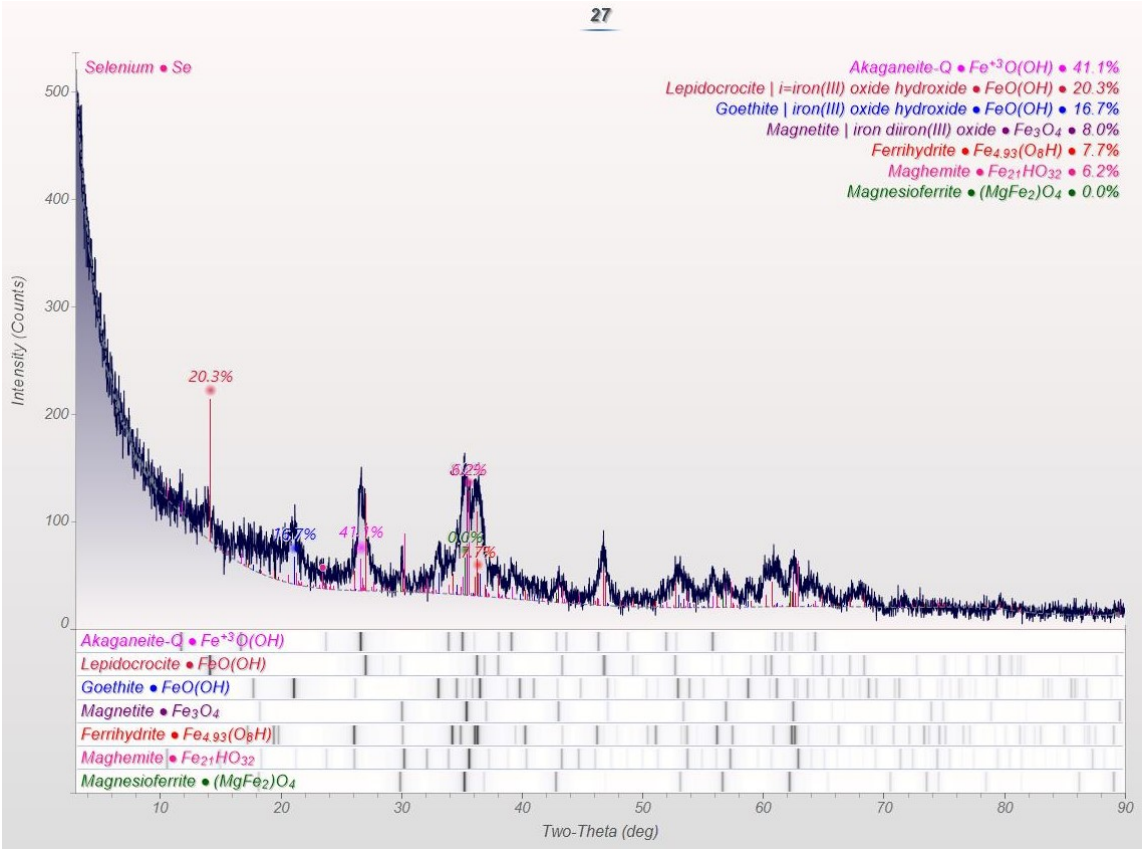

Figure 4.28: Pipe 27 XRD analysis

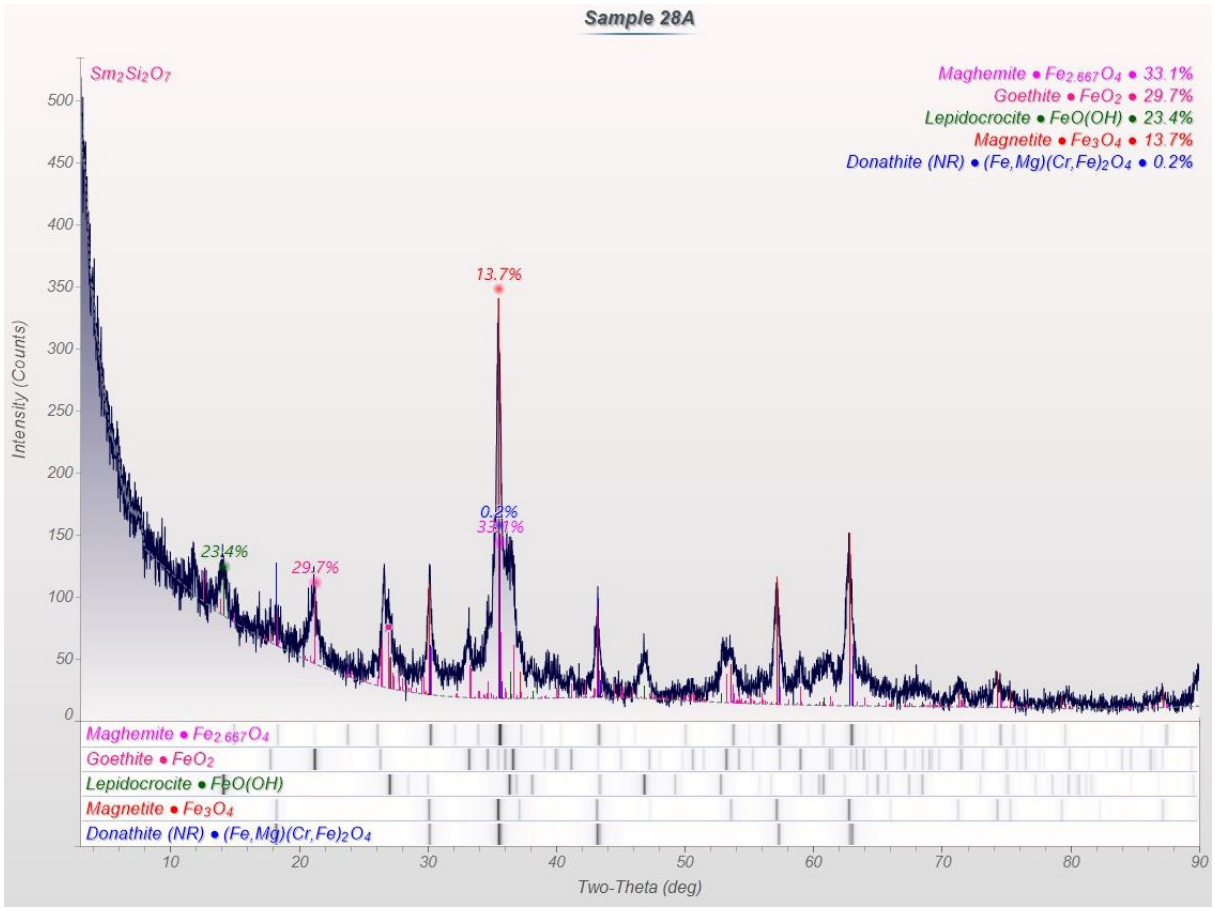

Figure 4.29: Pipe 28 XRD analysis

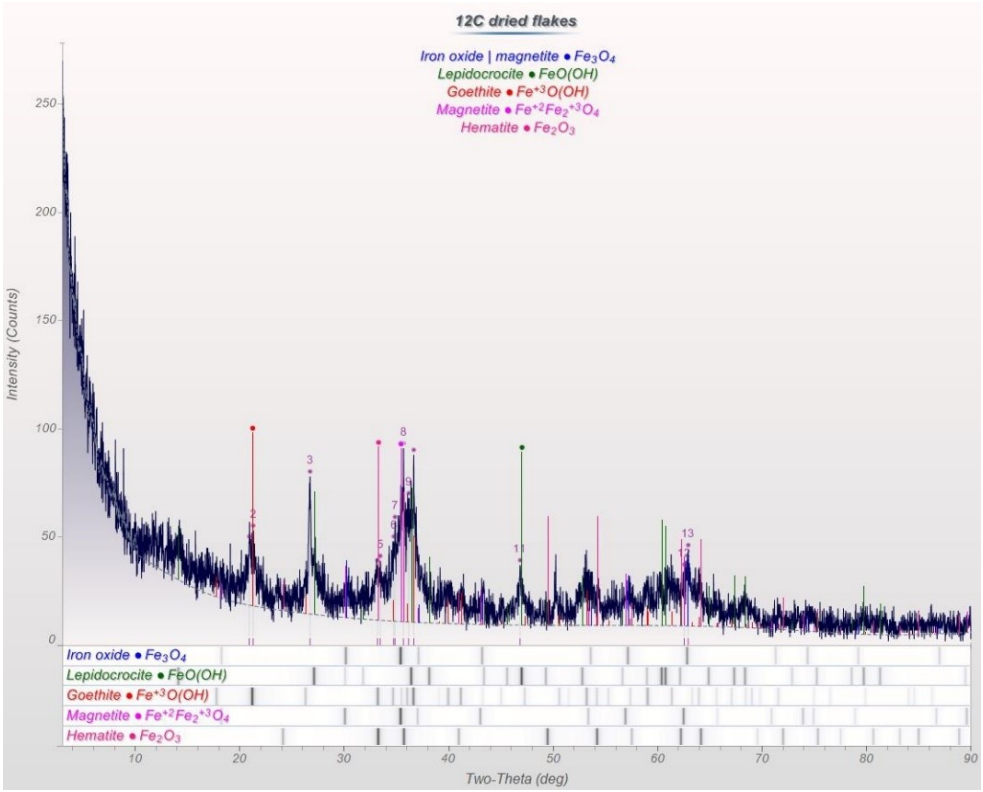

Figure 4.30: Pipe 12 XRD analysis

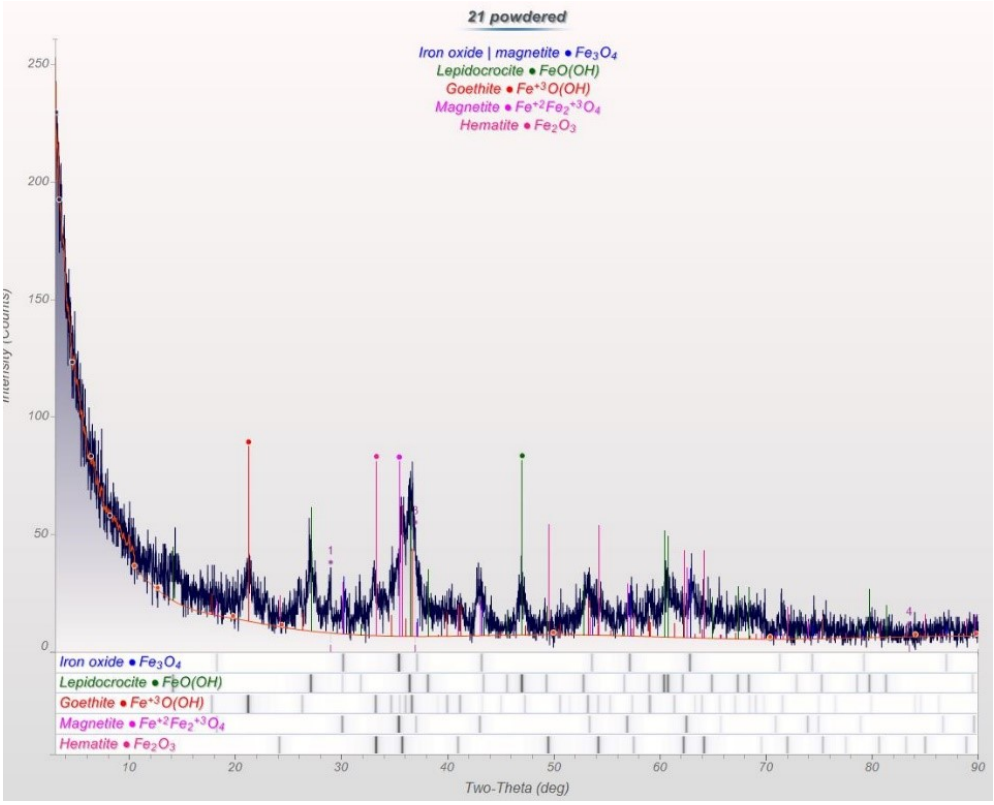

Figure 4.31: Pipe 21 XRD analysis

4.5 Discussion and Conclusion

According to (Alhawat et al., 2021) and references in the Introduction section, when steel is attacked by chloride the first corrosion product is lepidocrocite, and this was seen clearly on insulated and coated samples in the experiment section. Due to insulation and coating which protects the steel if not broken, the attacked surface on uninsulated pipes displayed a much different SEM image than pipes which were protected. I.e., new lepidocrocite over a cracked surface in Figure 4.13 compared to Figure 4.7 with less pronounced smoothed surface with deeper less pronounced valleys.

Magnetite can be considered a final phase of iron oxide passivating the surface. In samples from the first year, no magnetite was found but in the second year, magnetite had formed. Authors in (Refait et al., 2015) used steel over seven years in marine atmosphere and found that magnetite, and iron oxyhydroxides were present. This was also found in the present study.

Previously, in (Hillier et al., 2021), for the first year in marine atmosphere, pipelines which were uncoated (both insulated and uninsulated) had the deepest pits, and the highest percent mass loss. The reason for this occurring is likely due to the presence of akageneite and ferrihydrite. Ferrihydrite was found in samples in Table 10 for uncoated pipes, both insulated and not. For long term studies of medieval iron and weathering steel, ferrihydrite has been reported frequently (Bouchar et al., 2017, 2013). It is formed by iron corrosion in the presence of oxygen and water and stabilized by the adsorption of Si, P, and S (Furukawa et al., 2002). These elements were found on EDS scans in Table 4.3, Table 4.4,

Table 4.5 and others. Ferrihydrite forms small discrete clusters away from the surface and is highly reactive, like lepidocrocite and akageneite (Bouchar et al., 2013). When ferrihydrite, lepidocrocite, iron sulphites, and magnetite are close, (Furukawa et al., 2002) mentioned they stabilize ferrihydrite and reduced formations of passivating lepidocrocite and goethite. Thus, reducing oxide protection. Magnetite is present with ferrihydrite, but it should be noted it is one of the primary products of microbial ferrihydrite reduction (Roh et al., 2003) and magnetite formed in this way may not passivate as it not bound to the uncorroded surface, instead forming islands away. Comparable results of high pitting and CR are found in the present study with pipes having those oxides/hydroxides in Section 4.4.5 which add an interesting mechanism for corrosion in Argentia, NL.

The deepest pits and most mass loss percent occurred in samples with ferrihydrite and high amounts of akageneite (i.e., pipes uncoated with and without insulation). Further research is necessary to detect if microbial corrosion occurs at Argentia, NL, however, authors (Furukawa et al., 2002) had a similar environmental species, corrosion products, and elements (even though it was not the same environment) and mentioned three possible explanations for the combinations seen in Table 4.10. 1. Active metal reducing bacteria, 2. heterogeneous redox environment supporting simultaneous oxic and anoxic activities, and 3. Heterogeneous geochemical regimes which concentrate species that stabilize ferrihydrite (such as Si, P, Cu, S) and green rusts (C, Cl, S). Coating, insulation, and pits on pipelines limit free flow surface oxygen, and seawater spray with chloride promotes akageneite and increase localized corrosion on steels. Thus, it is possible the corrosion mechanism experienced at Argentia, NL is a combination of ferrihydrite formation with possible metal reducing bacteria and akageneite, or just species which stabilized ferrihydrite, which would be the main contributor for pits and high corrosion rates observed. Another clear mechanism present is exfoliation, which occurred Figure 4.7 and Figure 4.14 and is common in marine atmosphere with chlorides.

The largest to smallest reported oxides by XRD were as follows; for uncoated and uninsulated pipes, akageneite, lepidocrocite, and goethite. When akageneite was not detected, the largest to smallest detected were maghemite/hematite, lepidocrocite, and goethite. For uncoated and insulated pipes: goethite, lepidocrocite, and akageneite. Coated pipelines in the first year had one random sample for XRD. The most prevalent to least reported phases were goethite, maghemite/hematite, and lepidocrocite. Randomly selected coated and insulated samples for XRD did not have corrosion present. This makes sense that over two years the insulation and coating was rare to fail, as reported elsewhere (Geary, 2013; Geary and Parrott, 2016).

Table 4.9: Pitting and corrosion results from (Hillier et al., 2021). Pit depth +/- 3% error. CR +/- 0.6% error.

Pipe - 2017 June	Average % Mass Loss	Average Pit Depth (microns)	Max Pit Depth (microns)	CR
Ins. Uncoated	0.47	203	240	0.019
Ins. Coated	0.00	0	0	n/a
Unins. Coated	0.00	0	0	n/a
Unins. Uncoated	0.70	139	165	0.028

Pipe - 2017 Dec	Average % Mass Loss	Average Pit Depth (microns)	Max Pit Depth (microns)	CR
Ins. Uncoated	0.84	207	271	0.023
Ins. Coated	0.62	156	180	0.017
Unins. Coated	0.49	177	210	0.014
Unins. Uncoated	0.72	156	199	0.019

Table 4.10: XRD results

Pipe	I	C	Maghemite /Hematite	Lepidocrocite	Goethite	Akaganiete	Magnetite	Ferrihydrite	Year sample
9	X		6	15	79				1
26	X		31	16	53				1
28	X		33	23	30		14		2
3	X		4	18	19	34	7	16	2
21		X	18	16	66				1
12			46	33	21				1
27			7	20	17	41	8	8	2
9			2	18	22	40	7	9	2

4.6 Acknowledgements

The authors deeply appreciate and thank the late Dr. John Shirokoff for his help and input throughout this research. Thanks to Dr. Wanda Alyward for her help, some imaging, and use of lab for XRD, EDS, and SEM imaging.

4.7 References

Alcántara, J., Chico, B., Díaz, I., de la Fuente, D., Morcillo, M., 2015. Airborne chloride deposit and its effect on marine atmospheric corrosion of mild steel. Corrosion Science 97, 74–88. https://doi.org/10.1016/j.corsci.2015.04.015

Alcántara, J., Fuente, D. de la, Chico, B., Simancas, J., Díaz, I., Morcillo, M., 2017. Marine Atmospheric Corrosion of Carbon Steel: A Review. Materials (Basel) 10. https://doi.org/10.3390/ma10040406

Alhawat, M., Zinkaah, O.H., Araba, A., 2021. Study of corrosion products induced under different environmental conditions. IOP Conf. Ser.: Mater. Sci. Eng. 1090, 012050. https://doi.org/10.1088/1757-899X/1090/1/012050

An attempt to classify the morphologies presented by different rust phases formed during the exposure of carbon steel to marine atmospheres, 2016. . Materials Characterization 118, 65–78. https://doi.org/10.1016/j.matchar.2016.04.027

Antunes, R.A., Costa, I., Faria, D.L.A. de, 2003. Characterization of corrosion products formed on steels in the first months of atmospheric exposure. Materials Research 6, 403–408. https://doi.org/10.1590/S1516-14392003000300015

Antunes, R.A., Ichikawa, R.U., Martinez, L.G., Costa, I., 2014. Characterization of Corrosion Products on Carbon Steel Exposed to Natural Weathering and to Accelerated Corrosion Tests. International Journal of Corrosion 2014, 1–9. https://doi.org/10.1155/2014/419570

Armacell USA [WWW Document], 2018. URL http://www.armacell.us/home/

Bouchar, M., Dillmann, P., Neff, D., 2017. New Insights in the Long-Term Atmospheric Corrosion Mechanisms of Low Alloy Steel Reinforcements of Cultural Heritage Buildings. Materials (Basel) 10. https://doi.org/10.3390/ma10060670

Bouchar, M., Foy, E., Neff, D., Dillmann, P., 2013. The complex corrosion system of a medieval iron rebar from the Bourges' Cathedral. Characterization and reactivity studies. Corrosion Science 76, 361–372. https://doi.org/10.1016/j.corsci.2013.07.007

Caines, S., Khan, F., Shirokoff, J., 2013. Analysis of pitting corrosion on steel under insulation in marine environments. Journal of Loss Prevention in the Process Industries 26, 1466–1483. https://doi.org/10.1016/j.jlp.2013.09.010

Caines, S., Khan, F., Shirokoff, J., Qiu, W., 2015. Experimental design to study corrosion under insulation in harsh marine environments. Journal of Loss Prevention in the Process Industries 33, 39–51. https://doi.org/10.1016/j.jlp.2014.10.014

Cano, H., Neff, D., Morcillo, M., Dillmann, P., Diaz, I., Fuente, D. de la, 2014. Characterization of corrosion products formed on Ni 2.4wt%–Cu 0.5wt%–Cr 0.5wt% weathering steel exposed in marine atmospheres. Corrosion Science 87, 438–451. https://doi.org/10.1016/j.corsci.2014.07.011

Cook, D.C., Oh, S.J., Balasubramanian, R., Yamashita, M., 1999. The role of goethite in the formation of the protective corrosion layer on steels. Hyperfine Interactions 122, 59–70. https://doi.org/10.1023/A:1012685320582

Cornell, R.M., Schwertmann, U., 2006. The Iron Oxides: Structure, Properties, Reactions, Occurrences and Uses. John Wiley & Sons.

de la Fuente, D., Díaz, I., Simancas, J., Chico, B., Morcillo, M., 2011. Long-term atmospheric corrosion of mild steel. Corrosion science 53, 604–617. https://doi.org/10.1016/j.corsci.2010.10.007

Furukawa, Y., Kim, J., Watkins, J., Wilkin, R.T., 2002. Formation of Ferrihydrite and Associated Iron Corrosion Products in Permeable Reactive Barriers of Zero-Valent Iron. Environmental science & technology 36, 5469–5475. https://doi.org/10.1021/es025533h

Geary, W., 2013. Analysis of a corrosion under insulation failure in a carbon steel refinery hydrocarbon line. Case Studies in Engineering Failure Analysis 1, 249–256. https://doi.org/10.1016/j.csefa.2013.09.001

Geary, W., Parrott, R., 2016. Two corrosion under insulation failure case studies. Loss Prevention Bulletin 2–6.

Hillier, A., Khan, F., Caines, S., 2021. Pitting and corrosion rates of coated, uncoated, and insulated A333 steel pipelines in marine harsh environment. Proceedings of the ASME 2021 40th International Conference on Ocean, Offshore and Arctic Engineering OMAE2021.

Jaen, J., Iglesias, J., Hernandez, C., 2012. Analysis of Short-Term Steel Corrosion Products Formed in Tropical Marine Environments of Panama. Hindawi Publishing Corporation, International Journal of Corrosion 2021, 11. https://doi.org/10.1155/2012/162729

Javaherdashti, R., 2014. Corrosion under insulation (CUI): A review of essential knowledge and practice. Journal of Materials Science and Surface Engineering.

Melchers, R.E., 2012. Long-term corrosion of cast irons and steel in marine and atmospheric environments. Centre for Infrastructure Performance and Reliability, The University of Newcastle, NSW 2308, Australia, Corrosion Science Elsevier.

Morcillo, M., Díaz, I., Cano, H., Chico, B., de la Fuente, D., 2019. Atmospheric corrosion of weathering steels. Overview for engineers. Part I: Basic concepts. Construction and Building Materials 213, 723–737. https://doi.org/10.1016/j.conbuildmat.2019.03.334

Oh, S.J., Cook, D.C., Townsend, H.E., 1998. Study of The Protective Layer Formed on Steels. Hyperfine Interactions c3 84–87.

Raman, A., Razvan, A., Kuban, B., Clement, K.A., Graves, W.E., 1986. Characteristics of the Rust from Weathering Steels in Louisiana Bridge Spans. Corrosion 42, 447–455. https://doi.org/10.5006/1.3583050

Refait, Ph., Jeannin, M., Sabot, R., Antony, H., Pineau, S., 2015. Corrosion and cathodic protection of carbon steel in the tidal zone: Products, mechanisms and kinetics. Corrosion Science 90, 375–382. https://doi.org/10.1016/j.corsci.2014.10.035

Roh, Y., Zhang, C.-L., Vali, H., Lauf, R.J., Zhou, J., Phelps, T.J., 2003. Biogeochemical and environmental factors in Fe biomineralization: magnetite and siderite formation. Clays Clay Miner. 51, 83–95. https://doi.org/10.1346/CCMN.2003.510110

Surnam, B.Y.R., Chui, C.-W., Xiao, H., Liang, H., 2016. Investigating atmospheric corrosion behavior of carbon steel in coastal regions of Mauritius using Raman Spectroscopy. Matéria (Rio de Janeiro) 21, 157–168. https://doi.org/10.1590/S1517-707620160001.0014

CHAPTER 5 – Electro-potential Noise Experiments Varying Electrode Size, Temperature, and Electrolyte

5.1 Preface

This paper will be submitted to a journal after appropriate editing is completed. The primary author is Alan Hillier and co-authors for this manuscript include Dr. Faisal Khan and Dr. Susan Caines. The primary author setup experiment, performed testing, lab analysis, completed literature review and prepared the draft manuscript. Dr. Susan Caines developed the concept of experiment, provided equipment, LabVIEW software, and provided feedback on manuscript. The co-author Dr. Faisal Khan provided feedback on the manuscript.

5.2 Abstract

In the present work, A36 rolled steel was used in novel 3 working electrode experiments measuring electrochemical potential noise (EPN). Twenty twelve-hour experiments with similar and asymmetrical electrodes of ~230 to 400mm^2 were placed in distilled water, seawater, and 3.5 weight percent NaCl. Temperatures varied with room, 40°C, and 70°C. A Keithly 3706A digital multimeter recorded EPN at 3hz using LabVIEW software. Statistical time and frequency analysis performed included skew, standard deviation (SD), kurtosis, transients, wavelet response, and Fast Fourier transform (FFT) power spectral density (PSD). Results were compared to physical features (microscope, SEM) and mass loss. Simplified-EPN method using potential area alone did not correlate with corrosion rate (CR). Statistical time and frequency FFT PSD and wavelets were best at determining corrosion mechanism, while standard statistical analysis did not work well for raw potential time records. These results confirm different types of corrosion can be detected using

only potential on common steel electrodes after manipulation to frequency spectrum using simple methods and equipment.

5.3 Introduction

Electrochemical noise (EN) describes fluctuations in potential and current on metal surfaces in electrolyte. Iverson (Iverson, 1968) used a voltmeter and different metals to show that unique potential fluctuations occur on corroding surfaces. Sometime afterwards Hladky and Dawson (Hladky and Dawson, 1981) found that crevice and pitting corrosion produced "noise signatures". Since then, methodologies such as ASTM G199 ("Standard Guide for Electrochemical Noise Measurement," n.d.) and different use cases and experiments have been performed by Bihade (Bihade et al., 2013) and Cottis (Cottis, 2001), and stress corrosion cracking (Ricker and Bertocci, 1996). EN analysis has also been used to test organic coatings (Jamali and Mills, 2016). Some recent reviews include practical applications of electrochemical noise by Obot et al (Obot et al., 2019) and another by Xia et al (Xia et al., 2020) completed a review on instruments, procedures, and traditional electrode setups. EN is a powerful passive measurement technique which can allow early-stage corrosion identification and does not require external signal applied (Caines et al., 2017a).

It is rare to use raw noise data without manipulation, however, Caines et al in (Caines et al., 2017b) related electrochemical potential noise (EPN) to corrosion rate using novel 3 working electrodes. A relationship was found where corrosion rate (CR) correlated highly with potential area (on potential-time curve). The highest EPN generated from a corroding electrode were related to highest mass loss in the same electrode for a given experiment. No other studies were found relating potential area curves to overall mass loss. Therefore, it should be further investigated.

However, many researchers have commented that “transients” in raw data correspond to localized corrosion, while “smoother” time series corresponded to more uniform corrosion.

For most researchers, potential is recorded from electrodes and afterwards other analysis performed to find underlying corrosion information (Mahjani et al., 2014). In time domain, statistical analysis of noise takes place to quantify (and predict) the corrosion mechanism using skew, kurtosis and standard deviation (SD) calculated from the raw time domain data. Going from time to frequency domain is especially useful, where often power spectra density (PSD) and wavelets are used to create energy density plots (EDP) which gives insight to corrosion activities (Smith and Macdonald, 2009). In the frequency domain signals are easily seen compared to raw data, for example, in wavelet plots, waves present in the time domain are separated and placed into separate series based on their crest-to-crest wavelength so that frequency specific corrosion processes can be noticed and compared for different experiments.

Some authors modified traditional methods, using just two or even four electrodes, some with large ($400mm^2$) or small areas ($<5mm^2$) (Bertocci et al., 2003), though typically authors used areas up to $200mm^2$ to measure potential and current (Cappeln et al., 2005), (Girija et al., 2005) (Mahjani et al., 2014). Area changes may greatly modify the readings of potential and current and so some recommended different size electrodes to enhance noise pattern recognition for different types of corrosion (Pistorius, 1997). Potential readings in free corroding situations are rich in information (Cheng et al., 2003). Later other authors changed the area and found more details compared to symmetrical electrodes (Shahidi et al., 2012). This area has an inversive effect on potential readings (the larger the electrode the smaller the readings) (Cottis, 2001) and it may reduce the SD (Xia et al., 2020). Later it was reported when electrode areas were increased, the SD decreases because of the increase of the interfacial capacitance and area for the cathodic reaction (Ma et al.,

2017). and some Researchers recently were still curious about the effect of modifying area while recording EN (Xia et al., 2020). Therefore, modifying electrode area is still an area of interest and rarely found, so, asymmetrical, and symmetrical working electrodes should be investigated to observe results.

In the present work, EPN generated from steel coupons was recorded while varying electrode size, temperature, and electrolytes to gain insights while using simple and standard equipment and bulk materials. S-EPN method, as well as statistical and time-frequency domains were used to further understand if S-EPN and/or using potential alone can account for meaningful corrosion data.

The paper organization is as follows, first the experiment details are summarized, then methodologies presented. Results discuss statistical analysis, S-EPN, wavelets with surface features, and then FTT PSD which are then compared to physical features and mass loss.

5.4 Experiment

In this study two types of electrodes were used, with 3 temperature settings, and 3 electrolytes. Therefore for 3 different factors, and 2 and 3 levels were used. While considering 2^k and 3^k factorial experiments, the number required (with one added for error) is a minimum of 17 + 1 experiments are required. A36 hot rolled steel was used as electrode with dimensions of 0.25 thickness, 0.75-1-1.25in width, and 1.25in height, with total area 230-400mm^2. 60 electrodes were used in 20 experiments (originally 18 was planned but two had to be redone). Prior to experiment each was sanded in stages to 1200 grit, cleaned with ethanol, dried, and weighted prior to experiment following (ASTM G1-03, 2003).

Copper wires attached to alligator clips were used as connection to electrodes. Transparent glass container was used for experiments and to hold electrolyte. Keithly 3706A as a digital multimeter

was connected to electrode wires and LabVIEW software was used to record EPN data over experiment at a rate of ~3Hz over 3 data points (data points ~130000 in 12hours) which is of a resolution capable to record EN data (Cottis, 2001). Simplified EPN method (Caines et al., 2017b) was used to calculate individual potential from each electrode and check potential time area compared to CR. Background noise was recorded from electrodes before being placed simultaneously in electrolyte. Baseline electrical recordings of potential were recorded between 0.0000013-0.0000017V, compared to 0.001-0.03V when in contact. A ceramic heater under glass was used to heat electrolyte. Experiments were ~12 hours in length, except in one case where building access was unavailable, and the experiment was ~24 hours.

Three electrolytes: distilled water, seawater with corrosive ions (Cl-, Na+, SO4, Mg2, dissolved gasses and others), and 3.5 wt. percent NaCl (similar Cl- in seawater but without other elements) were used in experiments (Acosta et al., 2014). Three different temperatures were used, room (18-22), 40°C, and 70°C.

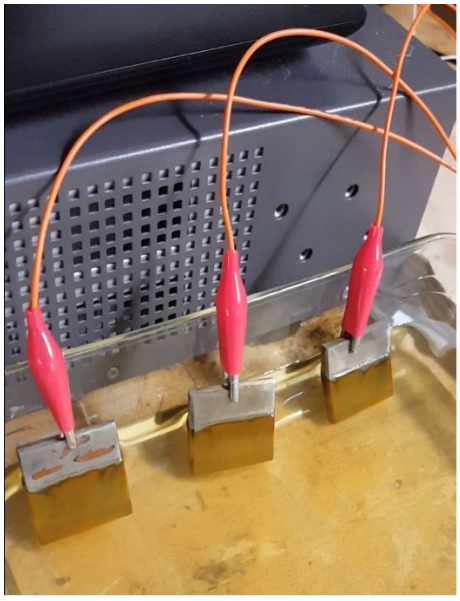

Figure 5.1: Experiment test of the system, light red/brown oxide clear on the electrodes.

Table 5.1: Experiment overview and trends for raw data. S is similar electrodes, and D is different.

Details For Each Experiment									
Experiment Number	Electrodes		Temperature			Electrolyte			Trends
	S	D	~18-22	40	70	Distilled	3.5% NaCl	Seawater	Most Potential with Highest CR
1	x		x			x			N
2	x		x			x			Y
3	x		x					x	Y
4	x		x				x		Y
5		x	x				x		N
6		x	x					x	N
7	x			x				x	N
8		x		x				x	N
9		x		x		x			N
10	x			x		x			Y
11		x			x	x			N
12	x				x	x			N
13		x		x			X		Y
14	x				x			x	N
15		x			x			x	Y
16	x			x			x		N
17		x			x		x		N
18	x				x		x		N
19	x				x		x		N
20		x			x		x		N

Following experiments, coupons were wiped of debris, photographed, weighted, and cleaned and reweighed (*NACE RP 0775-2005*, 2005). Post corrosion electrodes were cleaned using a 15% hydrochloric acid (HCL) solution inhibited with 10 g/L Dibutylthourea (DBT). Electrodes were randomly selected for SEM and microscope analysis.

5.5 Methodology

EN signals are composed of random, stationary, and direct current variables. It is important that noise not related to corrosion be removed before analysis ("Standard Practice for Preparation of

Metallographic Specimens," n.d.). As such, EN can be represented by equation below (Jáquez Muñoz et al., 2021):

$$x(t) = m_t + s_t + Y_t \quad (2)$$

Where *x(t)* is the EN time series, m_t is the DC component, s_t is the random component, and Y_t is a stationary component. The latter two are functions that define the corrosion system (Girija et al., 2005). This linear relationship was used as it can compare the potential vs time progression while removing the noise.

The component to remove the noise is below:

$$y_n = x_n - \sum_{i=0}^{p_o} a_i n^i \quad (3)$$

Therefore, to find signal without trend noise, Equation 3 is used where x_n is the noise signal, and the polynomial of "n" grade p_o at n^{th} term a_i in "n" time ("Electrochemical Noise Measurement for Corrosion Applications," n.d.) , (Liu et al., 2010). Figure 5.3 shows an example of original and potential with trend removed.

Time-domain statistical methods used in this research are skewness, kurtosis, transients measured with a moving average, and potential noise SD. If total sampling points on corroding electrode is *N* and the potential is *p*, then the expressions according to Mansfeld (Mansfeld, 2005) are below:

$$\text{Mean} = \mu_x = \frac{1}{N}\sum_{i=1}^{N}(\mu_i) \quad (4)$$

$$\text{Standard deviation} = \sigma_x = \sqrt{\frac{1}{N}\sum_{i=1}^{N}(X_i - \mu_x)^2} \quad (5)$$

$$\text{Skew} = \frac{\frac{1}{N}\sum_{i=1}^{N}(x_i - M_x)^3}{x_i^3} \quad (6)$$

$$\text{Kurtosis} = \frac{\frac{1}{N}\sum_{i=1}^{N}(x_i - M_x)^4}{(\sigma_x)^4} \quad (7)$$

Statistical calculations have a standard error (SE) that cause uncertainty in results. Where N is the number of data studied. Over larger data sets the SE is decreased (Eden, 1998).

$$SE = \sqrt{\frac{24}{N}} \qquad (8)$$

Time domain statistical analysis has been used extensively (Cappeln et al., 2005; Jamali and Mills, 2016; Shahidi et al., 2012) often referencing a patent to determine the corrosion mechanism from the calculations (*Official Gazette of the United States Patent and Trademark Office*, 1992). The direct current drift was removed prior to data analysis by a nine-order polynomial fitting for FFT, similarly, used by others (Jáquez M. et al., 2021).

5.5.1 Wavelet Analysis

Wavelet time-frequency statistical analysis was used to identify corrosion form at different wavelet crystals. The energy contribution of each crystal in the overall signal is given by Equation 8.

$$E_j^d = \frac{1}{E}\sum_{k=1}^{\frac{N}{2j}} d_{j,k}^2 (j = 1,2, \dots J) \qquad (9)$$

$$E_J^s = \frac{1}{E}\sum_{k=1}^{\frac{N}{2J}} s_{J,k}^2 \qquad (10)$$

Where $s_{J,k}$, $d_{j,k}$ are the wavelet coefficients, E_j^d is energy of wavelet detail of j level, E_J^S is energy of wavelet approximation $J(J = E + 1)$, $E$is wavelet level number, and N is the sampling number. Orthogonality of wavelets allow calculation of overall energy by the sum of $E_J^S$and E_j^dat each wavelet level:

$$E{=}E_J^s + \sum_{j=1}^{J} E_j^d \qquad (11)$$

Energy contribution of wavelet crystals has been related to corrosion type (Ma et al., 2017). Short time scale crystals (D1-D3) have been associated with activation-controlled processes. Medium time scale (D4-D6) crystals provide information on localized corrosion, while long time scale

processes (D7 and D8) relate to diffusion controlled/general corrosion and DC drift (Ma et al., 2017) (Homborg et al., 2012). Some have said that D8 to D12 are related to pitting corrosion (Smith and Macdonald, 2009). Determining time range from crystals is given by the following equation (Jáquez Muñoz et al., 2021)

$$\left(c_1^j, c_2^j\right) = (2^{-j}\Delta t, 2^{j-2}\Delta t) \quad (12)$$

where c is crystal and Δt is time display. Table 6 shows each crystal scale range in seconds and in Hz. High-frequency crystals are the first, and low-frequency phenomena are presented in the last crystals. For wavelet analysis both D1 to D8 and S8, as well as higher resolution D8-D16 as some other researchers with original time domain (Smith and Macdonald, 2009; Wharton et al., 2003). Percentages not displayed above D8 and D16 total 100. Wavelets are unique in that the DC drift component doesn't need to be removed from the raw data (Xia et al., 2020) as it is found in specific frequencies (Cao et al., 2006). No overfitting or data loss is present compared to polynomial fitting of other methods (FFT). Daubechies level 4 (db4) wavelet is highly localized in time and good for EN studies where short time duration events happen (Smith and Macdonald, 2005), as such, it was selected for use.

5.5.2 Power Spectral Density using FFT

Often EPN are analyzed using FFT technique to obtain the PSD plot which is used to find the corrosion characteristics (Yi et al., 2018) by plotting power per unit frequency on a logarithmic scale (Bertocci et al., 1997). The slopes of PSD plots reflect the corrosion mechanism by the linearity of slope (either entirely or after roll-off), the degree of the slope, and the frequency dependent area (flat slope can indicate passivation). When the slope is ~-4, it tends to represent general corrosion, while slopes ~-2 indicate pitting (Acosta et al., 2014).

Before the data was transformed to frequency domain with FFT, a Hann window was applied (Oppenheim et al., 1999):

$$w(n) = 0.5(1 - \cos(2\pi \frac{n}{N})), \ 0 \leq n \leq N \quad (13)$$

$$R_{xx}(m) = \frac{1}{N}\sum_{n=0}^{N-m-1} x(n) * x(n+m) \quad (14)$$

While (13) is from $0 < m < N$

$$\varphi_{x(k)} = \frac{\gamma * t_m}{N}\sum_{n=1}^{N}(x_n \bar{x}_n)e^{\frac{-2\pi k n^2}{N}} \quad (15)$$

$$log\varphi_x = -\beta_x log f \quad (16)$$

The frequency zero limit (Ψ0) gives material dissolution information because the PSD is related to total energy present in the system (Mehdipour et al., 2014).Results and Discussion

Here, characteristics of the potential time series, corrosion mechanism and analysis of findings are discussed. Statistical time domain (Skew, kurtosis, SD, variance), S-EPN procedure, frequency domain (FFT PSD), and time-frequency (wavelets) were applied to potential-time series to extract corrosion information.

5.5.3 Statistical Analysis, EPN, and Sample Area

Skew and kurtosis of EPN was used to determine corrosion mechanism based on kinetic. The application of statistical results to determine mechanism was discussed previously by many authors, Cottis, Eden and others (Montoya-Rangel et al., 2020) (Gaona-Tiburcio et al., 2014) (Eden et al., 1987) (Eden, 1998) (Al-Mazeedi and Cottis, 2004). Looking for a better method, Eden and Reid proposed corrosion type by skewness and kurtosis (Reid and Eden, 1999). Some authors agreed with the method (Cappeln et al., 2005) and it is still frequently found in literature, however, the results sometimes presented divergences in data and was inconsistent for some experiments

and electrolytes (Jáquez M et al., 2021). For this reason, it will be investigated it applies to the current research, or if it is not accurate.

From the procedure of the patent, two or more electrodes of the same material are measured regarding a third electrode. After trend removal (shown in Figure 5.3) statistical analysis is completed. When large skew is present, the data is "skewed" towards the side of +, -. A low skew means the data is generally presented around 0. In kurtosis, a 0 value is like a normal distribution, but a + value makes the mean higher, and tails shorter, while the opposite true for negative value. The patent (Reid and Eden, 1999) regards kurtosis <3 as general corrosion when skewness <+/-1, and pitting corrosion when skewness <-2 and kurtosis >>3. Though general and pitting corrosion occurred on many samples, the methodology of the patent did not apply to most of this data, and this was similarly found with other researchers who criticized its use (Obot et al., 2019). When comparing results in Table 5.2 and Table 5.3, there are no common signals to describe the corrosion mechanism based on skew and kurtosis. Significant error calculated for skew and kurtosis for experiments was ~0.025. From Table 5.2 skew calculation with or without error do not change the values enough to change its result definitions as recommended by the authors of the patent.

Experiments 5, 6, 8,9,11, 13, 15, 17, and 20 had three electrodes arranged ~235mm^2, ~313mm^2, and ~390mm^2 respectively (asymmetrical electrodes but otherwise identical). Other experiments were arranged as identical area (or as close as possible, sometimes due to the cutting large electrodes areas were slightly different). When recording EPN, it is assumed generally the smallest area exposed would generate the largest EPN area curves (v*s) due to lower capacitance while the system in the same electrolyte would have similar CR. However, in only 4/9 cases was the highest potential generated from the smallest electrode. Other researchers (Shahidi et al., 2012) found for

larger surface area differences (comparing current transients 4mm^2 vs 22mm^2 or 22 mm^2 vs 202 mm^2) in same material electrodes leads to overlapping of electrochemical events but reduces their detection. In other words, by increasing the area of similar electrodes in the same system, generally more transients would be detected but not increased in magnitude.

In the present case however, in Table 5.4, there appears no difference in SD for potential-time series for varied/symmetrical systems. One difference comparing results to Dr. Shahidi et al is their use of current noise and ZRA, while in the present case only potential from electrodes is being recorded.

Standard deviation results are presented in Table 5.4. Highlighted values are different sized electrodes (smallest to largest). X is the highest CR in each experiment. While the area of electrode size increases, the SD should decrease (Xia et al., 2020) but this was not shown in the majority of cases in highlighted cells. It may be that the difference in area is not great enough for observing differences. For similar corrosion behavior with different size electrodes, it should show that the SD is less on the third electrode, while this was not the case, and no trend was observed using SD and variance and area. However, highest variance and highest SD led to highest CR in 9/20 and 10/20 cases respectively. This may be due to the transients in data, where short term changes cause movements away from longer mean. Regarding SD and variance, in cases where highest CR was found, generally both values confirm the result, there may be no benefit in using both.

5.5.4 S-EPN Analysis

For individual electrode CR vs potential-time area, it did not correlate as compared to (Caines et al., 2017b). In 6/20 experiments (4 with similar/2 asymmetrical electrode sizes) electrodes with the highest mass loss/CR were largest in absolute potential recorded (v*s curve). Mirroring and removing the two electrode couples did not change this, also, it was previously reported (Caines

et al., 2017b) corrosion was similar when potentials of electrodes were similar in the same experiment, however, only 4/20 (1,2,3,19) experiments showed this clearly. Most raw EPN data in experiments looked like Figure 5.3. In Figure 5.3 applying S-EPN procedure, V2 being different than the other 2 electrodes was theorized to have the highest mass loss. In this case it was true, however for 14/20 experiments the largest potential area did not equate to highest CR. Detrended data was used for all calculations except wavelets, and is shown in purple, green, and light blue in that example.

Figure 5.2 shows the general trend for potential area (v*s) vs CR. High CRs may occur with low potential, and vice-versa which means that other methods are necessary to quantify/qualify corrosion. Linear trend didn't take place when experiments were considered in temperature or immersion times (considering EPN) vs CR. CR did generally increase with temperature as shown in Figure 5.4. Therefore, S-EPN was not accurate in these experiments regarding corrosion mechanism or quantification.

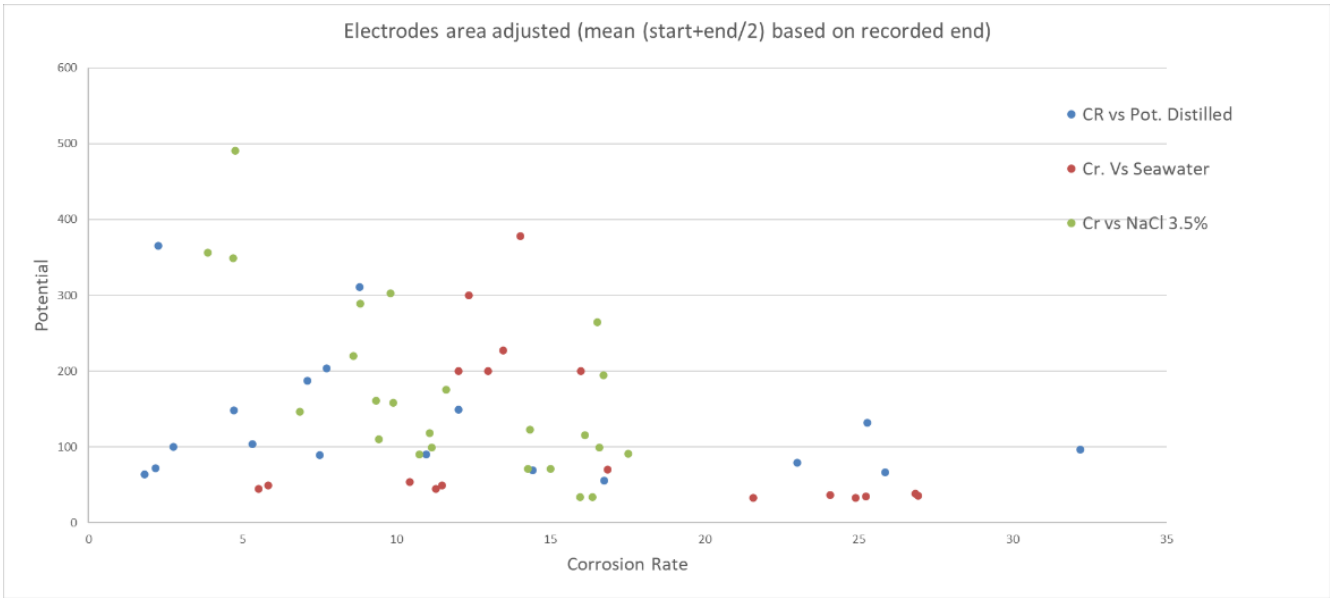

Figure 5.2: Total absolute electrode area vs CR. No clear trend was visible.

Table 5.2: Skewness values and the type of corrosion visible on the surface. Bold values are asymmetrical electrodes.

Experiment	Electrode			Type Corrosion
	1	2	3	
Data skewness towards +/-/0. Uni/Loc is SEM confirmed corrosion type				
1	0.1	0.1	0.1	uniform
2	2.6	12.4	9.4	uniform
3	16.5	21.4	30.9	localized
4	48.3	31.0	28.5	localized
5	31.1	32.3	24.6	localized
6	-1.2	-2.1	-5.6	localized
7	-0.7	0.1	0.1	localized
8	1.7	5.5	0.0	localized
9	0.9	1.2	0.9	uniform
10	0.1	0.2	-0.4	uniform
11	**-6.3**	**8.2**	**-1.4**	localized
12	**-6.4**	**-4.2**	**-3.0**	localized
13	-0.5	1.2	0.0	localized
14	**0.2**	**0.2**	**-0.8**	localized
15	**39.5**	**17.3**	**44.7**	localized
16	-0.5	-1.1	-0.5	localized
17	**0.1**	**1.2**	**1.7**	localized
18	**1.2**	**0.1**	**1.2**	localized
19	**18.0**	**11.5**	**11.6**	localized
20	**0.9**	**0.7**	**0.7**	localized

Table 5.3: Kurtosis values and type of corrosion visible on the surface. Bold values are asymmetrical electrodes.

Experiment	Electrode			Type Corrosion
	1	2	3	
Kurtosis: ++ has mean distinct and fall off to edges as in T-dist.				
1	17.0	13.1	15.3	uniform
2	472.0	87.0	297.0	uniform
3	0.0	0.0	0.0	localized
4	0.0	0.0	0.0	localized
5	0.0	0.0	0.0	localized
6	122.2	60.0	115.8	localized
7	168.9	55.3	55.3	localized
8	141.0	342.3	98.0	localized
9	7.1	12.1	8.3	uniform
10	11.4	10.4	15.1	uniform
11	**168.5**	**292.6**	**54.4**	localized
12	**116.5**	**121.1**	**101.0**	localized
13	12.2	29.2	14.3	localized
14	**106.9**	**75.1**	**94.3**	localized
15	**0.0**	**0.0**	**0.0**	localized
16	17.6	24.7	9.3	localized
17	**11.4**	**49.9**	**37.7**	localized
18	**18.8**	**34.9**	**22.9**	localized
19	**604.6**	**329.4**	**346.8**	localized
20	**18.5**	**22.1**	**14.5**	localized

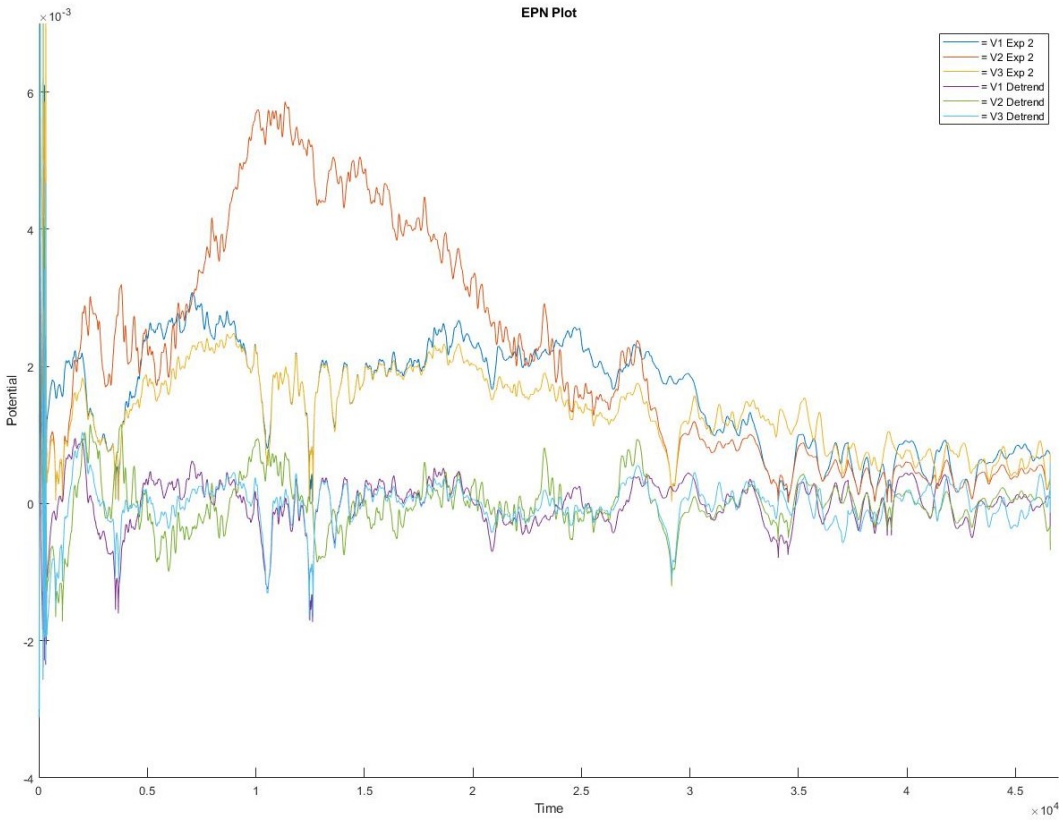

Figure 5.3: Experiment 2 distilled water plot. Upper blue, red, and yellow lines were V1, V2, and V3, respectively.

Table 5.4: Highlighted experiments have different sized electrodes; X marks highest CR. Bold is highest value in experiment.

	Electrode			Electrode		
	1	2	3	1	2	3
Experiment	Standard Deviation			Variance		
1	0.0032	**0.0045** X	0.0028	0.000010	**0.000020** X	0.000008
2	0.0008 X	**0.0017**	0.0007	0.000001 X	**0.000003**	0.000000
3	0.0033 X	**0.0034**	0.0030	0.000011 X	**0.000012**	0.000009
4	**0.0024**	0.0020 X	0.0022	**0.000006**	0.000004 X	0.000005
5	0.0015	**0.0022** X	0.0015	0.000002	**0.000005** X	0.000002
6	0.0012	0.0014	**0.0014** X	0.000001	0.000002	**0.000002 X**
7	**0.0047** X	0.0022	0.0042	**0.000022** X	0.000005	0.000017
8	0.0036 X	0.0043	**0.0057**	0.000013 X	0.000019	**0.000032**
9	0.0017	0.0022 X	**0.0050**	0.000003	0.000005 X	**0.000025**
10	0.0026 X	**0.0070**	0.0027	0.000007 X	**0.000048**	0.000007
11	0.0013	0.0013	**0.0015** X	0.000002	0.000002	**0.000002 X**
12	**0.0027** X	0.0019	0.0015	**0.000007** X	0.000004	0.000002
13	**0.0034** X	0.0014	0.0018	**0.000012** X	0.000002	0.000003
14	0.0020	**0.0022**	0.0018 X	0.000004	**0.000005**	0.000003 X
15	0.0013	**0.0015** X	0.0012	0.000002	**0.000002** X	0.000001
16	0.0014	**0.0018**	0.0013 X	0.000002	**0.000003**	0.000002 X
17	0.0014 X	**0.0034**	0.0018	0.000002 X	**0.000012**	0.000003
18	**0.0032**	0.0024 X	0.0032	0.000003	**0.000017** X	0.000011
19	0.0026	0.0029	**0.0030** X	0.000007	0.000008	**0.000009** X
20	0.0012	**0.0024** X	0.0010	**0.000009**	0.000006 X	0.000001

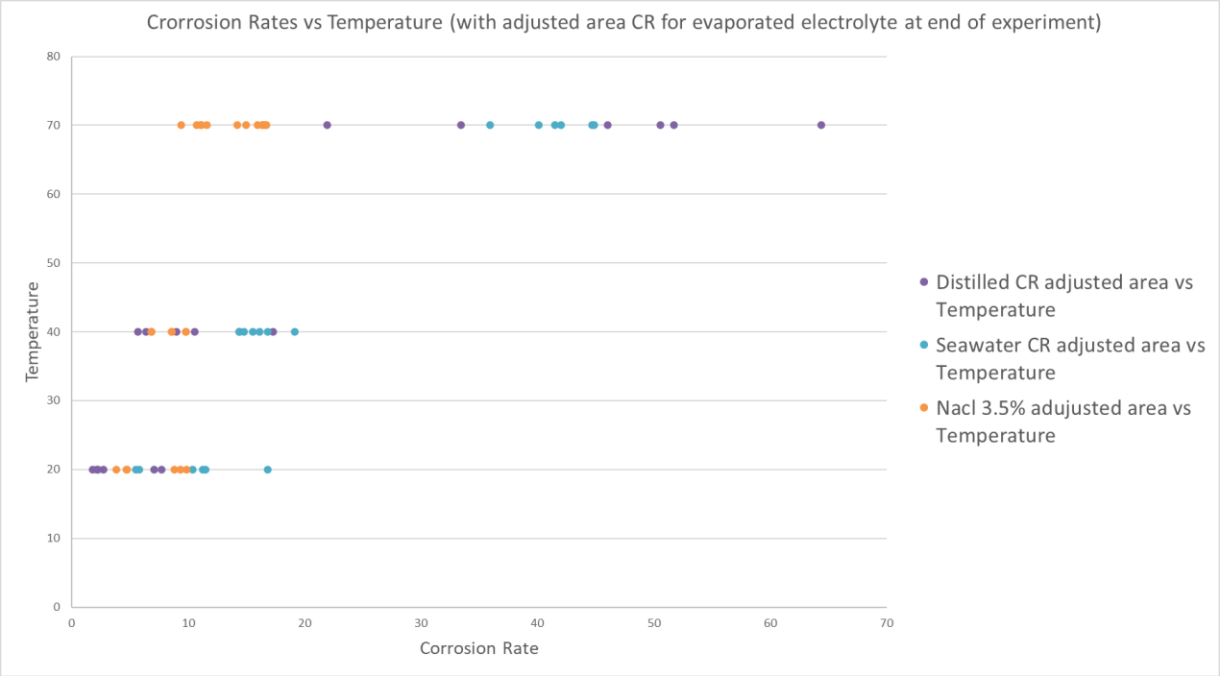

Figure 5.4: Consistently seawater has the higher corrosion rates as temperature is increased.

5.5.5 Wavelet Analysis

Wavelet analysis was used on potential time series to obtain information on corrosion mechanisms. A typical use is coefficient crystals D1 to D8 (Jáquez Muñoz et al., 2021, p. 04; Shahidi et al., 2012; Smith and Macdonald, 2009; Suresh and Mudali, 2014) and while some others have used to D16 against the time domain of the original signal (Moshrefi et al., 2014) to create energy distribution plots (EDP). Because different corrosion characteristics take place over the course of an experiment showing processes starting/dying they will be graphed compared to the original time domain. Because of the extent of the data, two of each type of experiment is presented, further data is available upon request.

The position of the maximum relative energy distribution of a crystal corresponds to the dominant process contributing to the signal. This can be shown as a cumulative total in the D1-D8 graphs, or instantaneously in D1-D16 vs original time series EDP. Time scale crystals are ranked from D1

to D8, where D1 is the lowest time frequency interval, while D8 is highest. For an eight-level decomposition of energy dispersion plot, it can be divided into three zones (Homborg et al., 2013). The distribution on smaller time scale crystals, D1-D3, gives information about high frequency events such as pitting. D3-D6 gives medium frequency signals associated with re-passivation or further propagation of pits. D6-D8 represent low frequency crystals and provide information on diffusion and growth of pits. Using the charts, D1 to D3 were of the range 1s to 8s, D3-D6s was 8s to 64s, and D5 to D8 was 32s to 256s. Time span per crystal is shown in Table 5.5. Each crystal corresponds to the time scale of corrosion events. As such, different wave time crests (with possibly different types of corrosion) will occur, and it will be shown on wavelet charts.

For (Suresh et al., 2005) it was said that pitting/nucleation process occurs in higher frequency processes (sharper waves on a potential-time graph are known as transients). At initial immersion, nucleation occurs as the steel passivates, and on most figures, there are initial spikes on immersion. In (Yi et al., 2018) copper was corroded at different temperatures and it was observed that metastable pitting/nucleation process occurs quickly and before general corrosion/diffusion processes as in the present cases. Large potential values at the start of the experiment are nucleation processes, and then become general corrosion later as passivation occurs. This was confirmed by SEM and FFT PSD figures in 5.7 Visual Comparison section.

The charts in (Yi et al., 2018) show that when temperature increases, potential values/transients change, and pitting/corrosion increase which was observed for higher temperature experiments in Figure 5.4. Experiment 10 had pits, unlike Experiment 2 as shown in the Section 5.7. This was observed with wavelet energies and for physical CR as in Figure 5.4 where seawater has the higher corrosion rates as temperature is increased. This chart included the change in height of the electrolyte through experiment verse the CR which shows that overall, higher temperatures

increase CR. Without area adjustment, generally, seawater had the highest CR and CR increased with temperature in most cases.

Note for the plots below that wavelet energy totals 100. After D1-D8, the remained of each electrode totals 100%. For example, in Figure 5.5 total energy seen in D1-D8 is ~4% while the remainder in the system is ~96%, most of which may be DC noise, as no localized corrosion was observed.

Table 5.5: Range of scale of each crystal

Crystal	Scale (s)	Scale (Hz)
1	1-2	1-0.5
2	2-4	0.5-0.25
3	4-8	0.25-0.125
4	8-16	0.125-0.0625
5	16-32	0.0625-0.03125
6	32-64	0.03125-0.015625
7	64-128	0.15625-0.00781
8	128-256	0.0078-0.0039

5.5.6 Distilled Experiments

Distilled water experiments for room and 40°C temperature show that D3/D6, and then D7 hold the most energy in EDP. Figure 5.5 shows that mixed activated processes are occurring. In Figure 5.6 when viewing at the start of the experiment D5, D12, D15 are active then drops to near 0 except the last half of the experiment, where again they raise in small amounts. Figure 5.7 with V2 is similar but during the last part of the experiment D10-D15 has increased readings, the same occurs on V1 in Figure 5.8. Having most energy above D8 is a large-scale time process, which can be DC drift, and/or general corrosion. Some processes happen after the halfway point in the experiment, but it is unknown which type, only that reactions are occurring. SEM microscope confirms the surface had general corrosion in Figure 5.42.

For Experiment 10 (details shown in Figure 5.9, Figure 5.10, Figure 5.11, Figure 5.12, and Figure 5.13), distilled with higher temperature V3 and V1 show similar energy profiles, while V2 shows general corrosion at the beginning and end of the experiment. However, different spikes in energy are recorded throughout the experiment in Figure 5.10. Corrosion rate was higher, and though general corrosion took place; some pitting was found on the surface of SEM microscope as shown in Figure 5.45.

Looking at Experiment 10 in Figure 5.9 show D7 peak. Because heated distilled water is present and most of the spikes occur in the first hours of immersion uniform corrosion is likely. However, SEM images confirm very few small pits Figure 5.45 and as such, some localized corrosion is occurring. D8-D15 crystals show considerable activity throughout the experiment compared to Experiment 2 and may be related to pitting activity (Smith and Macdonald, 2009).

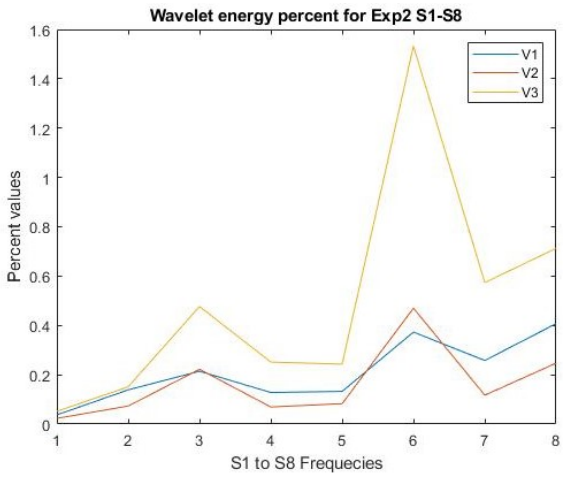

Figure 5.5: Experiment 2, room temperature distilled water.

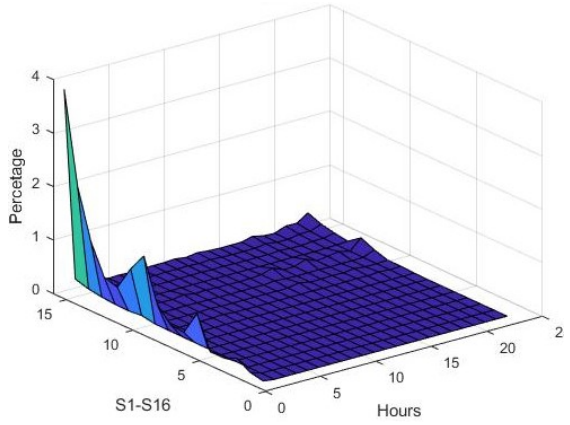

Figure 5.6: Experiment 2 V3

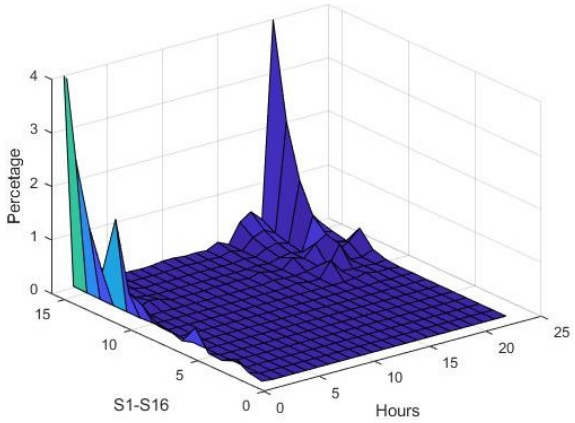

Figure 5.7: Experiment 2 V2

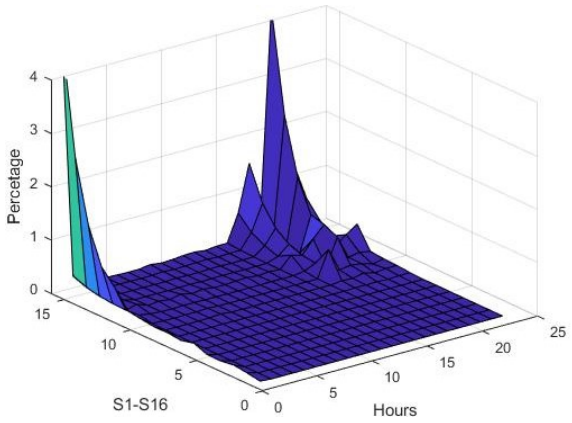

Figure 5.8: Experiment 2 V1

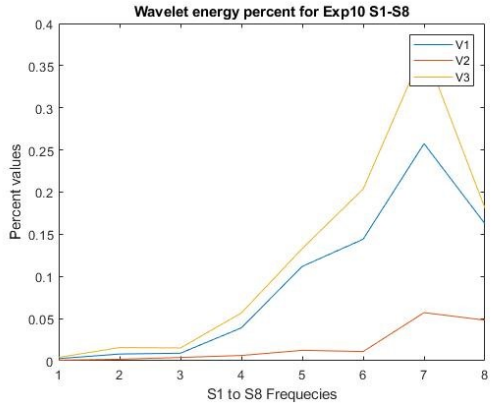

Figure 5.9: Peaks at D7, which sometimes is general corrosion or DC drift, in this case general and localized resulted from SEM images presented below.

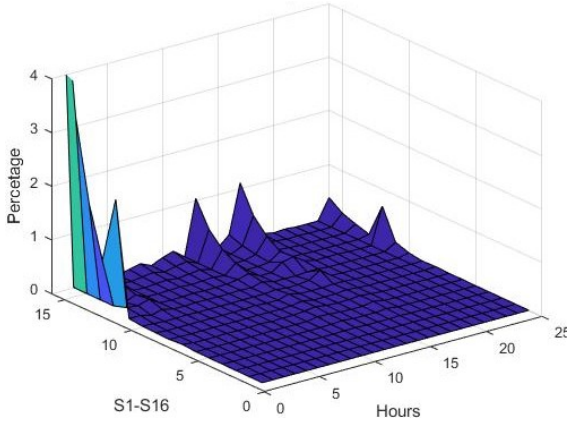

Figure 5.10: Experiment 10, V3

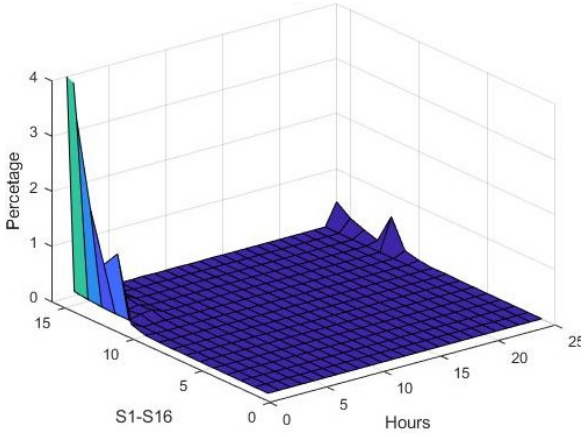

Figure 5.11: Experiment 10, V2

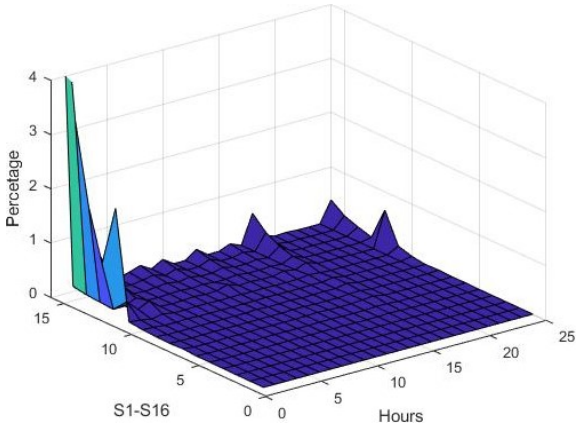

Figure 5.12: Experiment 10, V1

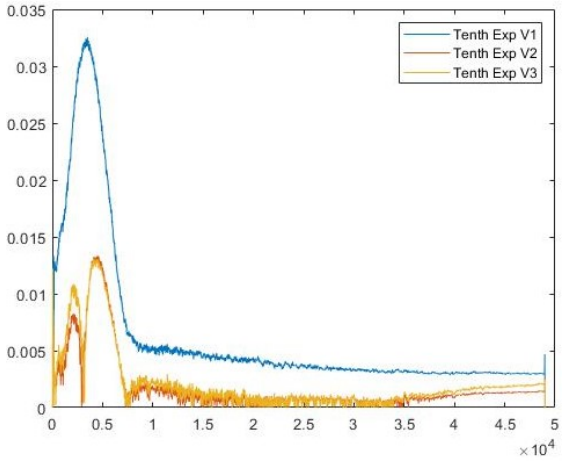

Figure 5.13: The EPN chart had transients like other seawater and NaCl. It may have been contaminated.

5.5.7 3.5% wt. NaCl Experiments

Room temperature Experiment 5 (shown in Figure 5.14, Figure 5.15, Figure 5.16, and Figure 5.17) has peak energy in D3/D4 and D7/D8 in Figure 5.14. D7-D12 show multiple times in wavelet plotted as original time below. Localized corrosion with pitted surface images confirmed in Figure 5.52 and Figure 5.51.

One difference to note with Experiment 18 (Figure 5.18, Figure 5.19, Figure 5.20, Figure 5.21, and Figure 5.22) is that, due to the high temperature much of the water evaporated by the end of the experiment, and concentration would have been higher. D8 was the highest energy crystal

overall, and high initial immersion jump showing on all electrodes starting in Figure 5.19 is very high.

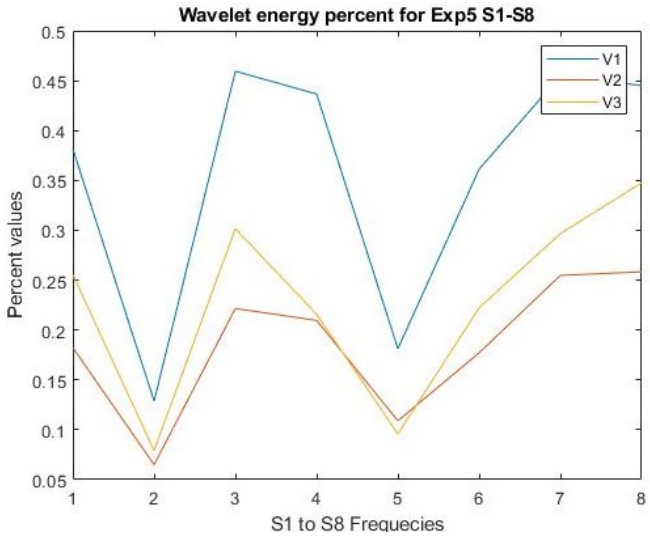

Figure 5.14:Smallest electrode area has higher energy.

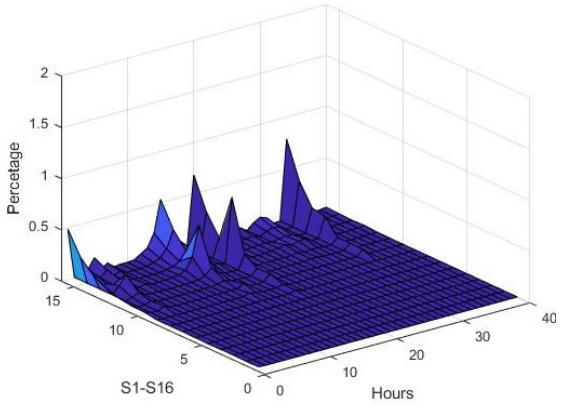

Figure 5.15: Experiment 5 V3

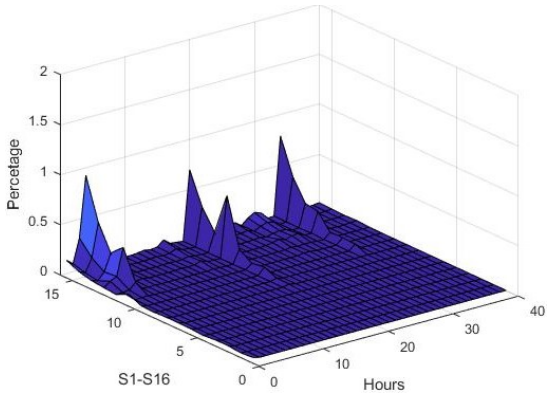

Figure 5.16: Experiment 5, V2

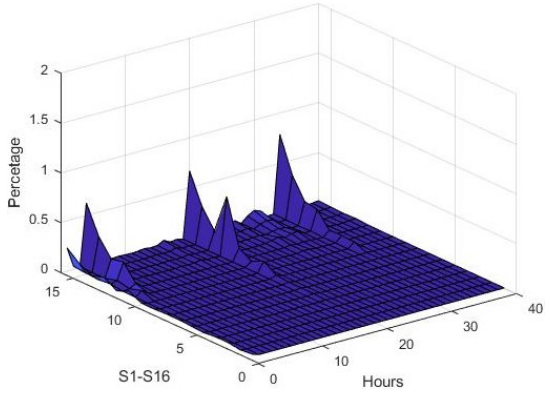

Figure 5.17: Experiment 5, V1

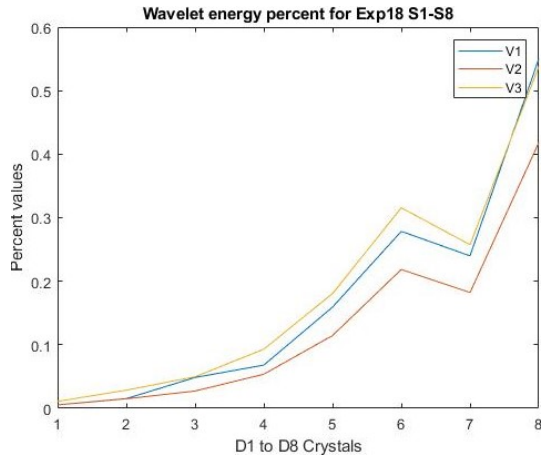

Figure 5.18: Experiment 18

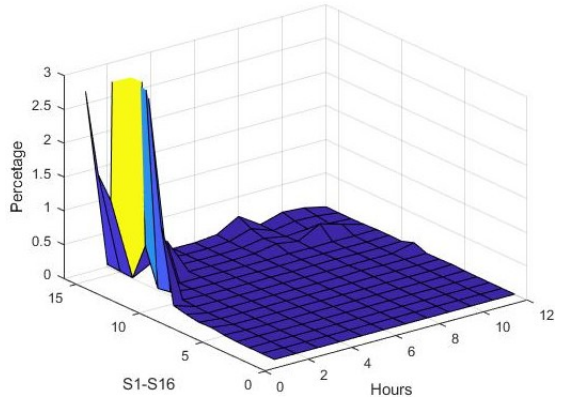

Figure 5.19:Experiment 18 V1

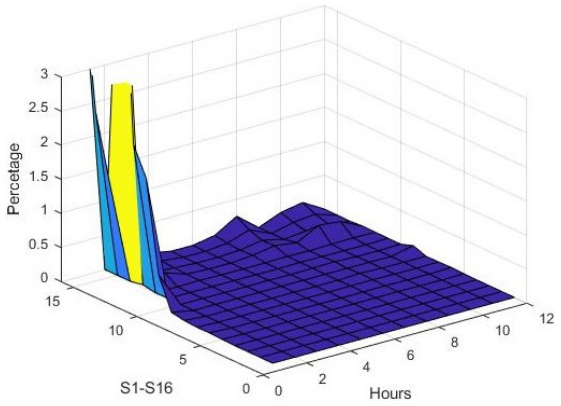

Figure 5.20: Experiment 18 V2

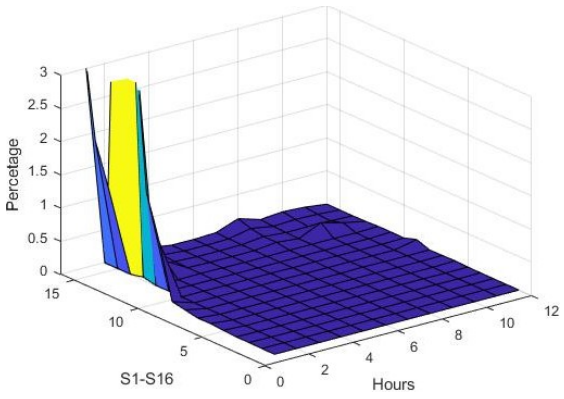

Figure 5.21: Experiment 18 V3

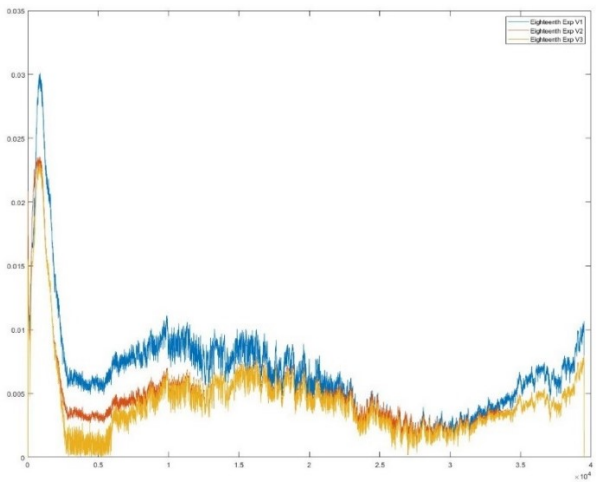

Figure 5.22: Raw EPN Experiment 18

5.5.8 Seawater Experiments

Experiment 6 (Figure 5.23, Figure 5.24, Figure 5.25 and Figure 5.26) was room temperature seawater, has highest energy occur in D5-D6, and saw activations through D7 to D16. Surface features shown in Figure 5.46. Experiment 8 (Figure 5.28, Figure 5.29, Figure 5.30, Figure 5.31 and Figure 5.32) was 40°C and exposed to seawater with similar findings to Experiment 6. Surfaces are shown in Figure 5.47 and Figure 5.48 confirming localized corrosion and common iron oxides formed in seawater atmospheric corrosion.

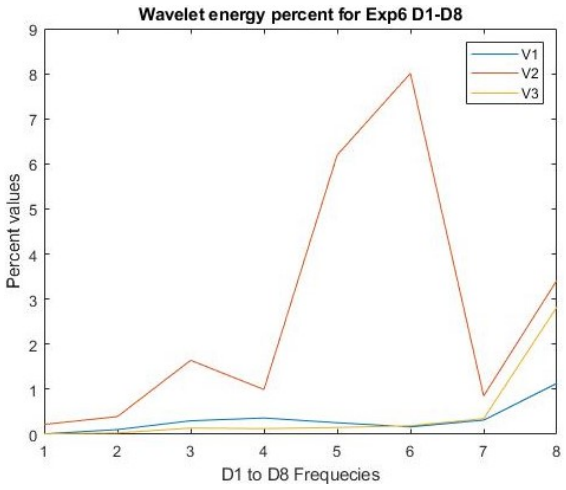

Figure 5.23: Experiment 6

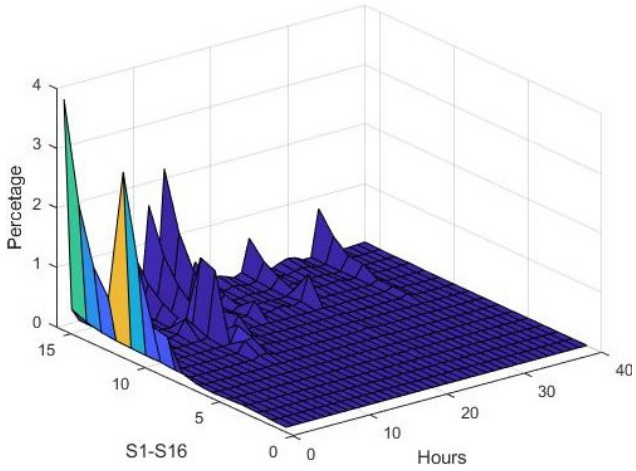

Figure 5.24: Experiment 6 V1

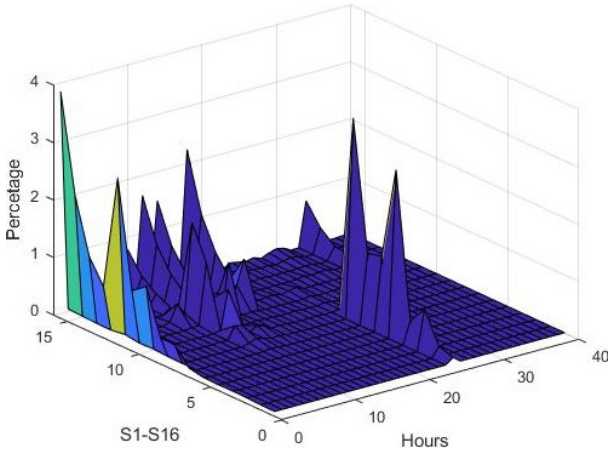

Figure 5.25: Experiment 6 V2

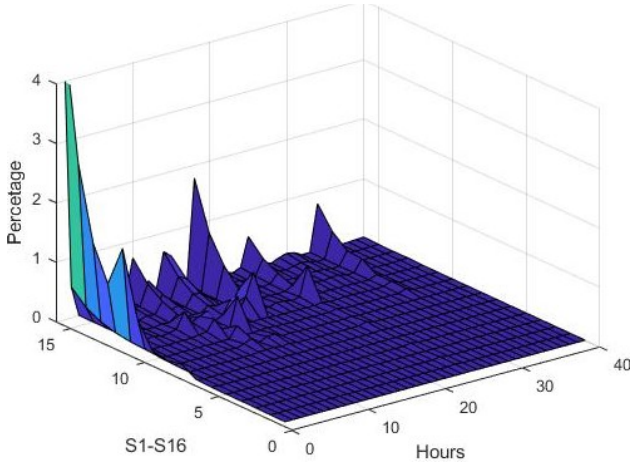

Figure 5.26: Experiment 6 V3

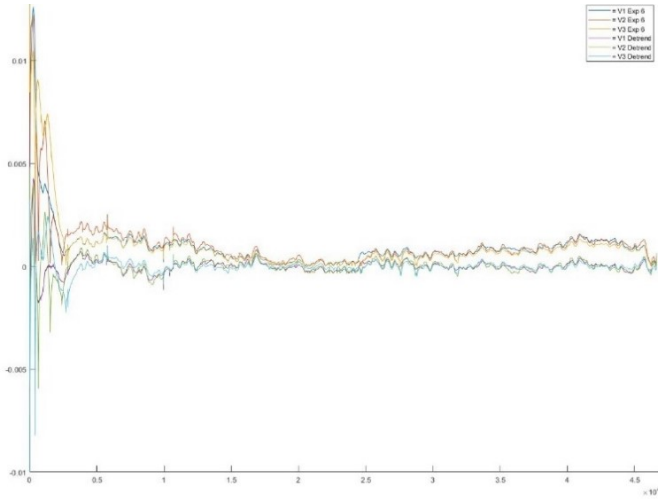

Figure 5.27: Experiment 8 EPN with detrend

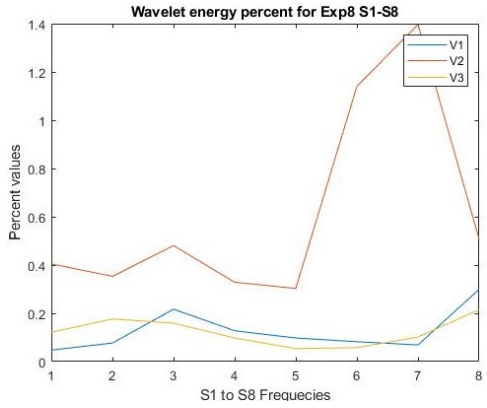

Figure 5.28: Experiment 8 D1-D8

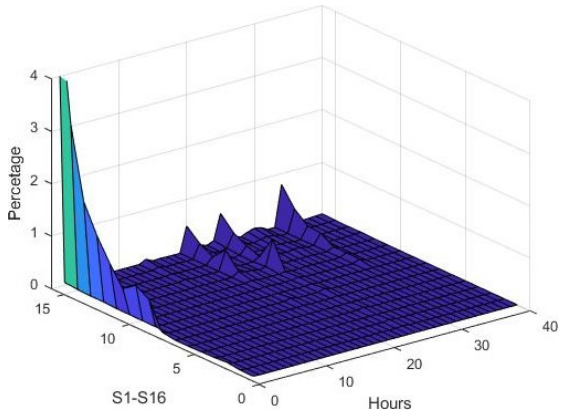

Figure 5.29: Experiment 8 V1

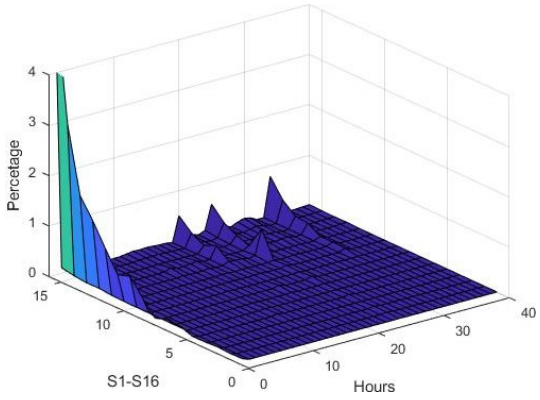

Figure 5.30: Experiment 8 V2

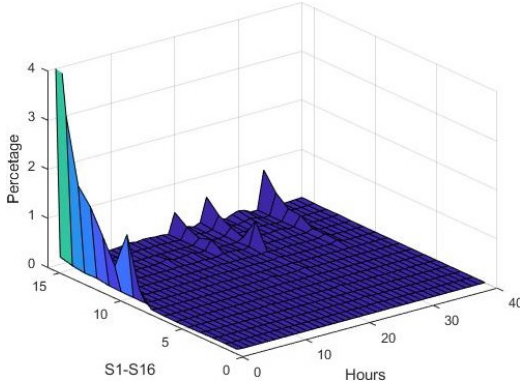

Figure 5.31: Experiment 8 V3

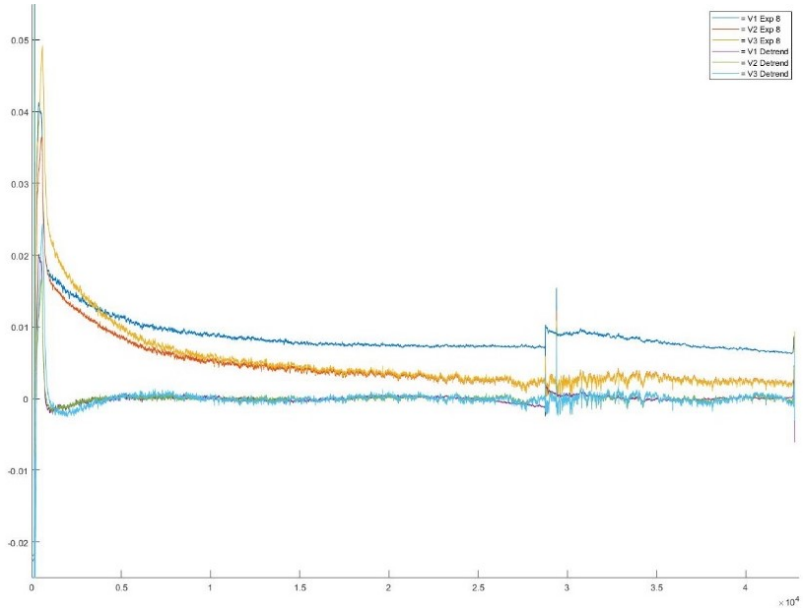

Figure 5.32: Experiment 8 EPN with detrend

5.5.9 Transients, Moving Average, Wavelets, Potential Area, and Average CR

For transients in EPN, 8/20 experiments showed highest moving averages related to highest mass loss, and some examples of transients and wavelet measuring are shown here. Measuring time from crest to crest shows the crystal(s) the waves would fall under, which are displayed in a wavelet plot.

Figure 5.33 EPN transients compare to Figure 5.28, where a large wave from 980 to 1020 ~40 seconds is shown corresponding to D6 energy. Larger D7 (not shown) were most common on the time series and correspond to pitting. Other waves shown are D3 ~8 seconds (980 to 988 and elsewhere in Figure 5.28). Figure 5.34 NaCl experiment 18, wavelets shown include, D2(~3s), D3(5s), D4 (10s). In that experiment D8 and higher represented the most energy, which can correspond to DC noise. In Figure 5.35 distilled water, D3 and D6 dominate. Also Figure 5.35, D5/D6 are shown from 3980 to 4010 and 3960 to 3990.

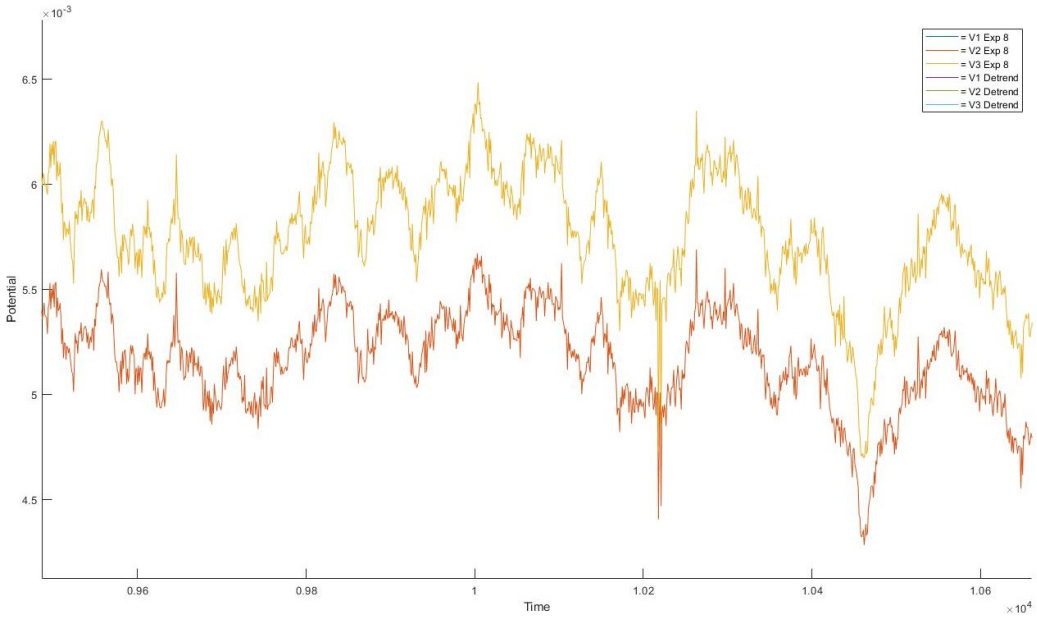

Figure 5.33: Seawater

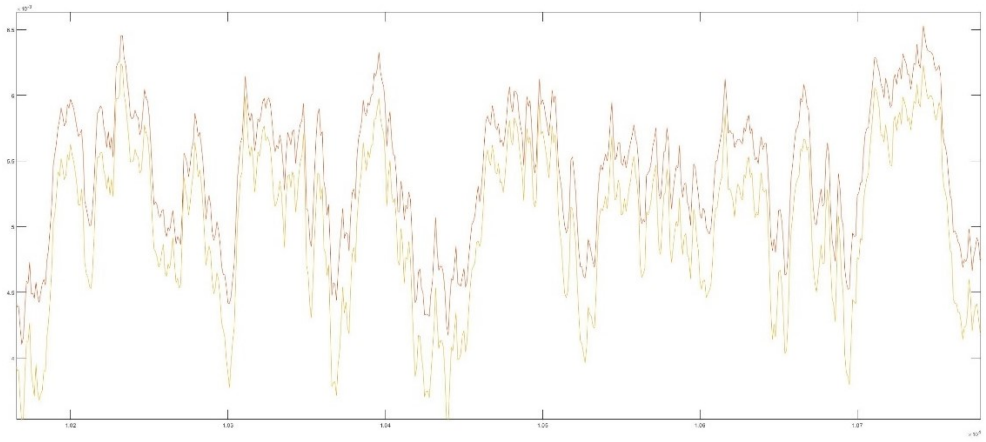

Figure 5.34: NaCl exp 18

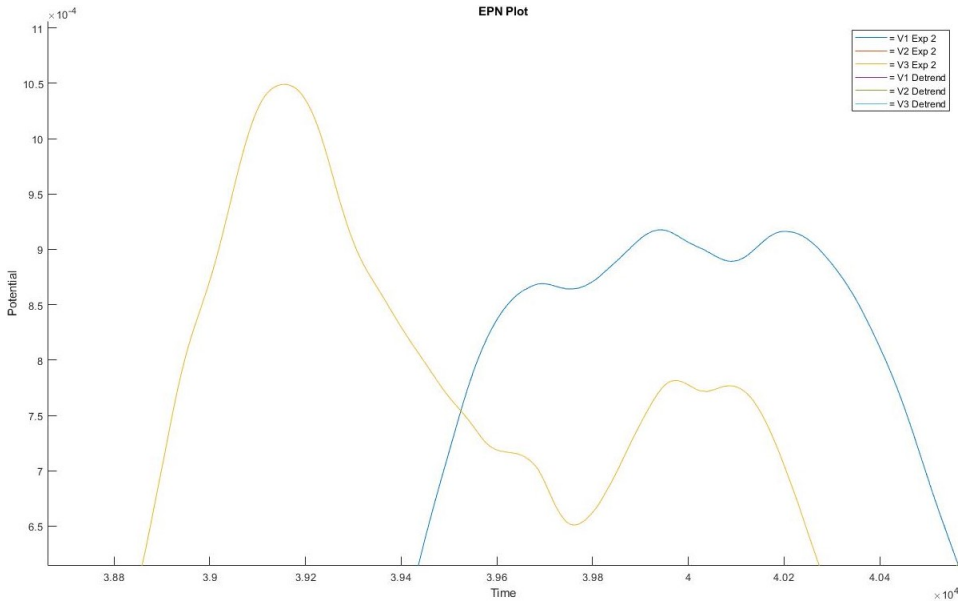

Figure 5.35: Distilled water

5.5.10 PSD FFT

In this section, using PSD FFT graphs showed different slopes were related to different types of corrosion. Searson, Dawson (Searson and Dawson, 1988) and others (Hladky and Dawson, 1981) (Smith and Macdonald, 2009) have obtained steep slopes of −4 for general corrosion and roll-off slopes of -2 or less for pitting in PSD FFT graphs. Comparable results are presented here. Linear slopes occur in most distilled samples verses a varied/changing slope in seawater and NaCl.

Average roll-off slopes were calculated for each experiment (1-20). Values for distilled, NaCl, and seawater were -3.9, -2.4, and -2.8 respectively as shown in Table 5.6. Typical general corrosion with constant slope shown in experiment 2 in Figure 5.36 that appears to be general corrosion which was confirmed by SEM and mass loss. Heated distilled water experiment 10 showed chart similar characteristics to localized corrosion, but with less slope after roll-off and more passivation in Figure 5.37. It is possible it was contaminated before experiment, or perhaps due to 40°C temperature. Seawater (Figure 5.38 and Figure 5.40) and NaCl (Figure 5.39) experiments showed typical localized corrosion roll-off slopes and sometimes passivation with frequency dependence at end of experiment as in Figure 5.41.

Table 5.6: PSD average slopes matching other researchers.

Slope Average Distilled	-3.9
Slope Average 3.5% NaCl	-2.4
Slope Average Seawater	-2.8

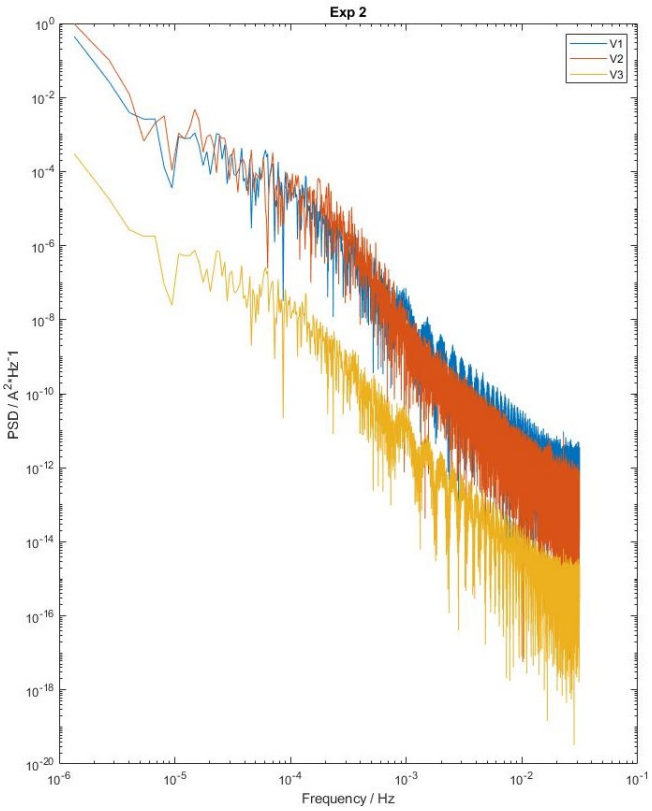

Figure 5.36: Slope generally unchanging, -4.8 slope, no passivation showing.

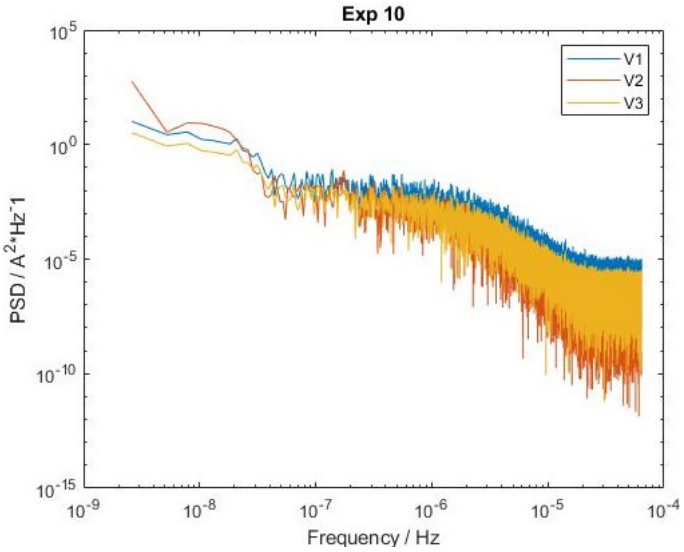

Figure 5.37: Distilled water heated to 40°C showing roll-off like localized corrosion and slope of -2.5 normal range of local corrosion, passivation at end due to flattened slope. On surface some minor pitting was observed.

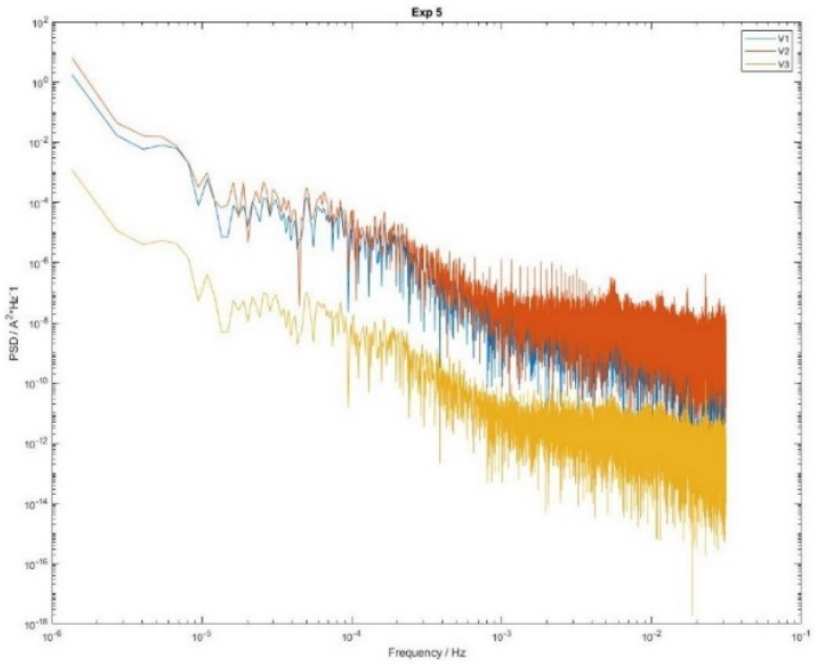

Figure 5.38: Room temperature seawater with slope -3.1 is indictive of localized corrosion. After slope, frequency dependent showing possible passivation near partly through end of experiment.

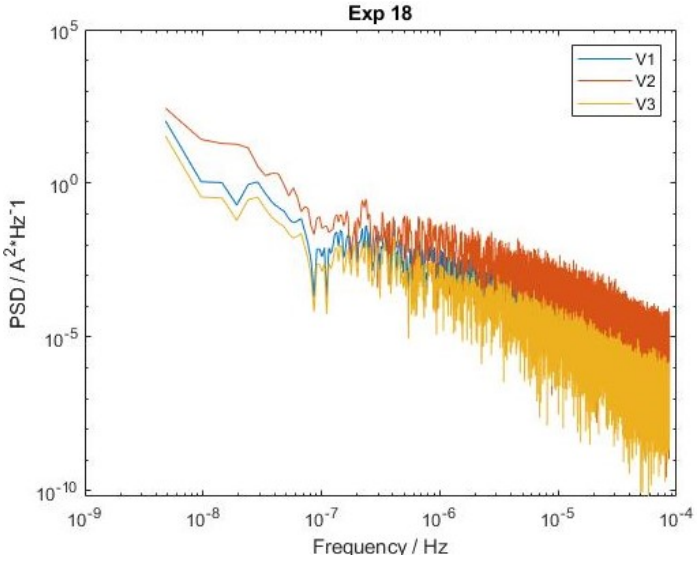

Figure 5.39: Heated NaCl slope near -2 and near constant after roll-off without any passivation. Due to evaporation, it could be the salt content was too high for passivation.

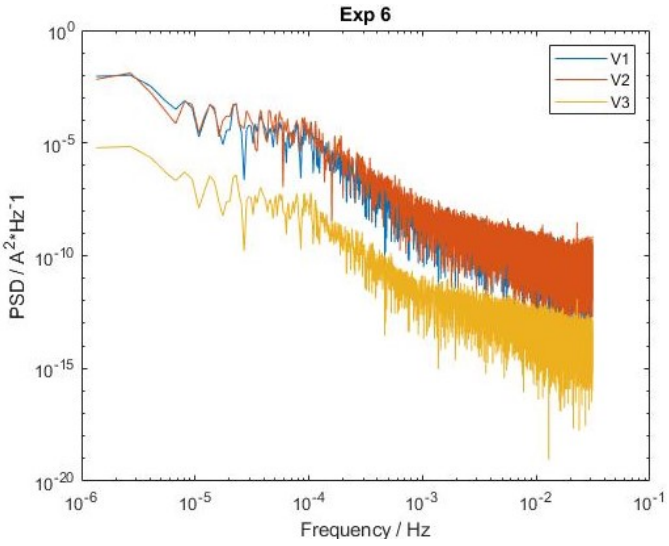

Figure 5.40: Room temperature seawater showing roll-off slope -3.5, and passivation at end.

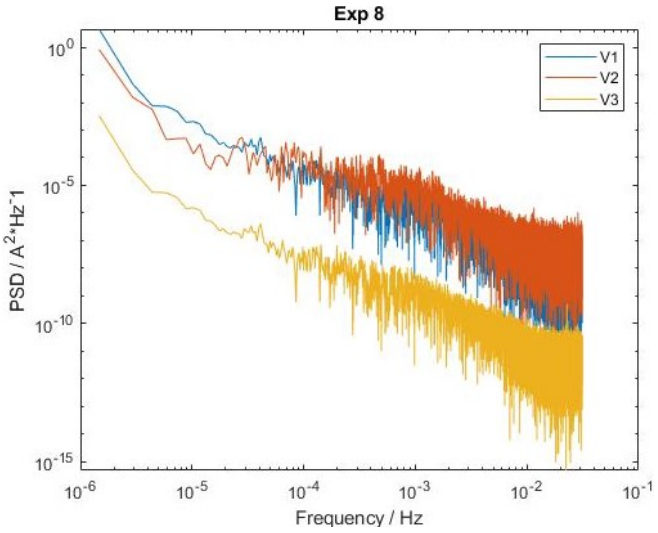

Figure 5.41: 40°C seawater showing roll-off slope -1.8 with passivation at end.

5.6 Visual Comparison

This section has microscope and SEM pictures (random selection of electrodes). Localized and general corrosion was observed. In early tests at room temperature water level was near identical to start of test, though with 40°C and 70°C water levels dropped over the course of the test. In general, distilled sample electrodes were very darkened, with batches of black as seen in Figure

5.42, Figure 5.43, Figure 5.44, and Figure 5.45. In cases of NaCl and seawater it was a lighter reddish colour as in Figure 5.46. 3.5% wt. NaCl at higher temperatures would have solidified salt crystals on removal.

5.6.1 Distilled Water

Darker areas on Experiment 2 could be seen without magnification. These occurred on distilled water and were seen under SEM below. Uniform corrosion seen across surfaces matching information from wavelet and FTT PSD plots. Experiment 10 minor localized corrosion on the surface and defects, perhaps due to higher temperature, or perhaps some contamination. CR was higher for most experiments as temperature was increased.

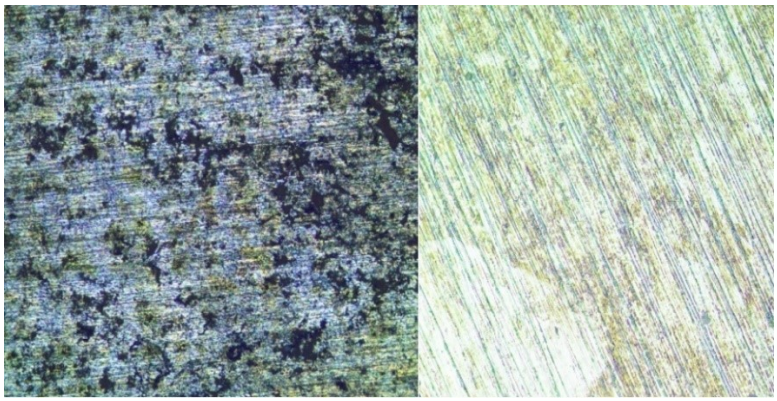

Figure 5.42: Room temperature distilled Experiment 2

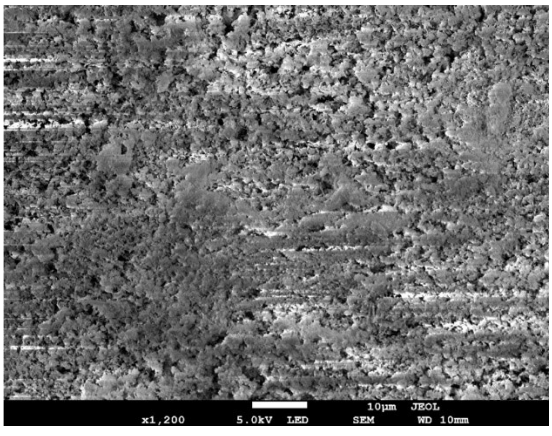

Figure 5.43: Experiment 2 surface before cleaning

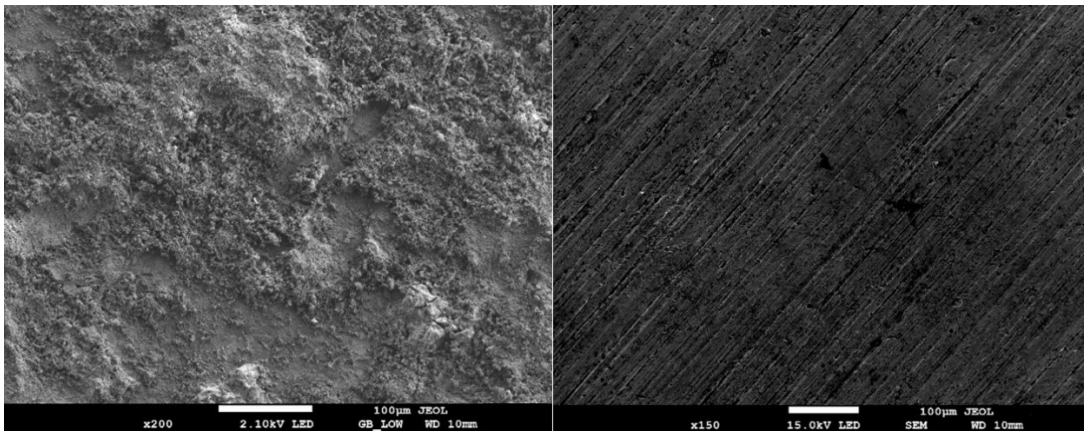

Figure 5.44: Experiment 10 heated distilled water pre and post cleaning, left and right, respectively.

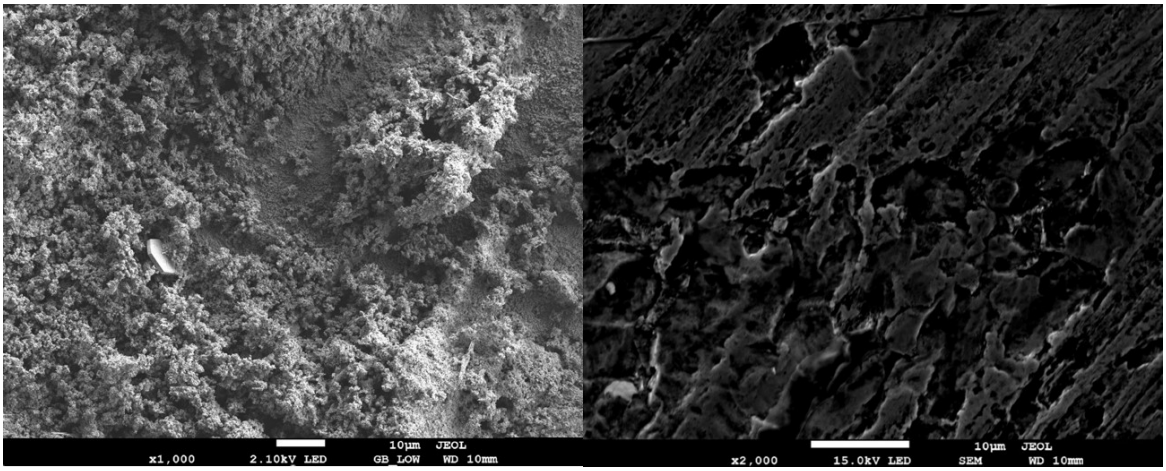

Figure 5.45: Experiment 10 surface pits

5.6.2 Seawater

Seawater samples (Figure 5.46 and Figure 5.47) shown below exhibit typical localized corrosion, reddish-brown oxide layer, and seawater environment oxide formation in Figure 5.48.

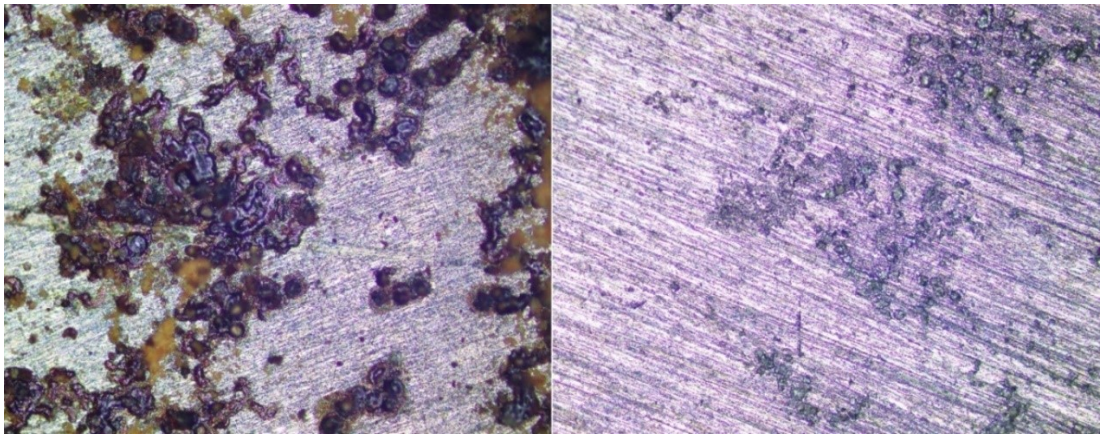

Figure 5.46: Experiment 6, room temperature seawater.

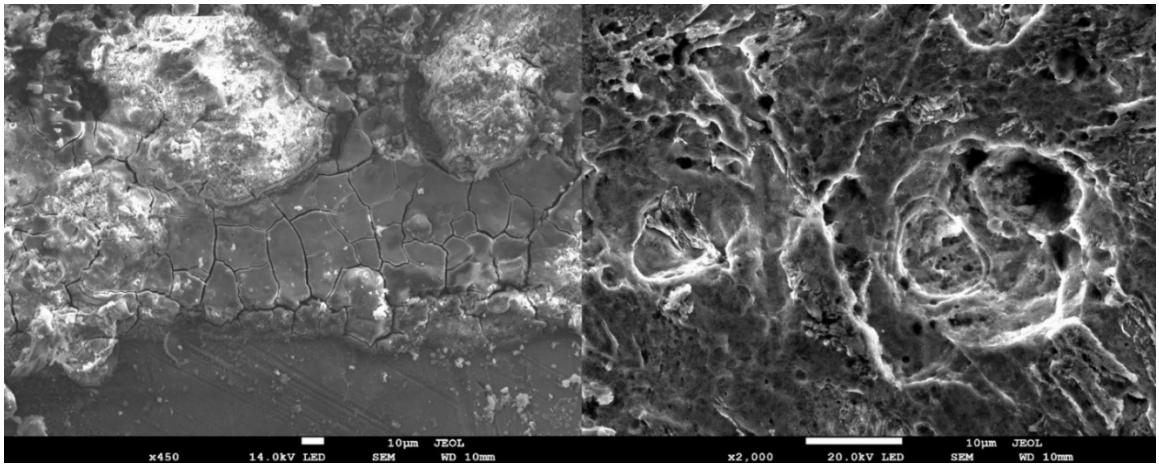

Figure 5.47: Experiment 8, heated seawater, uncleaned electrolyte interface zone, left, cleaned, right.

The surfaces for seawater seem rougher, and the cleaned surfaces seem to have more pits than NaCl in previous section. Cracking on surface also very apparent as seen in experiment 8 interface with electrolyte.

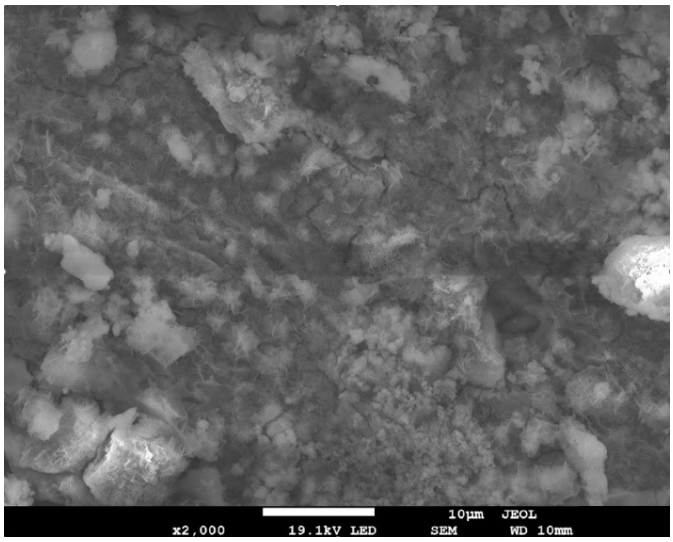

Figure 5.48: Experiment 8 with lepidocrocite, and/or akageneite, along with grain boundary cracks. Similarly found in Chapter 4

5.6.3 3.5% wt. NaCl Electrolyte

NaCl exposed electrodes are presented here. Black surface oxide was present (Figure 5.49), and reddish-brown (Figure 5.50) though it was not as coloured as seawater. After cleaning pitting was seen clearly.

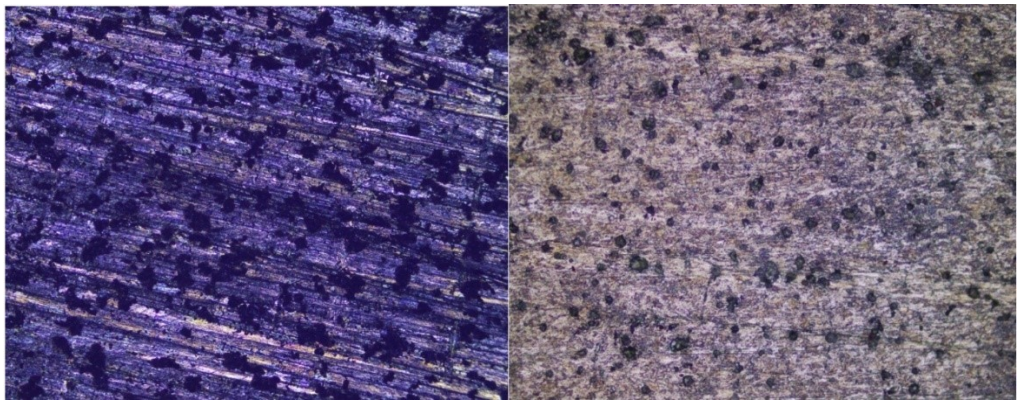

Figure 5.49: Experiment 5, NaCl, room temperature, left uncleaned, right, cleaned

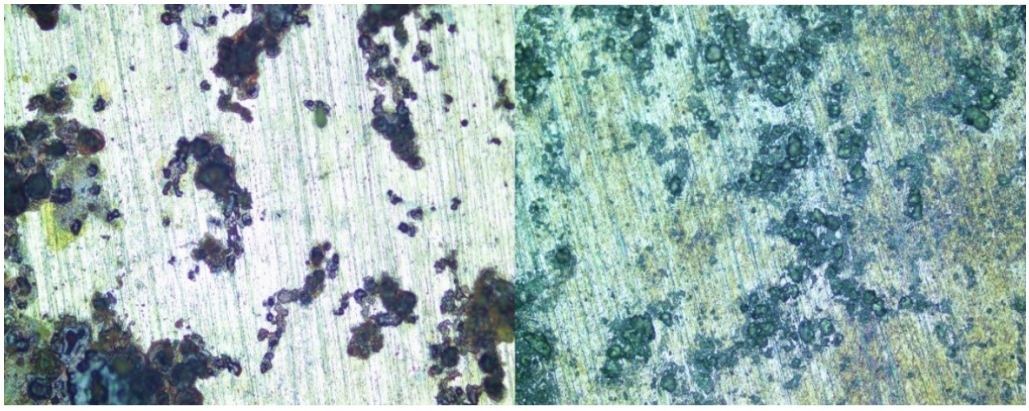

Figure 5.50: Experiment 5, 3.5% Room Temperature NaCl, left uncleaned, right, cleaned.

In higher temperatures of 40°C on zoom there is more attack on the surface microstructure in Figure 5.52. Figure 5.53 shows the cleaned surface of experiment 18, heated NaCl, showing more pitting than when unheated in Experiment 5.

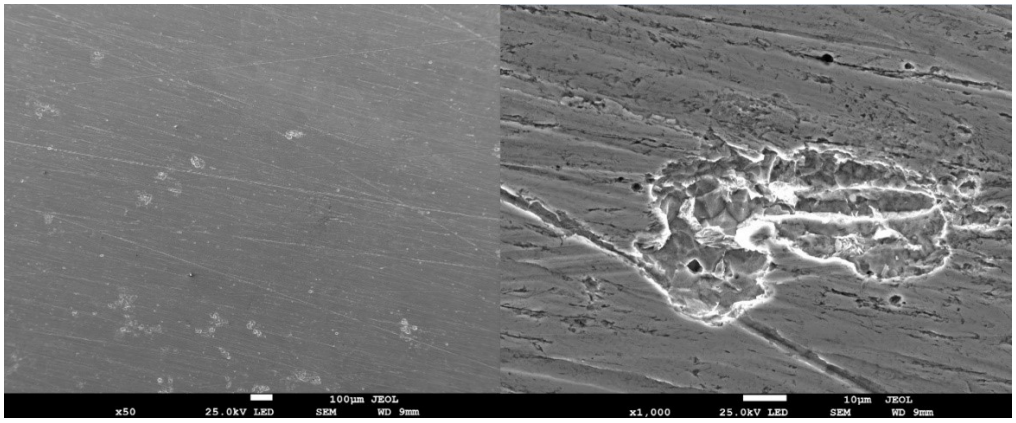

Figure 5.51: Experiment 5 NaCl, cleaned.

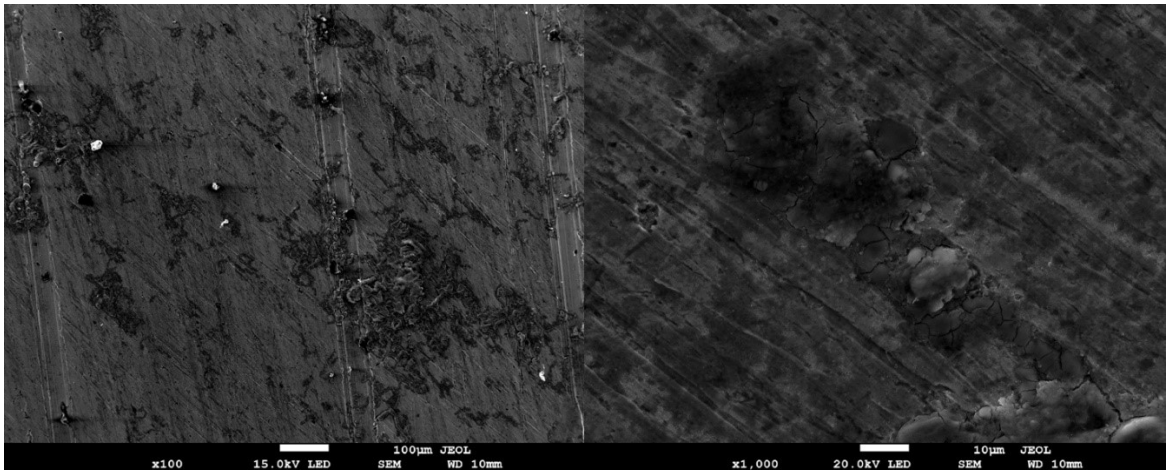

Figure 5.52: Experiment 18 heated NaCl, uncleaned.

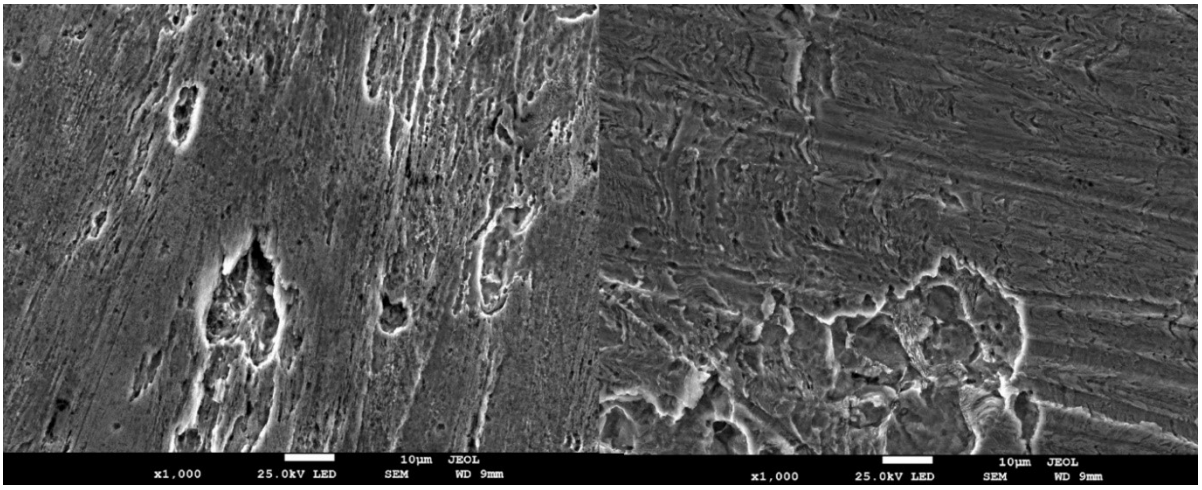

Figure 5.53: Experiment 18, heated NaCl, cleaned.

5.7 Mean CR and Potential Data

This research started to further explore the S-EPN method (Caines et al., 2017b). Though meaningful potential can be used and recorded using three electrodes with standard equipment, and without the use of a reference electrode, the methodology of using potential area curves relating CR for individual electrodes was not accurate. Total potential area did not relate to corrosion rate except in 6/20 cases where highest potential recordings on individual electrodes

having highest mass loss as shown in and Figure 5.2. Potential area alone in these experiments is not enough to find the quantification, or mechanism of corrosion.

Many graphs show large potential area vs time that occurred at start of experiments and tended towards 0 for the duration of the test. When metals are in contact with electrolyte, the first response is nucleation, and then afterwards different corrosion processes occur. Metals want to reduce to a lower energy state, and this was shown in wavelet frequency vs. time charts (i.e. Figure 5.7), as well as the raw EPN charts (i.e. Figure 5.3), meaning that potential may not increase over time with corrosion rate linearly. Rather, potential will fluctuate as charges move around the surface in electrolyte until some equilibrium is established. As the oxide is formed, stability is in the system increases as the base metal has an insulating layer reducing charge transfer. The metal surface becomes less active (until the system changes) as time goes on. This was observed in the present research. It is possible that, open systems with disturbances may change this result and new experiments could be designed based on this.

As shown in Figure 5.2 and other experiments in this work, high potential does not necessarily have high CR, and a lower potential does not equate to lower CR over the course of 12-hour (and one 24 hour) experiments. There are many factors contributing to corrosion and using only raw potential area/noise from electrodes was not able to determine corrosion rate or mechanism without manipulation. Some methods which worked to show mechanism are wavelets and PSD FFT.

Table 5.7: Mean CR, mass loss, and potential for different electrolytes, and calculations for evaporation area adjusted CR. The CR error was calculated as would be +/- 2%.

Electrolyte	Mean corrosion rate	Mean mass loss percent	Mean Potential
Distilled Water	11.7	5.0	132.4
Seawater	**15.8**	**7.2**	112.7
3.5% NaCL	8.3	3.6	**173.6**
Area Adjusted Distilled	19.7	n/a	
AA Seawater	**22.6**	n/a	
AA 3.5% NaCl	11.7	n/a	

5.8 Conclusions

Three symmetrical and asymmetrical (different area but otherwise identical) working electrodes were used to record EPN data over 20 experiments in 3 electrolytes and temperatures with 3Hz resolution for 3 electrodes and resulted in the following in statistical and frequency data (numerical findings were confirmed with microscope and SEM):

- Statistical analysis methods like kurtosis, skew, and SD did not represent the corrosion mechanism accurately. These methods have also been criticized by other researchers as insufficient (Cappeln et al., 2005).
- PSD slopes (linear gradient, roll-off, and flat) accurately portrayed corrosion mechanisms.
- Wavelet analysis showed energy contribution of short timescale crystals and were associated with general corrosion while long time scale crystals provided information on localized corrosion but, presentation was not as clear as FFT PSD graphs.
- For wavelets, large potential occurring at the beginning of most experiments were nucleation processes, and then become general corrosion/passivation. Other cases showed spikes of energy throughout experiment and occurred in localized corrosion cases. This was confirmed by FFT PSD graphs and SEM.

- Experiment 10 heated distilled water showed surface pitting in SEM, and the slope was like localized corrosion for FFT PSD, though with passivation at the end. Perhaps this was due to contamination and confirms FFT PSD as usable.

In regards of raw data information:

- Largest potential area on electrode (v*s) vs CR using S-EPN method did not result in greatest mass loss on electrode or trend linearly as reported previously in (Caines et al., 2017b). Largest/smallest potential does not equate to highest/lowest CR.
- Outliers in data series and high transients represented localized corrosion processes.
- Increase in temperature lead to higher CR, and increased FFT PSD slope.

Data is limited on varying electrode size/symmetry in experiments regarding EPN (Shahidi et al., 2012). Summary of data in the present work may be useful, and was briefly discussed, further analysis is outside the scope of this paper and should be pursued in future work. Below are noted about asymmetrical sized electrodes:

- For PSD plots, wavelets, skew and kurtosis and temperature changes, no major differences were noted comparing similar or asymmetrical electrodes.
- SD was not decreased for smaller size electrodes, and no major difference in potential and electrode area was noted though it was previously reported that smaller electrodes should display increased potential when in same electrolyte experiment.
- Where authors found differences, area was ~1:10 between electrodes or greater. Perhaps in future another experiment can be performed to confirm.

It should be noted that, due to the nature of using three identical electrodes in potential measurement without reference electrode, while unique and simpler to record data, some data may be different than other traditional methods (i.e., skew/kurtosis values related to specific corrosion

mechanism, or not viewing differences in different sized electrodes in the same system). Also, electrode asymmetry and trends cause by DC drift may challenge the reliability of some results presented (Obot et al., 2019).

In this research the best way to analyze corrosion was using the time-frequency domain from raw potential noise generated from A36 rolled steel electrodes. While EN has been in development for a long time, this method in the present research is not accurate in determining corrosion rate. In this research manipulation of the potential-time record to time-frequency domain allowed identification of corrosion mechanisms, but not severity. It is a tool which can work with other methods which add weight to an educated assessment of corrosion. To conclude, EPN can be used to determine corrosion mechanism when some analysis of raw potential is performed.

5.9 References

Acosta, G., Veleva, L., López, J., 2014. Power Spectral Density Analysis of the Corrosion Potential Fluctuation of Stainless Steel 316L in Early Stages of Exposure to Caribbean Sea Water. International journal of electrochemical science 9, 6464–6474.

Al-Mazeedi, H.A.A., Cottis, R.A., 2004. A practical evaluation of electrochemical noise parameters as indicators of corrosion type. Electrochimica Acta, Electrochemical Methods in Corrosion Research 49, 2787–2793. https://doi.org/10.1016/j.electacta.2004.01.040

ASTM G1-03, 2003. Practice for Preparing, Cleaning, and Evaluating Corrosion Test Specimens. ASTM International. https://doi.org/10.1520/G0001-03R17E01

Bertocci, U., Gabrielli, C., Huet, F., Keddam, M., Rousseau, P., 1997. Noise Resistance Applied to Corrosion Measurements: II. Experimental Tests. J. Electrochem. Soc. 144, 37. https://doi.org/10.1149/1.1837362

Bertocci, U., Huet, F., Nogueira, R.P., 2003. Use of Multiple Reference Electrodes in Electrochemical Noise Measurements. Corrosion 59.

Bihade, M.S., Patil, A.P., Khobragade, N.K., 2013. Analysis of Electrochemical Current Noise From Metastable Pitting of SS304L in NaCl Solutions. Trans Indian Inst Met 66, 155–161. https://doi.org/10.1007/s12666-012-0237-3

Caines, S., Khan, F., Shirokoff, J., 2017a. Demonstration of increased corrosion activity for insulated pipe systems using a simplified electrochemical potential noise method. Journal of Loss Prevention in the Process Industries 47, 189–202. https://doi.org/10.1016/j.jlp.2017.03.012

Caines, S., Khan, F., Zhang, Y., Shirokoff, J., 2017b. Simplified electrochemical potential noise method to predict corrosion and corrosion rate. Journal of Loss Prevention in the Process Industries 47, 72–84. https://doi.org/10.1016/j.jlp.2017.02.023

Cao, F.H., Zhang, Z., Su, J.X., Shi, Y.Y., Zhang, J.Q., 2006. Electrochemical noise analysis of LY12-T3 in EXCO solution by discrete wavelet transform technique. Electrochimica Acta 51, 1359–1364. https://doi.org/10.1016/j.electacta.2005.07.012

Cappeln, F., Bjerrum, N.J., Petrushina, I.M., 2005. Electrochemical Noise Measurements of Steel Corrosion in the Molten NaCl- K2SO4 System. J. Electrochem. Soc. 152, B228. https://doi.org/10.1149/1.1928187

Cheng, Y.L., Zhang, Z., Cao, F.H., Li, J.F., Zhang, J.Q., Wang, J.M., Cao, C.N., 2003. Study of the potential electrochemical noise during corrosion process of aluminum alloys 2024, 7075 and pure aluminum. Materials and Corrosion 54, 601–608. https://doi.org/10.1002/maco.200390132

Cottis, R.A., 2001. Interpretation of Electrochemical Noise Data. CORROSION 57, 265–285. https://doi.org/10.5006/1.3290350

Eden, D.A., 1998. Electrochemical Noise - The First Two Octaves. Presented at the CORROSION 98, OnePetro.

Eden, D.A., John, D.G., Dawson, J.L., 1987. Corrosion Monitoring.

Electrochemical Noise Measurement for Corrosion Applications [WWW Document], n.d. URL https://www.astm.org/stp1277-eb.html (accessed 10.17.22).

Electrochemical study of effect of the concentration of azole derivatives on corrosion behavior of stainless steel in H2SO4 - ScienceDirect [WWW Document], n.d. URL https://www-

sciencedirect-com.qe2a-proxy.mun.ca/science/article/pii/S0300944014001957 (accessed 10.19.22).

Gaona-Tiburcio, C., Aguilar, L.M.R., Robledo, P., Estupiñan Lopez, F., Miramontes, J.A., Nieves-Mendoza, D., Castillo-González, E., Almeraya Calderon, F., 2014. Electrochemical Noise Analysis of Nickel Based Superalloys in Acid Solutions. International Journal of Electrochemical Science 9, 523–533.

Girija, S., Mudali, U.K., Raju, V.R., Dayal, R.K., Khatak, H.S., Raj, B., 2005. Determination of corrosion types for AISI type 304L stainless steel using electrochemical noise method. Materials Science and Engineering: A 407, 188–195. https://doi.org/10.1016/j.msea.2005.07.022

Hillier, A., Khan, F., Caines, S., 2021. Corrosion Products and Surface Morphology for Coated, Uncoated, and Insulated A333 Steel Pipelines in Marine Harsh Environment. https://doi.org/10.1115/OMAE2021-63014

Hladky, K., Dawson, J.L., 1981. The measurement of localized corrosion using electrochemical noise. Corrosion Science 21, 317–322. https://doi.org/10.1016/0010-938X(81)90006-8

Homborg, A.M., Tinga, T., Zhang, X., van Westing, E.P.M., Oonincx, P.J., Ferrari, G.M., de Wit, J.H.W., Mol, J.M.C., 2013. Transient analysis through Hilbert spectra of electrochemical noise signals for the identification of localized corrosion of stainless steel. Electrochimica Acta 104, 84–93. https://doi.org/10.1016/j.electacta.2013.04.085

Homborg, A.M., Tinga, T., Zhang, X., Westing, E.P.M., Oonincx, P.J., Wit, J.H.W. de, Mol, J.M.C., 2012. Time-frequency methods for trend removal in electrochemical noise data. ELECTROCHIM ACTA 70, 199–209. https://doi.org/10.1016/j.electacta.2012.03.062

Iverson, W.P., 1968. Transient Voltage Changes Produced in Corroding Metals and Alloys. J. Electrochem. Soc. 115, 617. https://doi.org/10.1149/1.2411362

Jamali, S.S., Mills, D.J., 2016. A critical review of electrochemical noise measurement as a tool for evaluation of organic coatings. Progress in Organic Coatings 95.

Jáquez Muñoz, J., Gaona-Tiburcio, C., Miramontes, J.A., Nieves-Mendoza, D., Maldonado-Bandala, E., Olguín-Coca, J., López-Léon, L., Ríos, J.P., Almeraya Calderon, F., 2021. Electrochemical Noise Analysis of the Corrosion of Titanium Alloys in NaCl and H2SO4 Solutions. Metals 11, 105. https://doi.org/10.3390/met11010105

Liu, X., Zhang, T., Shao, Y., Meng, G., Wang, F., 2010. In-situ study of the formation process of stannate conversion coatings on AZ91D magnesium alloy using electrochemical noise. Corrosion Science 52, 892–900. https://doi.org/10.1016/j.corsci.2009.11.009

Ma, C., Song, S., Gao, Z., Wang, J., Hu, W., Behnamian, Y., Xia, D.-H., 2017. Electrochemical noise monitoring of the atmospheric corrosion of steels: identifying corrosion form using wavelet analysis. Corrosion Engineering, Science and Technology 52, 432–440. https://doi.org/10.1080/1478422X.2017.1320117

Mahjani, M.G., Moshrefi, R., Jafarian, M., Neshati, J., 2014. Detecting pitting corrosion and its severity using wavelet entropy in electrochemical noise measurement. Physical Chemistry Research 2, 116–122. https://doi.org/10.22036/pcr.2014.4561

Mansfeld, F., 2005. The Electrochemical Noise Technique — Applications in Corrosion Research. AIP Conference Proceedings 780, 625–630. https://doi.org/10.1063/1.2036830

Montoya-Rangel, M., Garza-Montes de Oca, N., Gaona-Tiburcio, C., Colás, R., Cabral-Miramontes, J., Nieves-Mendoza, D., Maldonado-Bandala, E., Chacón-Nava, J., Almeraya-Calderón, F., 2020. Electrochemical Noise Measurements of Advanced High-

Strength Steels in Different Solutions. Metals 10, 1232. https://doi.org/10.3390/met10091232

Moshrefi, R., Mahjani, M.G., Jafarian, M., 2014. Application of wavelet entropy in analysis of electrochemical noise for corrosion type identification. Electrochemistry Communications 48, 49–51. https://doi.org/10.1016/j.elecom.2014.08.005

Obot, I.B., Onyeachu, I.B., Zeino, A., Umoren, S.A., 2019. Electrochemical noise (EN) technique: review of recent practical applications to corrosion electrochemistry research. Journal of Adhesion Science and Technology 33, 1453–1496. https://doi.org/10.1080/01694243.2019.1587224

Official Gazette of the United States Patent and Trademark Office: Patents, 1992. . U.S. Department of Commerce, Patent and Trademark Office.

Oppenheim, A.V., Schafer, R.W., Buck, J.R., 1999. Discrete-Time Signal Processing. Prentice Hall, Upper Saddle River, NJ.

Pistorius, P.C., 1997. Design Aspects of Electrochemical Noise Measurements for Uncoated Metals: Electrode Size and Sampling Rate. CORROSION 53, 273–283. https://doi.org/10.5006/1.3280468

Preperation, Installation, Analysus, and Interpretation of Corrosion Coupons in Oilfield Operations, 2005. . NACE.

Reid, S.A., Eden, D.A., 1999. Assessment of corrosion. CA2320794A1.

Ricker, R., Bertocci, U., 1996. A Review of Electrochemical Noise and its Application to the Study of Stress Corrosion Cracking. pp. 235–245.

Searson, P.C., Dawson, J.L., 1988. Analysis of Electrochemical Noise Generated by Corroding Electrodes under Open-Circuit Conditions. J. Electrochem. Soc. 135, 1908. https://doi.org/10.1149/1.2096177

Shahidi, M., Jafari, A.H., Hosseini, S., 2012. Comparison of Symmetrical and Asymmetrical Cells by Statistical and Wavelet Analysis of Electrochemical Noise Data. Corrosion -Houston Tx- 68. https://doi.org/10.5006/0626

Smith, M., Macdonald, D., 2009. Wavelet Analysis of Electrochemical Noise Data. Corrosion 65. https://doi.org/10.5006/1.3319148

Smith, M.T., Macdonald, D.D., 2005. Wavelet Analysis of Electrochemical Noise Data. Presented at the CORROSION 2005, OnePetro.

Standard Guide for Electrochemical Noise Measurement [WWW Document], n.d. URL https://www.astm.org/g0199-09r20e01.html (accessed 10.17.22).

Standard Practice for Preparation of Metallographic Specimens [WWW Document], n.d. URL https://www.astm.org/e0003-95.html (accessed 10.17.22).

Suresh, G., Mudali, U.K., 2014. Electrochemical Noise Analysis of Pitting Corrosion of Type 304L Stainless Steel. Corrosion Science 70. https://doi.org/10.5006/1003

Suresh, G., U., K., Raju, V., Dayal, R., Khatak, H., Raj, B., 2005. Determination of corrosion types for AISI type 304L stainless steel using electrochemical noise method. Materials Science and Engineering A-structural Materials Properties Microstructure and Processing - MATER SCI ENG A-STRUCT MATER 407, 188–195. https://doi.org/10.1016/j.msea.2005.07.022

Wharton, J.A., Wood, R.J.K., Mellor, B.G., 2003. Wavelet analysis of electrochemical noise measurements during corrosion of austenitic and superduplex stainless steels in chloride media. Corrosion Science 45, 97–122. https://doi.org/10.1016/S0010-938X(02)00140-3

Xia, D.-H., Song, S., Behnamian, Y., Hu, W., Cheng, Y.F., Luo, J.-L., Huet, F., 2020. Review—Electrochemical Noise Applied in Corrosion Science: Theoretical and Mathematical Models towards Quantitative Analysis. Journal of The Electrochemical Society 167, 081507. https://doi.org/10.1149/1945-7111/ab8de3

Yi, C., Du, X., Yang, Y., Zhu, B., Zhang, Z., 2018. Correlation between the corrosion rate and electrochemical noise energy of copper in chloride electrolyte. RSC Adv. 8, 19208–19212. https://doi.org/10.1039/C8RA01203B

CHAPTER 6 – Thesis Conclusion

The major focus of this research was to gain knowledge of CUI and other corrosion processes in a marine harsh environment. Data was gathered from a field experiment near seashore and included mass loss due to corrosion, pit depth, and discussions on pipe surface protections. Surface morphology was investigated using SEM, and XRD/EDS analysis was used for surface product identification.

Another key area of research was to determine corrosion monitoring capabilities of EPN using S-EPN method and was investigated through 20, 12-hour experiments with different electrode sizes, electrolytes, and temperatures. Physical mass loss and surface morphology was compared to EPN readings. All research conclusions are presented in this section.

6.1 Field Experiment Conclusions

An experiment in C5 harsh marine environment was recorded for more than 2 years. Two peer-reviewed conference papers (Chapter 3 and 4) were created, and three presentations were made detailing the challenges of the environment, data recorded, and future research (C-RISE 4th Conference, 2019, St. John's, OMAE 40th International Conference, and ASME Online 2021 A and B).

The work presented demonstrated differences in mass loss, CR, and pitting in pipelines for different surface protections leading to better understanding of coating and insulation in highly corrosive environments. Corrosion near the ends of the pipe were most severe, perhaps due to crevice corrosion, and ingress of moisture and chloride. Insulated uncoated pipes showed deepest pits, therefore when pipes are insulated, anti-corrosion protective coating should be applied. Corrosion and pitting rates were lowest in insulated and coated pipes.

Destructive testing results provided the following CRs (see Figure 3.8 for pitting, and Figure 3.12 for average CRs below, as bar charts):

- insulated coated 0.017mm/yr
- insulated uncoated 0.021mm/yr
- uninsulated coated 0.014mm/yr
- uninsulated uncoated 0.023mm/yr

Averaged corrosion rates were comparable with other harsh marine atmosphere researchers (Lins et al., 2018) but were lower than others in the literature review section of Chapter 3. This may be because of using LTCS with similar properties to weathering steels, or because of the added protection of coating and/or insulation. The deepest pits were in uninsulated coated and insulated uncoated was perhaps due to lack of oxygen access under the coating and insulation. It also retained moisture, thus accelerating corrosion.

Regarding conclusions related to surface morphological features in Chapter 4, it appears ferrihydrite reduced formations of lepidocrocite and goethite, thus reducing the protective ability of the oxide formed, and deepest pits were found in uncoated pipes containing ferrihydrite and akageneite (with or without insulation). Therefore, marine environment pipelines must have protection against chlorides and moisture to ensure design life. When coating fails, accelerated corrosion causes high volume oxide buildup and expansion, cracking the coating and increasing breaks the coat from the pipe (presented were cases of more than ~10x visual area of initial break). Pitting was most extreme just away from exposed metal surface and under coating, where oxygen and airflow would be less.

Further research is necessary to detect if microbial corrosion occurs at Argentia, NL, however, other authors (Furukawa et al., 2002) had a similar environmental species and corrosion products

mentioning that active metal reducing bacteria or heterogeneous redox environment were present stabilizing ferrihydrite (such as Si, P, Cu, S). Green rust presence (in environments containing C, Cl, S) can also cause ferrihydrite. Magnetite and other species are similarly found in the field test, however, when found with ferrihydrite the oxide does not protect as well due to the formation of islands away from the metal substrate. Coating, insulation, and pits on pipelines limit free flow surface oxygen, as well, seawater spray with chloride promotes akageneite and increases localized corrosion on steels. This was observed. Mechanisms clearly present at Argentia, NL include a combination of ferrihydrite formation, and chloride occurring akageneite, which would cause high pitting and corrosion rates. Exfoliation from expanding oxides created away from the surface also occurred, typical of many marine atmospheres (especially near seawater spray)

LTCS pipelines had lightly bound oxide on an outer layer with dark stronger bound oxide on the inner surface. For CS, thick layer exfoliation occurred after several months and by the end of the experiment the CS braces lost ~20% of their total thickness, while even the heaviest corroded LTCS pipes were near original mass in all surface conditions.

The largest to smallest reported oxides by XRD on uncoated and uninsulated pipes were akageneite, lepidocrocite, and goethite. When akageneite was not detected, the largest to smallest detected were maghemite/hematite, lepidocrocite, and goethite. Uncoated and insulated pipes had goethite, lepidocrocite, and akageneite. Coated pipes had goethite, maghemite/hematite, and lepidocrocite. Randomly selected coated and insulated samples for XRD did not have corrosion present which makes sense. It means that over two years the insulation and coating rarely failed, as reported elsewhere (Geary, 2013; Geary and Parrott, 2016), however, in those same reports the general life estimate is 5-13 years, while in the present case, some did fail below 2 years.

These results add knowledge of CUI, CRs, corrosion under coating, and pitting rates not available before for field tests using A333 steel (LTCS) in harsh marine environment. Some uses of this data may be new corrosion models, or new information for standard guidance on CUI and coating for assets in C5 marine environments. Also, industry can use this information to better plan maintenance and design life.

6.2 S-EPN Experiment Conclusions

Three symmetrical and asymmetrical area working electrodes were used to record EPN data over 20 12-hour experiments in 3 electrolytes and temperatures at ~1Hz per electrode.

Statistical analysis methods like kurtosis, skew, and SD did not represent the corrosion mechanism accurately from raw EPN data. These methods have been criticized by other researchers as insufficient (Cappeln et al., 2005), however, PSD slopes (linear gradient, roll-off, and flat) accurately portrayed corrosion mechanisms. Wavelet analysis showed the energy contribution of short timescale crystals, are associated with general corrosion while long time scale crystals provided information on localized corrosion, but presentation was not as clear as PSD. When wavelet signal was placed alongside original time domain, large potential shifts occurring at the beginning showed nucleation processes, and then became general corrosion/passivation later. Often when this occurred it was confirmed by FFT PSD slope and SEM physical observations. I.e., when wavelets potential changed through experiment it often matches with FFT PSD, and physically shows localized corrosion. Increases in temperature lead to higher CR, and increased PSD slope on all samples.

S-EPN was new research from (Caines et al., 2017) which related individual electrode potential to CR using bulk materials and simple instruments where the largest potential area on an electrode

(v*s) often showed a high CR, and that it trended linearly. Investigation of this method over 20 experiments did not show electrode area relate to CR, or trend linearly. Largest/smallest potential did not equate to highest/lowest CR and the methodology was not applicable.

20 experiments performed under different conditions in the present research found that potential was not related directly to corrosion rate/type on electrodes using S-EPN. However, when moving to frequency and time-frequency domain with FFT and wavelets, raw EPN qualified corrosion type using simple equipment with bulk materials from potential time records.

Asymmetrical electrodes are seldom studied, and controversial opinions exist about them. In the present work for PSD plots, wavelets, skew, kurtosis and temperature changes, no major differences were noted comparing symmetrical or asymmetrical electrodes. SD was not decreased for smaller size electrodes, and no large differences in potential and electrode area were noted, though it was reported that the smaller electrode should display increased potential/DS when in same electrolyte experiment. Differences were noted by other researchers it only occurred when the ratio of electrode areas were greater than 1:10. In the present case the difference in electrode area was ~1:2.

It should be noted that, due to the nature of using three identical material electrodes in potential measurement without reference electrode, while unique to record data, it may be different than other traditional methods (i.e. skew/kurtosis values related to corrosion mechanism may have required a reference electrode similar to SCE etc).

As seen currently, the best way to analyze corrosion with EPN was using the time-frequency domain on raw potential noise generated from electrodes. EPN can be used to help in making decisions on corrosion mechanism, however, analyzing methods performed need to be understood so that those using them can use other means to fill in the blanks due to inconsistent data. I.e. in

cases where statistical data does not work, attempting frequency PSD or wavelet EDP may help determine what is occurring physically when metal surfaces cannot be physically observed (like in the case of CUI).

6.3 Future Work

Future research in harsh marine environment can include creating a models based on CRs, CUI, and coating information presented in this work and creating an accelerated test to match the timeline presented. Magnetite layers which are away from the surface in Chapter 4 may be from microbial reduction of ferrihydrite, or perhaps due to large formation of chloride oxides formed and should be investigated.

Longer term testing should be performed, 3+ years around Newfoundland, or different locations away/closer to sea while recording some atmospheric conditions throughout the time of the test. The corrosion rate was lower than many others in Chapter 2, and it should be tested if this is only related to using LTCS or something else.

Interestingly, there was a small plant on the surface of a metal pipe which had attached itself and started growing. It is unknown if this organism was from the sea or land, but further research should check on biological fowling in the area near seashore.

In regards of EPN experiments slopes and rates of change in PSD charts could be extracted and compared to mass loss on electrodes to try and relate slope to quantification. An algorithm in MatLAB should be created to determine the type of corrosion from wavelet chart/frequency domain PSD as corrosion was easily qualified in the present work using those methods.

Though electrode size was varied, no differences were found regarding corrosion rates or potential, as such, the electrode difference should increase to 1:10/1:100 and record results.

Though an initial plan was to included gathering EPN data in field, equipment was not working well to record long term data, and extreme humidity would turn off the power, and I could not have access to the network to check remotely. The data was also originally planned to be 3+ years, but the province closed the corrosion site due to budget cuts and only slightly more than 2 years was available.

Data recording of EPN on pipelines should be performed without a dielectric barrier, with only one large pipe section to simulate pipelines in field. Another test should include measurement of EPN while corrosive substances are inside pipelines to check ability to measure corrosion through pipe wall.

The original reason to use three identical electrodes was to compare electrode potential area on each and relate to physical mass loss. Because that is not applicable there is no reason to use a three identical electrode setup. Therefore, experiments should be performed with only 1 or 2 electrodes and then raw EPN can be checked to see if the PSD and wavelets work as well as in the present case to qualify corrosion.

6.4 References

Caines, S., Khan, F., Zhang, Y., Shirokoff, J., 2017. Simplified electrochemical potential noise method to predict corrosion and corrosion rate. Journal of Loss Prevention in the Process Industries 47, 72–84. https://doi.org/10.1016/j.jlp.2017.02.023

Cappeln, F., Bjerrum, N.J., Petrushina, I.M., 2005. Electrochemical Noise Measurements of Steel Corrosion in the Molten NaCl- K2SO4 System. J. Electrochem. Soc. 152, B228. https://doi.org/10.1149/1.1928187

Furukawa, Y., Kim, J., Watkins, J., Wilkin, R.T., 2002. Formation of Ferrihydrite and Associated Iron Corrosion Products in Permeable Reactive Barriers of Zero-Valent Iron. Environmental science & technology 36, 5469–5475. https://doi.org/10.1021/es025533h

Geary, W., 2013. Analysis of a corrosion under insulation failure in a carbon steel refinery hydrocarbon line. Case Studies in Engineering Failure Analysis 1, 249–256. https://doi.org/10.1016/j.csefa.2013.09.001

Geary, W., Parrott, R., 2016. Two corrosion under insulation failure case studies. Loss Prevention Bulletin 2–6.

Lins, V., Gomes, E.A., Costa, C.G., Castro, M. das M.R., Carneiro, R.A., 2018. Corrosion behavior of experimental nickel-bearing carbon steels evaluated using field and electrochemical tests. Metallurgy and materials 71(4), 613–620. https://doi.org/10.1590/0370-44672016710173

Appendix 1 – Argentia Files

The files for Argentia will be uploaded to https://github.com/FieldExperiment/Argentia

Appendix 2 – LabVIEW pages

These are the screenshots of the active pages used for Keithly device measurement from electrodes.

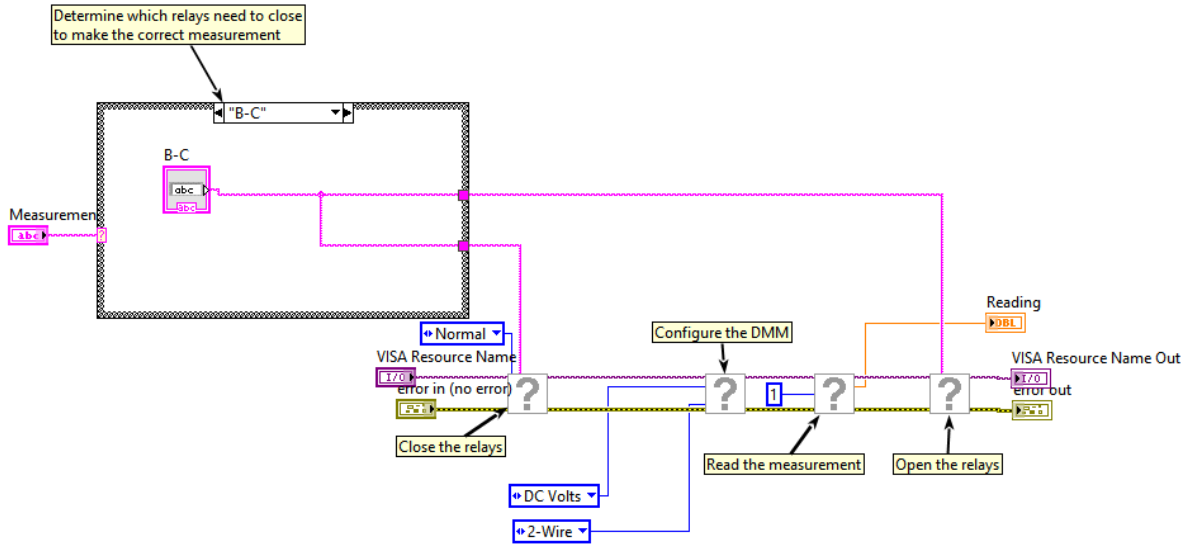

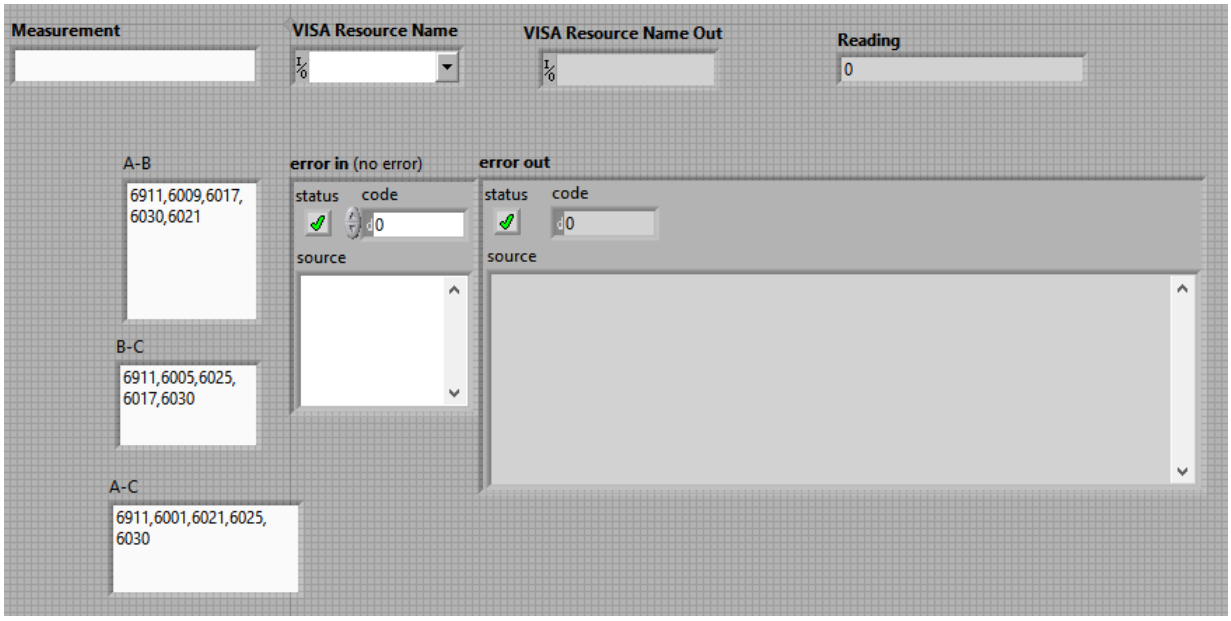

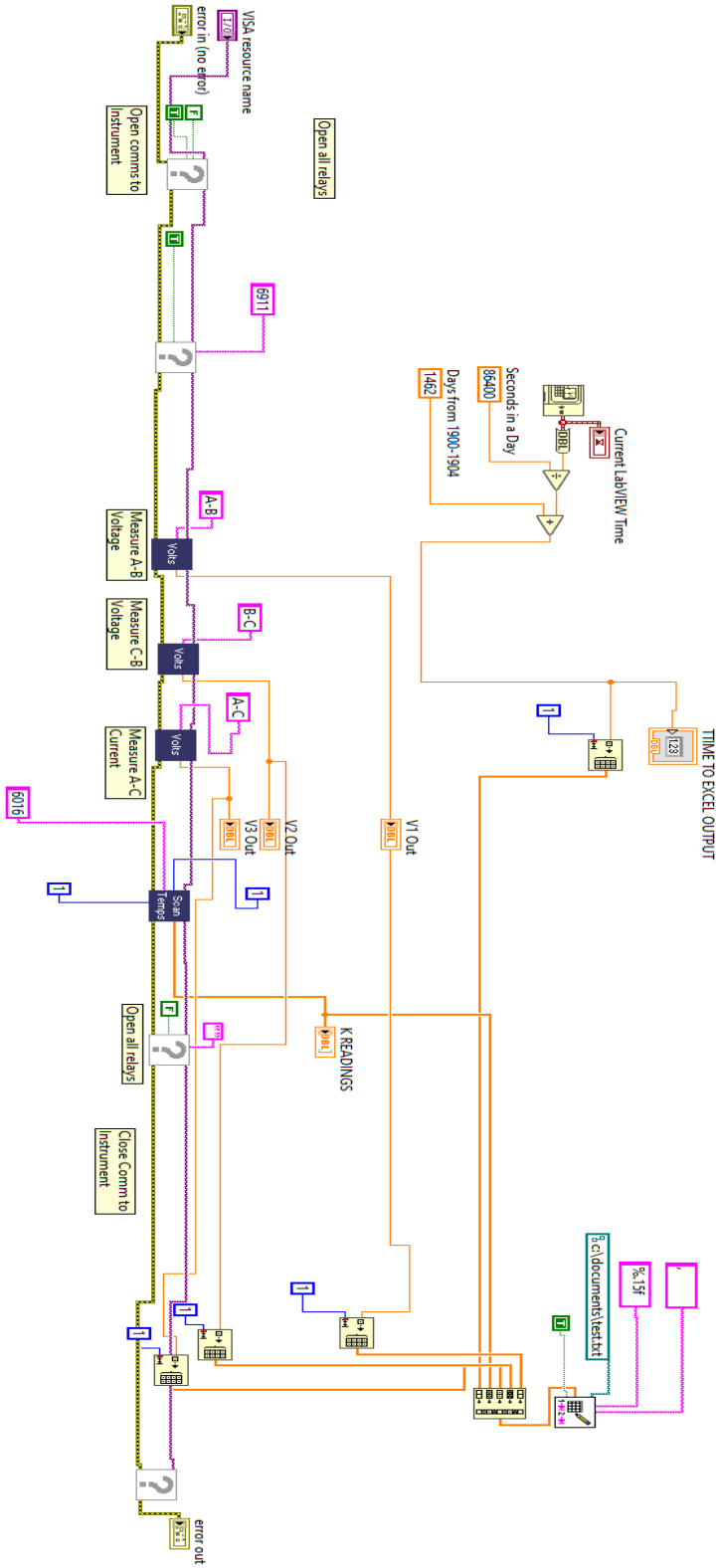
VISA resource name
error in (no error)
Open comms to Instrument
Open all relays
6011
A-B
Measure A-B Voltage
Volts
B-C
Measure C-B Voltage
A-C
Measure A-C Current
6016
Scan Temps
V2 Out
V3 Out
V1 Out
K READINGS
Open all relays
Close Comm to Instrument
error out
Days from 1900-1904
1462
Seconds in a Day
86400
Current LabVIEW Time
TIME TO EXCEL OUTPUT
c:\documents\test.txt
%.15f

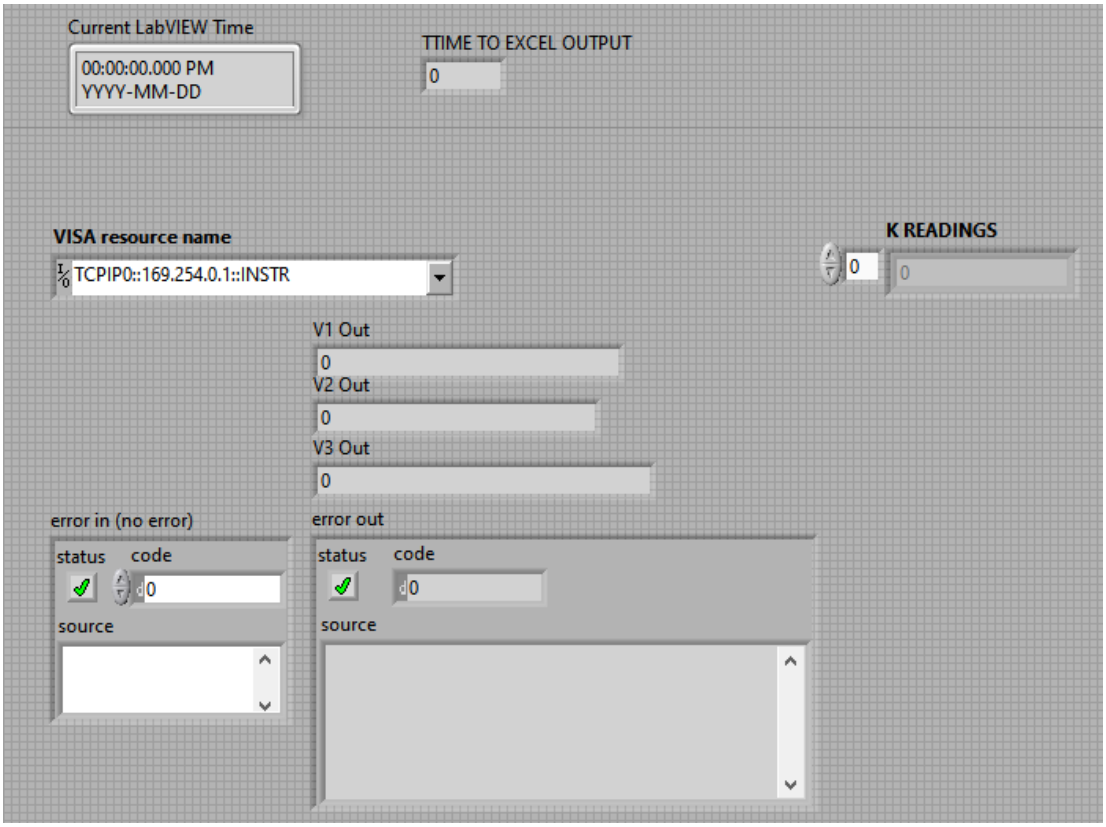
Current LabVIEW Time
00:00:00.000 PM
YYYY-MM-DD
TTIME TO EXCEL OUTPUT
0
VISA resource name
TCPIP0::169.254.0.1::INSTR
K READINGS
0
0
V1 Out
0
V2 Out
0
V3 Out
0
error in (no error)
status
code
0
source
error out
status
code
0
source